Universidad de Valparaíso CHILE | Doctorado en Ciencias Mención Neurociencia

GLUCAGON AS A NOVEL NEUROMODULATOR OF RETINAL ROD BIPOLAR CELL INHIBITORY ACTIVITY, POSSIBLE IMPLICATIONS IN MYOPIA PATHOGENESIS

Tesis entregada a

LA UNIVERSIDAD DE VALPARAÍSO

en cumplimiento parcial de los requisitos para optar al grado de

Doctor en Ciencias con Mención en Neurociencia

Facultad De Ciencias

Por

Felipe Alejandro Tapia Pérez

Septiembre 2022

Dirigida por: Dr. Oliver Schmachtenberg

Codirigida por: Dr. Alex Vielma

FACULTAD DE CIENCIAS

UNIVERSIDAD DE VALPARAÍSO

INFORME DE APROBACIÓN

TESIS DE DOCTORADO

Se informa a la Facultad de Ciencias que la Tesis de Doctorado presentada por:

FELIPE ALEJANDRO TAPIA PÉREZ

Ha sido aprobada por la Comisión de Evaluación de la tesis como requisito para optar al grado de Doctor en Ciencias con mención en Neurociencia, en el examen de Defensa de Tesis rendido el día 21 del mes de octubre de 2022.

Director de Tesis:
Dr. Oliver Schmachtenberg .....

Co-Director de Tesis:
Dr. Alex Vielma .....

Comisión de Evaluación de la Tesis

Dr. Andrés Chávez .....

Dra. Ana María Cárdenas .....

Dra. Georgina Renard .....

AGRADECIMIENTOS

Quisiera partir agradeciendo a mi familia, ya que su apoyo siempre ha sido fundamental para mí, y en especial ahora para salir adelante durante estos extraños tiempos de pandemia y cuarentenas.

También quiero agradecer a mis tutores, por su ayuda para rediseñar la tesis después del fallido primer intento y para luego llevarla en la dirección correcta con sus comentarios, críticas y felicitaciones. Agradezco también a la comisión de tesis por su guía, sobre todo para encausar y acotar los objetivos a cumplir.

Muchas gracias también a mis compañeros del LFS, por toda la ayuda y el apoyo en el día a día de las actividades del laboratorio, y por las discusiones y comentarios que me ayudaron a completar esta tesis.

Quiero agradecer también de forma especial a Valentín Peñaloza por su ayuda con los ratones modelo de miopía, que fueron parte fundamental para cimentar las conclusiones de la tesis. También a Sebastián Estay y los demás miembros del laboratorio del profesor Andrés Chávez por su ayuda y la disposición cada vez que iba a pedirles materiales y reactivos.

Finalmente, agradecer a las fuentes de financiamiento que hicieron posible esta tesis, la Beca Doctorado Nacional ANID, la Beca del Programa de Neurociencias UV y los proyectos FONDECYT Regular No. 1210790 y FONDECYT Iniciación No. 11191211.

TABLE OF CONTENTS

LIST OF FIGURES AND TABLES

LIST OF ABBREVIATIONS

AMPAR	AMPA receptor
cAMP	Cyclic adenosine monophosphate
CNQX	6-cyano-7-nitroquinoxaline-2,3-dione
CNS	Central nervous system
D	Diopter
D1R	D1-like dopamine receptor
D2R	D2-like dopamine receptor
DAC	Dopaminergic amacrine cell
D-AP5	D(−)-2-amino-5-phosphonopentanoic acid
EAAT	Excitatory amino acid transporter
ECDF	Empirical cumulative distribution function
FDM	Form deprivation myopia
GCL	Ganglion cell layer
GCR	Glucagon receptor
GLP	Glucagon-like peptide
GlyR	Glycine receptor
GPCR	G-protein coupled receptor
HK-ECS	High-potassium and high-calcium extracellular solution
INL	Inner nuclear layer
IPL	Inner plexiform layer
IPSC	Inhibitory post-synaptic current
IV	Current-voltage
KDF	Kernel density function
KO	Knock-out
L-AP4	L-(+)-2-amino-4-phosphonobutyric acid
LIM	Lens-induced myopia
ONL	Outer nuclear layer
OPL	Outer plexiform layer
PACAP	Pituitary adenylate cyclase-activating polypeptide
PG	Proglucagon
PHI	Peptide histidine isoleucine
PPG	Preproglucagon
RBC	Rod bipolar cell
SARS-CoV-2	Severe acute respiratory syndrome coronavirus 2
TPMPA	(1,2,5,6-Tetrahydropyridin-4-yl)methylphosphinic acid
VEC	Voltage-evoked currents
VIP	Vasoactive intestinal peptide

ABSTRACT

Myopia incidence is steadily increasing worldwide, but the underlying pathophysiologic mechanisms are still only partially understood. Glucagon is a peptide thought to signal image defocus in the eye, which is considered the first step in myopia induction, and dopamine is known for its key role in myopia, being proposed as the main signaling molecule linked to its pathogenesis. The aim of this study was to corroborate glucagon signaling in the mammalian retina and find a possible link with dopaminergic signaling. To this end, whole-cell patch-clamp and bath application of selective pharmacological agents were used to study the inhibitory activity of rod bipolar cells (RBCs), as this activity is known to be regulated by dopamine and has been linked in other parts of the central nervous system to regulation by members of the glucagon/secretin family, and also since RBCs have been implicated in glucagon-related activity. Inhibitory post-synaptic currents (IPSCs) under 0 mV voltage-clamp mode were measured in RBCs from wild-type and lens-induced myopia model mice. Glucagon produced a dose-dependent and glucagon receptor-dependent increase in RBC glycinergic IPSC frequency. This effect was also dependent on dopaminergic activity as it was abolished by dopamine type 1 receptor (D1R) antagonism and in scotopic conditions. The effect was also abolished in the myopia murine model but could be recovered using D1R agonism in model animals for up to 2 weeks of induction. Glucagon is a novel retinal neuromodulator in mammals, regulating the glycinergic inhibitory activity acting on RBCs in a D1R-dependent manner. Its effects are abolished in a myopia model, suggesting it is one of the pathways affected in this condition. More research will be required to determine whether this pathway could be a target for myopia prevention or treatment.

INTRODUCTION

Myopia, an increasing worldwide concern

Myopia is a common refractive error, where the image of distant objects is focused in front of the retina, resulting in blurry vision when not corrected (Y. Zhang & Wildsoet, 2015). This condition entails an imbalance between the refractive power of the eye, that is close to normal, and an excessive elongation of the eye, dependent on the posterior chamber (McBrien & Millodot, 1987; Y. Zhang & Wildsoet, 2015). As a consensus, in the clinical setting myopia is more strictly defined as a spherical equivalent refractive error ≤ -0.5 diopters (D) (Flitcroft et al., 2019).

The incidence of myopia has increased in the recent decades, reaching levels that warrant the designation as an “epidemic” (Dolgin, 2015). A global epidemiologic study estimated a myopia prevalence of 1,950 million people worldwide in 2010 (28.3 % of the population), and projected an increase to 2,620 million people in 2020 and up to 4,758 million people in 2050 (49.8% of the global population) (Holden et al., 2016) (Fig. 1). An important regional variability can also be observed, with East Asian countries showing greater numbers (Holden et al., 2016; Matsumura et al., 2020), with reports of a prevalence of up to 96.5% of 19-year-old male conscripts in Seoul, South Korea (Jung et al., 2012).

These figures will most likely need to be revised following the effects of the spread of the severe acute respiratory syndrome coronavirus 2 (SARS-CoV-2) pandemic that started on December 2019. The government of China, the country where the outbreak started, ordered multiple contention measures including home quarantine, prohibition of outdoor activities, and a nationwide

schools closure, requiring students to study using digital devices (Parmet & Sinha, 2020; G. H. Wang et al., 2020). As SARS-CoV-2 spread to other countries, similar measures started to be adapted.

Recent epidemiologic studies in China have shown significant myopic shifts in 6-8 years-old children during school screening in 2020, when compared to the previous 5 years (J. Wang et al., 2021). Follow-up studies of myopic children 7-12 years-old showed a faster progression of myopia, up to 3 times higher when compared to the previous visit before quarantine. This increase in progression was also correlated with digital screen use time (Ma et al., 2021). Future studies will be needed to corroborate these results and help to improve our picture of how the control measures associated with the SARS-CoV-2 pandemic affected myopia progression in the rest of the world.

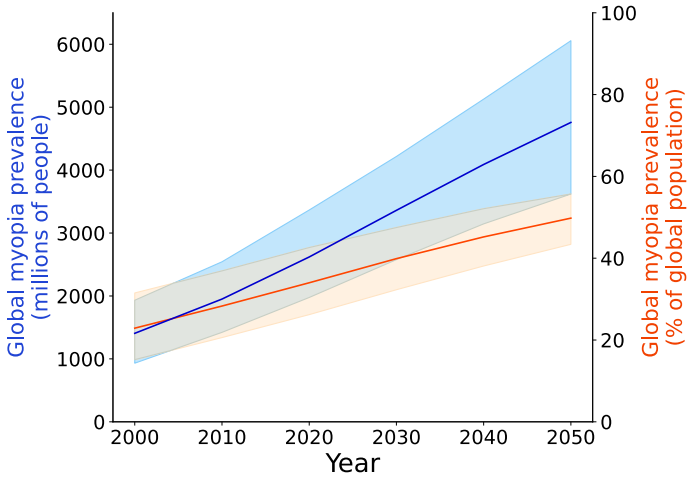

Figure 1. Predictive studies show a progressive increase in myopia prevalence worldwide. The estimation of the worldwide prevalence of myopia from the year 2000 up to year 2050 shows a marked increase, with a projected 49.8% of the global population affected by 2050. The estimated global prevalence in millions of people worldwide (blue) and as a percentage of total world population (orange) are shown. Adapted from (Holden et al., 2016), shaded areas show 95% confidence intervals.

Myopia is associated with an increased risk of multiple complications that can severely affect vision, potentially even leading to vision loss. These pathologies include myopic maculopathy, retinal detachment, choroidal neovascularization, cataracts and glaucoma, with high myopia (a spherical equivalent refractive error ≤ -6 D) having a higher risk (Saw et al., 2005).

Despite this epidemiological importance, the etiology of myopia and other refractive errors, and the reasons behind the increase in prevalence are still poorly understood (Stone, 2008). Most of the knowledge available so far about the mechanisms underlying the development of myopia come from studies in animal models, being the chicken (*Gallus domesticus* (Linnaeus, 1758)) one of the major models to date (Schaeffel & Feldkaemper, 2015).

These studies in animal models have made fundamental contributions to our understanding of the signals linking image defocus with axial elongation in the retina (M. Feldkaemper & Schaeffel, 2013; Pardue et al., 2013). Two main procedures have been used to model myopia development in animals, form deprivation myopia (FDM) and lens-induced myopia (LIM). FDM was the first method to be used for myopia induction in animals (Wallman & Turkel, 1978), and it was performed by either suturing the eyelids or by using translucent googles (Fig. 2, left). This method has been successfully used in multiple animals, including chicken and mammals such as tree shrews, mice and monkeys (Rymer & Wildsoet, 2005; Schaeffel & Feldkaemper, 2015). In the case of LIM, negative lenses are used to induce hyperopic defocus, which in turn leads to axial eye elongation. This model has been used with multiple animals too, such as chickens, tree shrews, guinea pigs, mice and monkeys (Rymer & Wildsoet, 2005; Schaeffel & Feldkaemper, 2015) (Fig. 2, right).

Figure 2. Methods for myopia induction in animal models. Chicks fitted with the two main methods for myopia induction, on the left fitted with a translucent goggle to induce myopia via form deprivation, on the right, fitted with a negative lens to produce lens-induced myopia. Adapted from (Rymer & Wildsoet, 2005).

It is important to note that the changes observed in eye anatomy in animal models are confined to the posterior chamber, as is the case of human myopia (Rymer & Wildsoet, 2005), with an increase in axial length and scleral and choroidal thinning posterior to the eye equator (Jonas et al., 2014, 2016; Kim et al., 2017). This increase in size is also finely regulated by the characteristics of the visual stimulus, as myopia induction using lenses covering only half of the visual field produces the enlargement only of the half of the eye associated with the affected hemi-retina (Diether & Schaeffel, 1997; E. L. Smith et al., 2009). Further evidence suggests these morphological changes are mediated by local mechanisms within the eye, as optical nerve section, producing the physical isolation of the retina from the brain, and the use of tetrodotoxin to in turn produce functional isolation, are not able to prevent the development of myopia using either FDM or LIM (Mcbrien et al., 1995; Norton et al., 1994; Troilo et al., 1987).

Glucagon, a peptide signaling visual defocus

Glucagon is a peptide produced from the cleaving of proglucagon (PG), a 160-aminoacid protein codified by the preproglucagon (PPG) gene (GCG gene in humans) (Müller et al., 2017). The post-

translational modification of PG gives origin to multiple tissue-specific derivates. In the brain for example, PG can be cleaved into glucagon-like peptide 1 (GLP-1), GLP-2, glicentin, oxyntomodulin and intervening peptide 2 (Müller et al., 2017).

Glucagon and GLP belong to the evolutionarily-linked secretin/glucagon superfamily, comprised of highly homologous peptides (Müller et al., 2017; Tam et al., 2014) that perform their function through equally related and homologous class B G protein-coupled receptors (GPCR) (Müller et al., 2017). Glucagon in particular acts through the glucagon receptor (GCR), which when activated signals using at least two G proteins, $G_{s\alpha}$ y $G_{q\alpha}$, increasing intracellular levels of cyclic AMP (cAMP) and calcium, respectively (Jelinek et al., 1993).

There is evidence showing the presence of both glucagon and GCR in the retina of multiple vertebrate species. In the case of chickens, glucagon has been shown to be present in the retina and to play a role in the development of myopia (Carr & Stell, 2017). In-situ hybridization in chicken retina has localized GCR in close to 50% of the cells in the ganglion cell layer (GCL) and inner nuclear layer (INL), especially closer to the border with the inner plexiform layer (IPL) (M. Feldkaemper et al., 2004).

Production of glucagon inside the retina has been linked to a group of glucagonergic amacrine cells (Fischer et al., 2006b). A subgroup of these glucagonergic amacrine cells is immunoreactive for both glucagon and ZENK, responding to the sign of image defocus with a down-regulation of ZENK under negative lenses (Bitzer & Schaeffel, 2002; Fischer et al., 1999) and under FDM (Ashby et al., 2010). ZENK is a member of the immediate early gene family of transcriptional regulators, genes that are induced rapidly and transiently following neuronal activation, and is the avian ortholog of the mammalian immediate early gene Egr-1 (Ashby et al., 2010; Patton et al., 2017).

In mammals, EGR-1 has been shown to undergo changes homologous to those seen in chickens. Mice knocked-out (KO) for Egr-1 show myopic changes in their refractive characteristics and eyes with greater axial longitude (Schippert et al., 2007). Similar results were found in rhesus

macaques, with a decrease in the expression of EGR-1 in myopia induction conditions (diffuser) and an increase in the opposite condition (+3 D lens) (Zhong et al., 2004).

Furthermore, in the retina of mice and rats, glucagon immunoreactivity has been detected in the INL, GCL and the feet of Müller cells (Das et al., 1985). In the rat retina, high affinity binding sites for glucagon suggesting the presence of GCR have also been documented (Fernandez-Durango et al., 1990) and PPG and GCR mRNA have been evidenced using PCR (M. Feldkaemper et al., 2004). Immunohistochemical studies have shown the presence of multiple members of the secretin/glucagon family in the mouse retina, including vasoactive intestinal peptide (VIP), peptide histidine isoleucine (PHI) and pituitary adenylate cyclase-activating polypeptide (PACAP), with VIP co-localizing with PHI and EGR-1 in amacrine cells (Mathis & Schaeffel, 2007). It is of note that the levels of EGR-1 expression were associated with the level of retinal illumination, as higher illumination was associated with higher numbers of EGR-1 positive cells (Mathis & Schaeffel, 2007).

Due to the high degree of homology of the peptides and receptors in the secretin/glucagon family, it is also possible that peptides other than glucagon could signal focus-related information. Studies in chickens have shown an effect homologous to that of glucagon for VIP (Cakmak et al., 2017) and oxyntomodulin (Vessey, Rushforth, et al., 2005). Also, population genetics studies in China have shown an association of polymorphisms of the gene for the VIP-2 receptor and high myopia (Yiu et al., 2013).

Dopamine and the dopaminergic hypothesis of myopia

Other than glucagon, multiple molecular signals such as neurotransmitters, neuromodulators and growth factors have been related to the development of myopia. Of all of them, dopamine is perhaps the most researched. One of the first studies linking dopamine and ocular growth was performed by Stone et al. in 1989, showing a decrease in the retinal content of dopamine and its

metabolite 3,4-dihydroxyphenylacetic acid in chicken eyes under FDM (Stone et al., 1989). Since then, a large number of studies have linked dopamine with myopia, leading to what is called the “dopaminergic hypothesis of myopia”, which suggests that dopamine is the main signaling molecule involved in emmetropization and myopia development, as retinal dopamine release plays an antagonistic role to myopia development (Zhou et al., 2017).

In the retina, dopamine is released by dopaminergic amacrine cells and interplexiform cells (Frederick et al., 1982), and acts both at the synaptic level and through volumetric transmission (Bjelke et al., 1996). Production and release of dopamine in the retina is dependent on illumination levels (Iuvone et al., 1978) and shows a circadian rhythm dependent on photoreceptor activity (Doyle et al., 2002). The amacrine cells in charge of its production are in turn regulated by inhibitory activity originating in different groups of GABAergic and glycinergic amacrine cells (Qiao et al., 2016).

Dopamine exerts its effects through GPCRs that can be classified in two families, D1-like receptors (D1R), which act increasing intracellular levels of cAMP, and D2-like receptors (D2R), which inhibit its synthesis (Beaulieu & Gainetdinov, 2011). These two families are in turn divided into five receptor subtypes, with subtypes 1 and 5 being part of the D1R family, and subtypes 2, 3 and 4 being part of the D2R family (Beaulieu & Gainetdinov, 2011).

Both families have been shown to be present in the retina (Djamgoz & Wagner, 1992; Veruki & Wässle, 1996), but their roles in myopia pathogenesis are not clearly understood. In general, the use of non-selective dopamine receptor agonists, like apomorphine, inhibits the development of myopia (Dong et al., 2011; Gao et al., 2006; Rohrer et al., 1993; Schmid & Wildsoet, 2004), while studies using specific agonists and antagonists suggest a shared role of D1R and D2R.

In the case of D1R, its selective agonism does not seem to have an effect on the development of either LIM or FDM (McCarthy et al., 2007; Nickla et al., 2010) while its selective antagonism limits the protective effects of unrestricted vision under FDM, in which removal of the lens used to induce myopia for periods of time during the day ameliorates or prevents myopia induction (Nickla et al.,

2010). Later studies contradicted these results, showing that this effect is only present in LIM (Nickla & Totonelly, 2011) and not in FDM (McCarthy et al., 2007). The authors propose a differential effect of D1R antagonism for LIM and FDM (Nickla & Totonelly, 2011).

In the case of D2R, selective agonism of this family inhibits myopia development under FDM (McCarthy et al., 2007) and LIM (Nickla et al., 2010). The antagonism of D2R has been shown to prevent the protective effects of unrestricted vision in FDM but not in LIM (McCarthy et al., 2007; Nickla & Totonelly, 2011), while having no direct effect on the development of FDM (McCarthy et al., 2007). Furthermore, co-application of apomorphine and spiperone, a D2R antagonist, blocks the protective effect of apomorphine (Rohrer et al., 1993), suggesting this effect to be mediated by D2R. It is of interest however, that D2R antagonism alone does not seem to be sufficient for myopia induction (Huang et al., 2014).

The ambiguity of the aforementioned results could be related to the methodology, as these studies were performed using intravitreal injections, making it difficult to control the exact concentrations acting on the retina, and also to the possibility of biphasic effects of the drugs used (M. Feldkaemper & Schaeffel, 2013).

A series of studies in KO mice for either dopamine receptor family showed that, on one hand, D1R play a fundamental role in the protective effect of apomorphine on myopia, as it was abolished in D1R KO mice (Huang et al., 2018). On the other hand, KO mice for D2R showed an hyperopic state during the first two post-natal months (Zhou et al., 2010) and the effect of FDM was attenuated (Huang et al., 2014).

Taken together, the available data suggest a complex interaction between D1R and D2R signaling in myopia pathogenesis and progression.

Glucagon and dopamine, a possible signaling pathway linking image defocus and axial growth

Since glucagon and dopamine have been implicated in myopia development, the question arises as to whether there exists a retinal signaling pathway involving the interaction between these two neuromodulators.

To date, no studies have reported a direct relationship between dopaminergic and glucagonergic signaling at the retinal level, but there are studies linking dopamine with the expression of ZENK. In two studies in chickens, intravitreal injection of 2-amino-6,7-dihydroxy-1,2,3,4-tetrahydronaphthalene hydrobromide, a non-selective dopaminergic agonist, reverted the decrease in ZENK levels observed in FDM, leading to an increase in its expression over controls (Ashby et al., 2007, 2010).

Expression of ZENK/EGR-1 has also been associated in chicken (Fischer et al., 1999) and in rhesus macaques (Zhong et al., 2004) to bipolar cells expressing PKCα, a marker abundantly expressed in rod bipolar cells (RBC) (Xiong et al., 2015). In the case of the study in rhesus macaques, the levels of EGR-1 in RBCs and in subgroups of GABAergic amacrine cells showed a bimodal response to the direction of the image defocus (Zhong et al., 2004).

The inhibitory activity acting on RBCs is dependent on the level of light adaptation of the retina (Eggers et al., 2013), which in turn is correlated with the levels of dopaminergic activity. Studies have shown that dopamine modulates the inhibitory activity acting on RBCs, specifically, dopamine acting through D1R decreases the frequency, but not the amplitude of spontaneous inhibitory activity in RBCs, suggesting a pre-synaptic mechanism (Flood et al., 2018). This inhibitory activity corresponds to non-reciprocal GABAergic signaling, arising from a subgroup of wide field amacrine cells signaling onto RBCs through $GABA_{A\text{-}\rho}$ receptors (Travis et al., 2018). Dopamine acts on these cells in an indirect way, inhibiting the activity of secondary amacrine cells, which in turn decreases the inhibition received by the primary amacrine cells through $GABA_A$ receptors, a configuration called serial inhibition (Travis et al., 2018) (Fig. 3). It is of note however,

that this study shows an inhibitory effect of D1R activation, with an increase in the $GABA_{A-\rho}$ receptor-dependent inhibitory activity acting on RBCs (Travis et al., 2018).

This dopamine-regulated RBC inhibitory activity is also of interest as a possible target for a confluence with glucagonergic activity. The literature regarding the role of glucagon in the mammalian central nervous system (CNS) has focused mostly on its metabolic effects (Abraham & Lam, 2016), and is severely lacking in regard to its possible role as a neuromodulator. On the other hand, multiple studies have shown that GLP-1, the molecule sharing the most homology to glucagon in the secretin/glucagon family (Adelhorst et al., 1994), has roles as a neuromodulator of both excitatory and inhibitory activity in the CNS. In the case of its role as a modulator of inhibitory activity, GLP-1 has been shown to increase both the amplitude and frequency of spontaneous IPSCs in hippocampal CA3 pyramidal neurons by pre- and post-synaptic mechanisms (Korol et al., 2015). GLP-1 has also been shown to regulate the activity of GABAergic neurons in the nucleus tractus solitarius (Fortin et al., 2020) and in the mouse cortex and hippocampus (Rebosio et al., 2018). The use of the GLP-1 analog exenatide has also been shown to increase the levels of GABA in the brain of a murine autism model (Solmaz et al., 2020). In isolated rat retinal ganglion cells, the GLP-1 agonist exendin-4 has been shown to suppress GABA receptor-mediated currents, and also to suppress light-induced GABAergic currents in retinal ganglion cells from rat retinal slices, in a pathway dependent on IP_3 and CaMKII activity (T. Zhang et al., 2022).

Taking all this information into account, RBCs emerge as an interesting target to study a possible interrelation between dopaminergic and glucagonergic activity in myopia development, since these cells show dopamine-dependent inhibitory activity and EGR-1 expression dependent on the sign of image defocus, a molecule that has also been associated with the activity of glucagonergic amacrine cells.

The present study thus set out to record the inhibitory activity of RBCs and to test whether glucagon plays a role in its regulation and its relationship with dopaminergic signaling in the mouse retina, both in wild type animals and a murine myopia model, using whole cell patch-clamp recordings and calcium imaging.

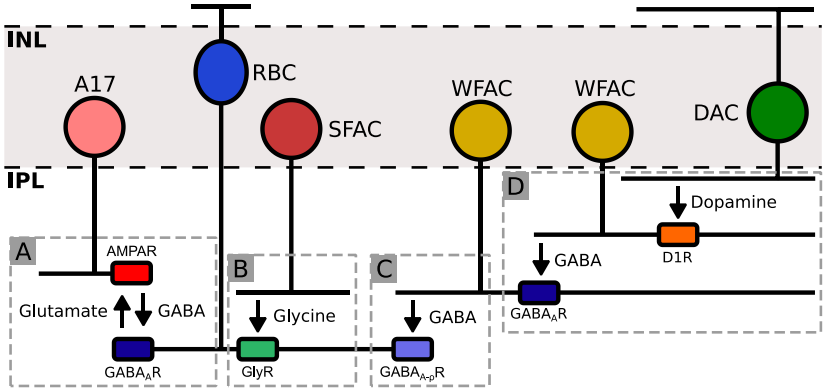

Figure 3. Inhibition pathways of retinal RBCs in the IPL. Diagram showing the main pathways of inhibition acting on RBCs present in the IPL. **(A) Reciprocal inhibition:** RBCs form reciprocal synapses with A17 amacrine cells (A17). Glutamate released from RBCs acts on A17 amacrine cell AMPA receptors (AMPAR) producing feedback GABA release from these cells, which in turn activates $GABA_A$ receptors ($GABA_AR$). **(B-C) Non-reciprocal inhibition: (B)** RBCs receive glycinergic inputs from small field amacrine cells (SFAC), acting on glycine receptors (GlyR). **(C)** RBCs also receive GABAergic inputs from wide field amacrine cells, acting on $GABA_{A-\rho}R$. **(D) Serial inhibition:** GABAergic input from primary wide field amacrine cells (WFAC) is in turn regulated by secondary wide field amacrine cells, the activity of these secondary cells is regulated by dopamine, acting through dopamine D1 receptors (D1R). This dopamine is produced by dopaminergic amacrine cells (DAC). INL: Inner nuclear layer; IPL: Inner plexiform layer.

Hypothesis

Glucagon modulates the inhibitory activity received by RBCs, in a mechanism dependent on dopaminergic signaling acting through GABAergic amacrine cells. This dopaminergic mechanism is altered in a myopic animal model.

Objectives

Main objective:

- To study the effect of glucagon on the inhibitory activity received by RBCs and its dependency on dopaminergic activity and to compare it with the results obtained in a myopic animal model.

Secondary objectives:

- To evaluate the effect of glucagon application on the inhibitory activity received by RBCs.
- To evaluate the dependence on dopaminergic signaling of the effect of glucagon on the inhibitory activity received by RBCs.
- To compare the effect of glucagon on the inhibitory activity received by RBCs observed in wild-type animals with a myopic animal model.

METHODOLOGY

Animals

The experiments were conducted on C75BL/6 mice, regardless of sex and weight, 32-40 days of age, as this is the period were mice eyes reach emmetropic refraction values (Tkatchenko et al., 2010). The animals are housed in the institutional animal facility of the Universidad de Valparaíso and are held at 20 - 25°C under a 12-hour light/dark cycle with water and food ad libitum. Procedures were conducted with approval and according to the norms of the bioethics committee of the Universidad de Valparaíso.

Preparation of retinal slices

Animals were deeply anesthetized by inhalation using isoflurane and euthanized via decapitation. Eyes were enucleated and kept in extracellular solution during the remainder of the procedure, composed of (in mM): 119 NaCl, 23 $NaHCO_3$, 1.25 NaH_2PO_4, 2.5 KCl, 2.5 $CaCl_2$, 1.5 $MgSO_4$, 20 glucose, 2 Na^+ pyruvate, aerated with 95% O_2 and 5% CO_2, reaching a pH of 7.4. The eye is then cut along the ora serrata to separate the anterior and posterior chambers, and the retina is separated carefully from the choroid-sclera. The retina is embedded in type VII agarose (Sigma) dissolved in a solution composed of (in mM): 119 NaCl, 25 HEPES, 1.25 NaH_2PO_4, 2.5 KCl, 2.5 $CaCl_2$, 1.5 $MgSO_4$ at a pH of 7.4. The retina is then sliced using a vibratome (VT1000S, Leica

Microsystems) to obtain 200 µm thick retinal slices. Slices are kept in a chamber containing extracellular solution, aerated with 95% O_2 and 5% CO_2 at room temperature.

Patch-clamp recordings of rod bipolar cells

Recordings were obtained using the patch-clamp technique in whole-cell configuration. To record inhibitory activity, the holding potential was set to 0 mV in voltage-clamp mode, corresponding to the reversal potential of non-specific cationic currents under our recording conditions. Signals are processed using an EPC 7 Plus (HEKA Instruments) amplifier, filtered at 3 kHz, digitized and sampled at 10 kHz (Digidata 1440A, Molecular Devices) and recorded using pClamp 10.4 (Molecular Devices) software. Recording pipettes were pulled from borosilicate capillaries (1.5 mm OD, 0.84 mm ID, WPI), to resistances between 10-15 MΩ (Sutter P-97, Sutter Instruments). The solution used to fill the recording pipette was composed of (in mM): 125 K+ gluconate, 10 KCl, 10 HEPES, 2 EGTA, 2 Na_2ATP, 2 NaGTP and 1% Lucifer Yellow, pH 7.4 adjusted with KOH. The calculated liquid junction potential of 14 mV was corrected before the recordings. The access resistance was assessed periodically during the experiments, and recordings were discarded when a variation larger than 15% was observed.

Patch-clamp recordings were performed in RBCs visualized under an Eclipse FN1 (Nikon) microscope, equipped with a 40x water immersion objective, using infrared light and differential interference contrast, and a TCH-1.4LICE (Tucsen Photonics) camera to capture bright field and fluorescence images.

Confirmation of the identity of the recorded cell was possible using Lucifer Yellow dye, dialyzed through the recording pipette, which allowed to assess the morphology and terminal stratification of the axon. RBCs display a characteristic morphology, with a soma in the upper part of the INL and an axon extending to the border of the IPL and the GCL, ending in multiple varicosities (Ghosh et al., 2004) (Fig. 4A). During the recordings, it was also possible to assess voltage-gated currents,

using a protocol consisting of multiple 10 mV steps between -100 and 50 mV, this protocol has been previously established to identify bipolar cell subtypes (Vielma & Schmachtenberg, 2016). RBCs showed a characteristic pattern under this protocol (Fig. 4C) with a positive deflection at the start of the -20 mV pulse corresponding to the reciprocal feedback from A17 amacrine cells (Elgueta et al., 2018) (Fig. 4D).

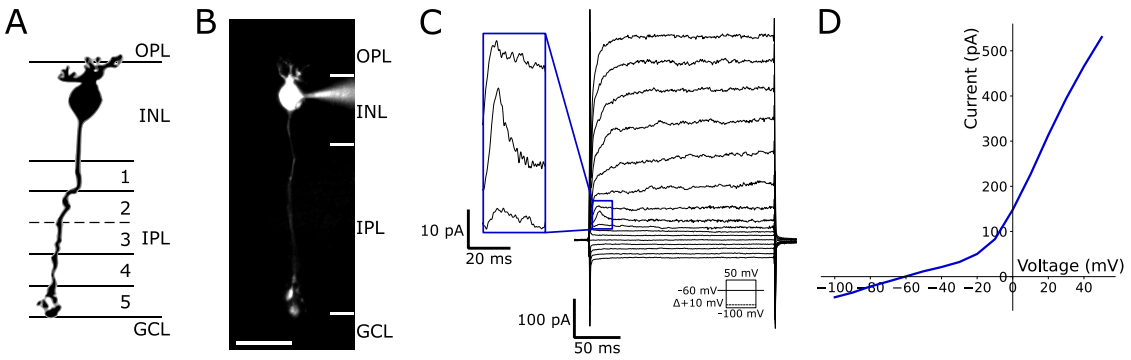

Figure 4. Characteristics used for the identification of RBCs. (A) Schematic representation of a mouse retinal RBC showing its morphological characteristics, with a soma ubicated high in the INL, and an axon terminal extending to the limit between the IPL and GCL and composed of multiple varicosities. Adapted from (Ghosh et al., 2004). **(B)** A lucifer yellow filled RBC showing the same morphological characteristics. Scale bar = 20 µm, magnification = 40x. **(C)** The family of voltage-gated currents obtained using a protocol of multiple 10 mV steps between -100 and 50 mV. The inset shows the characteristic reciprocal current from A17 amacrine cells. **(D)** The current-voltage curve obtained from the steady state region of the currents family shown in (C).

To elicit inhibitory postsynaptic currents (IPSCs), stimulation was performed using a puff of glutamate (500 µM) applied to the OPL from a single-barrel glass pipette operated by a custom-made picospritzer at 2 to 3 psi. An alternative stimulation method using high-potassium and high-calcium extracellular solution (HK-ECS), as described by (Ivanova et al., 2006), was delivered to the OPL using the same configuration, HK-ECS contained (in mM): 128 NaCl, 20.1 KCl, 3 $CaCl_2$, 1.2 $MgCl_2$, 5 HEPES, pH 7.4 adjusted with NaOH. This protocol was used to more reliably elicit glycinergic IPSCs.

To study the origin of the observed IPSCs, pharmacological inhibition was used to separate the different inhibitory pathway: SR-955531 10 μM to block $GABA_A$ receptors, (1,2,5,6-Tetrahydropyridin-4-yl)methylphosphinic acid (TPMPA) 50 μM, to block $GABA_{A\text{-}\rho}$ receptors and strychnine 5 μM to block glycine receptors were added as needed to the bath solution. The recording protocol consisted of 3 baseline 30 s recordings followed by bath application of the antagonist for a period of 15 min; after that 3 new 30 s recordings were performed.

To study the effect of glucagon on the recorded inhibitory activity of RBCs, glucagon 1 μM (Sigma) was added to the bath solution. The recording protocol consisted of 3 baseline 30 s recordings followed by application of glucagon for a period of 5 min and 3 new 30 s recordings. The concentration of glucagon was varied to produce a dose-response curve to concentrations of 250 nM, 500 nM and 2 μM.

To study the dependency of the observed effects of glucagon application on GCR activity, the non-peptidyl allosteric GCR antagonist L168,049 was added to the bath solution. L168,049 inhibits glucagon binding to its receptor, with an IC50 of 3.7 nM in the case of human glucagon receptor, without inhibiting the binding of GLP to its receptor using concentrations up to 10 μM (Cascieri et al., 1999). In the case of the murine glucagon receptor, L168,049 has an IC50 of 0.25 μM in the presence of Mg^{+2} (De Laszlo et al., 1999). The protocol consisted of 3 baseline 30 s recordings followed by bath application of L168,049 for a period of 15 min, after that 3 new 30 s recordings were performed, finally after a period of 5 min co-application of L168,049 and glucagon 1 μM, 3 final 30 s recordings were performed. L168,049 was used at concentrations of 1 μM, 500 nM and 250 nM.

To study the dependency of the effects of glucagon on dopaminergic activity, SCH 23390 10 μM, to block D1 dopamine receptors, sulpiride 10 μM, to block D2 dopamine receptors, SKF 81297 10 μM as a D1 receptor agonist and quinpirole 10 μM were added to the bath solution as needed. The protocol used the same scheme described before, with 3 control recordings, 15 min

application of the tested drug followed by 3 recordings, and 5 min co-application of the drug and glucagon 1 µM followed by 3 final recordings.

To isolate RBCs and study possible post-synaptic events, a cocktail of blockers was applied to the extracellular solution used to keep the cells during the experiments. This cocktail contained L-(+)-2-amino-4-phosphonobutyric acid (L-AP4) 20 µM as a mGluR III agonist, 6-cyano-7-nitroquinoxaline-2,3-dione (CNQX) 20 µM to block AMPA/kainate receptors, D(−)-2-amino-5-phosphonopentanoic acid (D-AP5) 25 µM to block NMDA receptors, SR-95531 10 µM to block $GABA_A$ receptors and TPMPA 50 µM to block $GABA_{A\text{-}\rho}$ receptors. For these experiments, glycine was used at a concentration of 300 µM, described previously as a saturating concentration for this type of cell (Ivanova et al., 2006), applied with a puffer pipette to the axon terminal of the recorded cell. The protocol used bath solution containing the described cocktail for the total duration of the experiments, with 3 control recordings, 5 min application of glucagon 1 µM and 3 final recordings.

Glucagon was obtained from Sigma; the other pharmacologic agents used for these experiments were obtained from Tocris.

Murine model of myopia

Myopic changes were induced in mice using -10 D lenses, positioned in front of one of the eyes at day PN27, and kept for either 2 or 3 weeks. The contralateral eye was kept without a lens as a control. The lenses are kept in place using a plastic support glued to the cranium of the animal.

To position the support armature, the mouse is anesthetized via inhalation of isoflurane (4-5%) in a chamber and kept under a lower dose (1-2%) for the rest of the protocol. An analgesic (carprofen 5 mg/kg s.c.) and an antibiotic (enrofloxacin 10 mg/kg s.c.) were also administered.

The surgical area on the head of the animal is shaved and disinfected using 70% ethanol and chlorhexidine. A 1.5 mm diameter incision is opened using a surgical blade to access the cranium.

Using dental cement, two screws are affixed to the bone and used as a support for the lens armature.

After the surgery, animals are kept for a week with their litter, and after that moved to an independent cage at 20 - 25 °C under a photoperiod of 12/12 h, with water and food ad libitum. The analgesic and antibiotics are continued for 2 days after surgery. The nails of the animals are kept trimmed to prevent lens scratching.

Calcium imaging

To study possible overall effects of glucagon on retinal activity, calcium imaging recordings were performed. 200 µm retinal slices were obtained as previously described and were then incubated in 2 ml of extracellular solution containing 5 µM fluo-4 AM (Thermo Fisher Scientific) and 0.04% pluronic for a period of 1 h in a dark room and at a temperature of 37°C. After incubation, the plate containing the slices is washed twice using 2 ml extracellular solution. The rest of the experiments are conducted in dark conditions.

Fluorescence recordings are performed under an Eclipse FN1 (Nikon) microscope, equipped with a 40x water immersion objective, using infrared light and differential interference contrast, equipped with a TCH-1.4LICE (Tucsen Photonics) camera and a LED stimulation system. To decrease the effect of photobleaching, periods of light stimulation last for 1 s and are followed by 5 s of darkness for the duration of the experiment.

Recordings consisted of 3 min of baseline recording, 5 min of glucagon 1 µM bath application and 9 min of wash-out. A single ROI was taken from each slice, and they were changed for each experiment.

Data analysis

Recordings were analyzed using a custom script written in Python 3.8.8 by the thesis author. The custom script first filters the signal using a 3rd order low pass Butterworth digital filter to reduce noise, and then uses the peak finding algorithm provided in the SciPy 1.8.0 package. The threshold amplitude to detect events is determined as two times the interquartile range of the noise sampled from the start of the recording, calculated over the average trace obtained using a gaussian filter to remove the high frequency activity of the signal. The functions used for these subsequent steps are also contained in the SciPy 1.8.0 package.

For transient events, the frequency is calculated as the number of events divided by the total recording time and the amplitude as the difference between the peak value of an event and the average of the signal at that point. The decay time was used as an approximation of the decay tau and calculated as the time from the peak of the event until the event amplitude has decreased to e^{-1} times the peak amplitude (Fig. 5).

For the sustained events, amplitude was calculated as the peak value over the signal average, time to peak as the time between stimulation start to the time of the measured maximum, charge transfer as the area under the curve, obtained by integrating the signal starting at the time of stimulation and decay tau as the value of τ after fitting the function (Fig. 5):

$$f_{(x)} = N_0 e^{-\frac{x}{\tau}}$$

For calcium imaging recordings, the time-lapse obtained was analyzed using the software ImageJ 1.53q, and photobleaching was corrected using the Bleach Correction ImageJ plug-in with the Histogram Matching Method (Miura, 2020). For analysis, the retina was subdivided by layer, the INL was further subdivided into the first two thirds (INL_A) and the last third (INL_B) to differentiate the lower part of the INL where the somata of amacrine cells are located (Remington, 2012). The IPL was subdivided into the sublamina a (IPL_A) and the sublamina b (IPL_B) to differentiate the OFF

and ON synaptic layers, respectively. The fluorescence for each area was measured as the average pixel value and then normalized as fluorescence change using the formula:

$$Fn_x = \frac{\Delta F}{F_0} = \frac{(F_x - F_0)}{F_0}$$

Where Fn is the normalized value, F_x is the raw fluorescence value and F_0 is the initial fluorescence (at time = 0).

Statistical analysis

Statistical analysis was performed using either the software Stata/SE 17.0 or jamovi 2.2.5. Data was first tested using the Shapiro-Wilk test to determine whether it conformed to a normal distribution. For parametric tests, comparison of means between two groups was performed using two-tailed paired samples t test and for more than two groups, either repeated samples ANOVA or one-way ANOVA were used. For repeated measures ANOVA tests, the sphericity assumption was assessed using Mauchly's sphericity test, and either the Greenhouse-Geisser or Huynh-Feldt corrections were used depending on the value of the ε estimation (the former in case of ε < .75, or else the latter). For post-hoc tests, in order to correct for multiple comparisons, in the case the sphericity assumption was met, Tukey correction was used, or else Bonferroni correction was used. For one-way ANOVA tests, the homogeneity of variances was assessed using Levene's test, in the case of violation of homogeneity, Welch's correction was used. For post-hoc tests, in order to correct for multiple comparisons, in the case the homogeneity assumption was met, Games-Howell correction was used, or else Tukey correction was used.

For non-parametric tests, comparison of means between two groups was performed using the Wilcoxon signed rank test and for more than two groups the Friedman test was used, followed with post-hoc tests using the Durbin-Conover method with Bonferroni correction for multiple comparisons.

To analyze the distribution of single events, the data from multiple recordings was pooled and the empirical cumulative distribution step function (ECDF) was calculated using the statsmodels v0.13.2 package for Python 3.8.8. For the construction of histograms, the number of bins to use was calculated from the pooled data using the maximum between the Sturge's rule and Freedman Diaconis estimators, the data was normalized to show the density for each bin. The histograms were overlaid with the kernel density estimate (KDE), which was calculated using the Epanechnikov kernel and the bandwidth was estimated with Scott’s rule, using the statsmodels v0.13.2 package for Python 3.8.8.

Principal component analysis was performed using the scikit-learn 1.1.1 package for Python 3.8.8, the data was first standardized using z score, with the following formula:

$$z = \frac{x - \mu}{\sigma}$$

Where x is the data point, μ is the mean and σ is the standard deviation of the sample. After performing the principal component analysis, the resulting principal components are sorted by the explained variance, and the raw variables and principal components are compared against the fold change in IPSC frequency using linear regression, the goodness-of-fit was calculated using the R^2 indicator.

All graphs were constructed using custom scripts for each type written in Python 3.8.8 and using the Matplotlib 3.5.0 library.

For all tests, the significance level was set a p = 0.05. Outliers were defined by a z score greater than 2.5. Unless otherwise specified, data are presented as mean ± s.e.m, and sample size values as number of cells recorded.

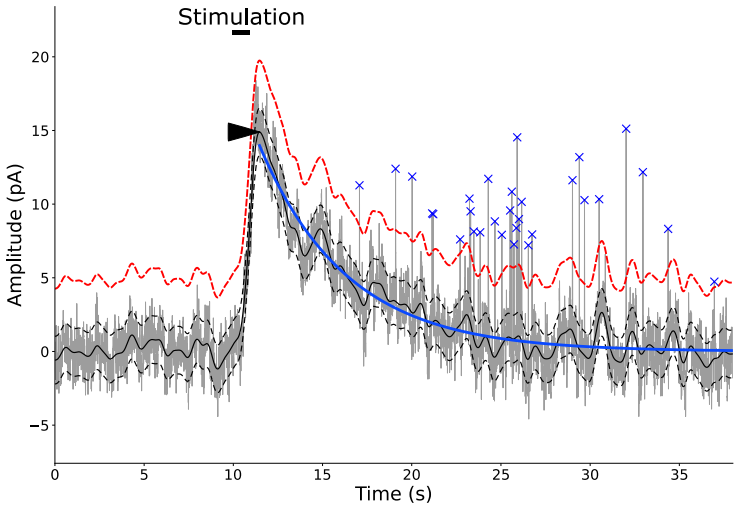

Figure 5. Representative trace of the analysis script output. Example trace showing the parameters returned by the analysis script. The filtered trace is shown in gray, the superimposed full black line shows the average of the trace and the segmented black lines the limits of the detected noise. The segmented red line above the trace shows the threshold amplitude for transient event detection, transient events are marked by the blue x symbols. For the sustained response, the start of the stimulus is marked above, and the peak amplitude is denoted by the black arrowhead. The decay part of the event is fitted with an exponential decay function and the result of the fitting is shown as a blue line.

RESULTS

Evoked inhibitory post-synaptic currents recorded in RBCs display two components

To study the inhibitory activity acting upon RBCs and further study the effects of the application of glucagon on their characteristics, two types of stimulation were used to elicit IPSCs. The first one was the application of a 1 s puff glutamate 500 µM in the OPL. This stimulation has been previously shown to evoke IPSCs in RBCs (Vielma et al., 2020).

When this stimulation was used, RBCs exhibited two types of responses, a sustained response characterized by a positive deflection of the baseline, which was observed in all the recorded cases (21/21 cells) and multiple concurrent transitory responses with faster kinetics, which were less common, appearing in 42.9% of the recordings (9/21 cells) (Fig. 6A). The first component will onwards be referred to as the sustained component and the second as the transient component.

A second method was the use of a high-potassium and high-calcium modification of the extracellular solution (HK-ECS). This method has been previously used to trigger glycinergic IPSCs (Ivanova et al., 2006) and was selected as it displayed a higher success rate in eliciting the transient component of the response (13/13 cells). HK-ECS was applied for a period of 30 s using a puffer pipette situated in the OPL. The sustained component was not observed using this type of stimulation (Fig. 6B).

In both cases, the cell was held at a membrane potential of 0 mV in whole-cell patch-clamp configuration in order to isolate IPSCs.

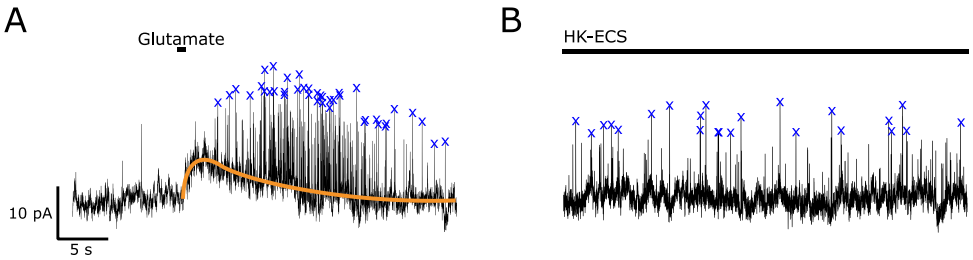

Figure 6. Representative traces of RBC IPSCs observed under glutamate and HK-ECS stimulation. (A) IPSCs observed after a 1 s puff administration of glutamate 500 µM in the OPL. A sustained response (orange line) can be observed, together with multiple transient events (blue x). (**B)** IPSCs observed after continuous puff administration high-potassium and high-calcium modification of the extracellular solution (HK-ECS) for a period of 30 s in the OPL. Multiple transient events can be observed (blue x), but not the sustained component. In both cases, only high amplitude transient events are marked for clarity.

The transitory component of RBC IPSCs corresponds to a glycinergic input, and its frequency is regulated by $GABA_A$ receptor activity

To characterize the nature of the observed IPSCs, selective blockers for GABA receptors ($GABA_A$ and $GABA_{A\text{-}\rho}$) and glycine receptors were used to isolate different sources of inhibitory activity known to act upon RBCs (Eggers & Lukasiewicz, 2006, 2011).

This pharmacologic approach was first used to study the two components observed using glutamate stimulation, via bath application of the different blockers for a period of 15 minutes.

In the case of GABA receptors, selective antagonism of $GABA_A$ receptors by bath application of SR-95531 10 µM produced an increase in the frequency of the transient activity (***control*** 2.34±0.84 Hz; ***SR-95531*** 3.21±0.98 Hz; paired t test, t(4) = -3.36, **p = 0.03**, n = 5) (Fig. 7B), with no change in the average amplitude (***control*** 15.1±3.52 pA; ***SR-95531*** 12.1±1.98 pA; paired t test, t(4) = 1.09, **p = 0.34**, n = 5) (Fig. 7C). No significant changes were observed in the characteristics of the sustained response (Fig. 7D-G).

These results suggest a modulator role of GABA over the transient activity, decreasing its frequency via $GABA_A$ receptor activity.

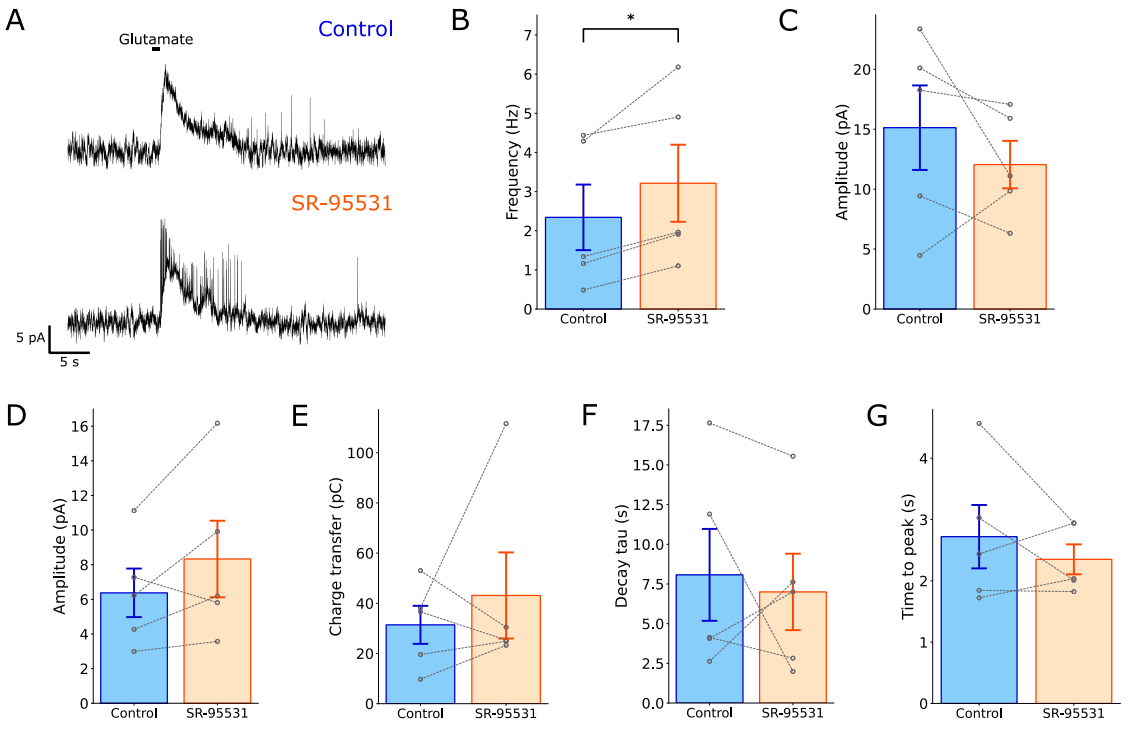

Figure 7. Bath application of SR-95531 10 µM increases the frequency of transient IPSCs. (A) Representative traces of RBC IPSCs after the application of a 1 s puff of glutamate 500 µM in the OPL in control conditions (top, blue) and after 15 min bath application of SR-95531 10 µM to block $GABA_A$ receptors (bottom, orange). **(B-C)** SR-95531 produced an increase in the frequency of the transient IPSCs **(B)**, with no change in amplitude **(C)**. **(D-G)** No changes in the amplitude **(D)**, charge transfer **(E)**, decay tau **(F)** or time to peak **(G)** of the sustained component were observed. *p < .05.

On the other hand, selective antagonism of $GABA_{A\text{-}\rho}$ receptors by bath application of TPMPA 50 µM did not produce statistically significant changes in the characteristics of either the transient (Fig. 8B-C) or the sustained components of the response (Fig. 8D-G).

This result argues against either a regulatory or causative role of $GABA_{A\text{-}\rho}$ receptor signaling in the observed inhibitory responses.

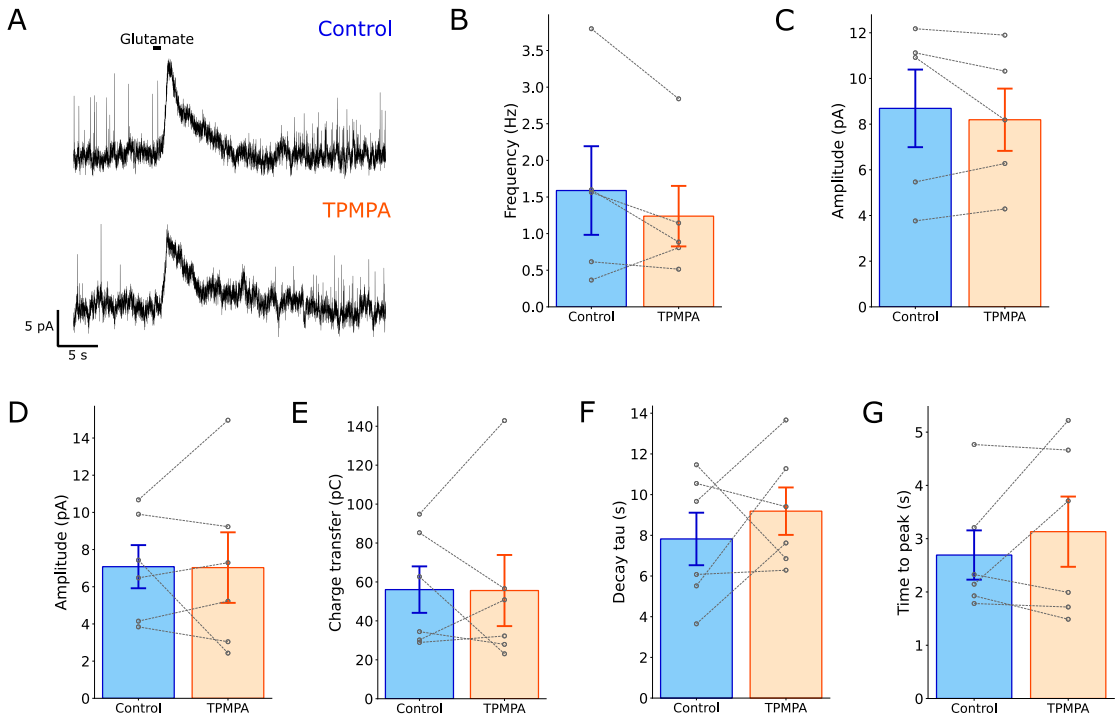

Figure 8. Bath application of TPMPA 50 µM did not induce changes on RBC IPSCs. (A) Representative traces of RBC IPSCs after the application of a 1 s puff of glutamate 500 µM in the OPL in control conditions (top, blue) and after 15 min bath application of TPMPA 50 µM to block $GABA_{A\text{-}\rho}$ receptors (bottom, orange). **(B-C)** TPMPA produced no changes in the frequency **(B)** or the amplitude **(C)** of the transient component. **(D-G)** No changes in the amplitude **(D)**, charge transfer **(E)**, decay tau **(F)** or time to peak **(G)** of the sustained component were observed either.

Finally, selective blocking of glycine receptors by bath application of strychnine 5 µM produced the abolition of the transient component (***control*** 1.83±1.05 Hz; ***strychnine*** 0±0 Hz; Wilcoxon signed-rank test, z = 2.2, **p = 0.03**, n = 6) (Fig. 9B-C), with no significant changes in the characteristics of the sustained response (Fig. 9D-G).

These results indicate the transient component of the observed response corresponds to glycinergic activity.

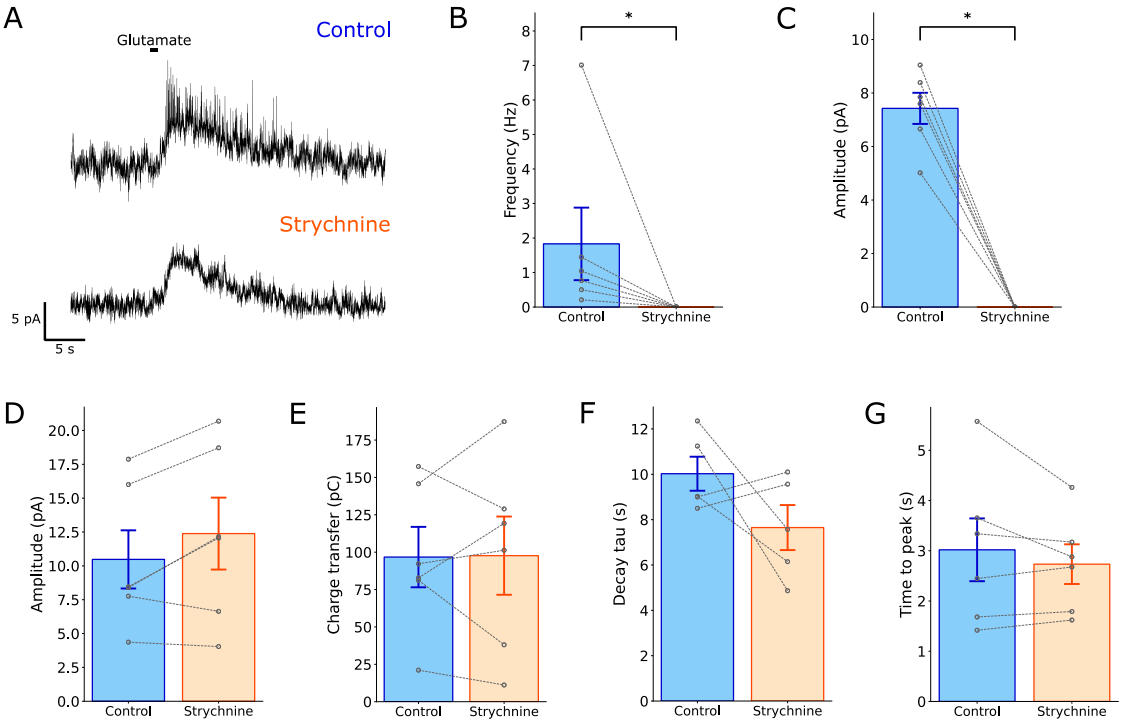

Figure 9. Bath application of strychnine 5 µM abolished the transient component of RBC IPSCs. (A) Representative traces of RBC IPSCs after the application of a 1 s puff of glutamate 500 µM in the OPL in control conditions (top, blue) and after 15 min bath application of strychnine 5 µM to block glycine receptors (bottom, orange). **(B-C)** Under these conditions, the transient component was abolished. **(D-G)** No changes in the amplitude **(D)**, charge transfer **(E)**, decay tau **(F)** or time to peak **(G)** of the sustained component were observed. *p < .05.

To further study the transient glycinergic activity, and because selective pharmacologic blocking showed that the source of the observed sustained component in response to glutamate application was not related to inhibitory activity, the HK-ECS stimulation method was used.

Bath application of strychnine 5 µM produced the abolition of the transient activity, with a decrease in both frequency (***control*** 1.79±0.35 Hz; ***strychnine*** 0.08±0.04 Hz; Wilcoxon signed-rank test, z = 3.37, **p = 0.0008**, n = 8) (Fig. 10B) and amplitude (***control*** 9.96±1.06 pA; ***strychnine*** 2.38±0.83 pA; paired t test, t(7) = 4.97, **p = 0.002**, n = 8) (Fig. 10C). This result confirms the glycinergic origin of the observed transient activity.

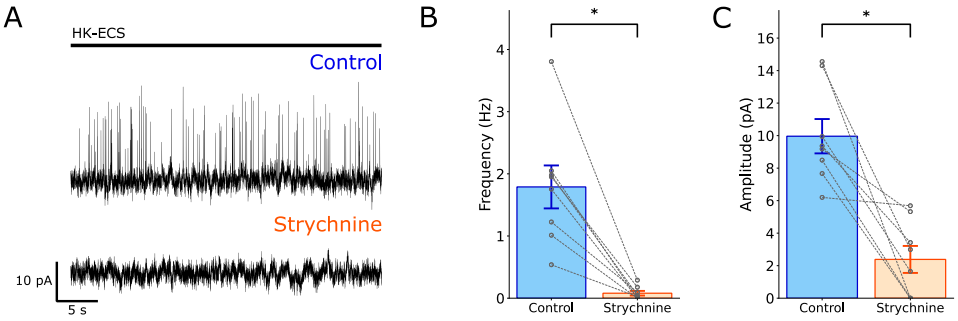

Figure 10. Strychnine abolishes RBC transient IPSCs under HK-ECS stimulation. (A) Representative traces of RBC IPSCs under control conditions (top, blue) and after 15 min of bath application of strychnine 5 µM (bottom, orange). **(B-C)** Application of strychnine produced an abolition of the glycinergic IPSCs, with a decrease both in frequency **(B)** and amplitude **(C)**. * p < .05.

As was observed with glutamate stimulation, selective antagonism of $GABA_A$ receptors by bath application of SR-95531 10 µM produced an increase in the frequency of transient activity (***control*** 1.17±0.28 Hz; ***gabazine*** 2.7±0.65 Hz; paired t test, t(5) = -2.96, **p = 0.03**, n = 6) (Fig. 11B), with no change in the average amplitude (***control*** 16.9±3.71 pA; ***gabazine*** 11±1.3 pA; paired t test, t(5) = 2.02, **p = 0.1**, n = 6) (Fig. 11C).

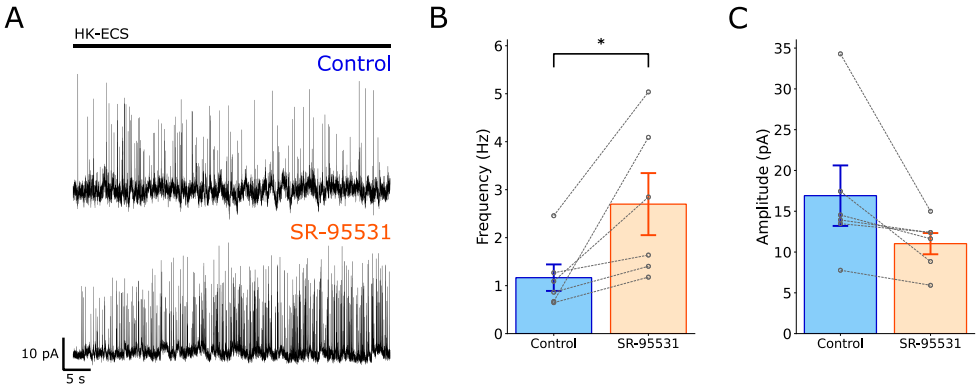

Figure 11. Bath application of SR-95531 10 µM increases the frequency of transient IPSCs under HK-ECS stimulation. (A) Representative traces of RBC IPSCs in control conditions (top, blue) and after 15 min bath application of SR-95531 10 µM (bottom, orange). **(B-C)** SR-95531 produced an increase in the frequency of the transient IPSCs **(B)**, with no change in amplitude **(C)**. *p < .05.

Finally, to study the stability of the recordings during the test periods, a 1 min recording using the HK-ECS stimulation protocol was repeated every 5 min for a period of 20 min, corresponding to the maximum recording time used during this study. When the characteristics of the transient component were analyzed as the change ratio compared to the initial recording at time = 0, no significant changes on frequency (Friedman test, $\chi^2(4) = 4.48$, **p = 0.35**, n = 7) (Fig. 12A) or amplitude (repeated measures ANOVA, F(4,24) = 0.06, **p = 0.99**, n = 7) were observed (Fig. 12B).

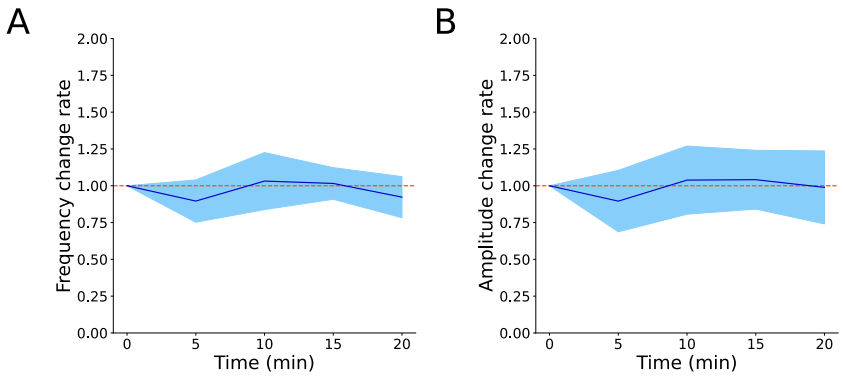

Figure 12. Recording characteristics were stable over the duration of the HK-ECS protocols. Repeated recordings of 1 min of RBC inhibitory activity using the HK-ECS protocol were performed every 5 min for a total period of 20 min to study recording stability. **(A-B)** Frequency **(A)** and amplitude **(B)** of transient IPSCs was measured and is reported as the change rate compared to the value at time = 0 min. No significant changes were observed on either parameter over the course of the recordings. Data are presented as mean ± s.d.

Glycinergic IPSCs arise in the axon terminal and their origin is local circuitry

To further characterize the IPSCs observed using HK-ECS stimulation, as this will be the main stimulation protocol used further in this study, first the effect of changing the distance of the puffer pipette to the soma was studied. To this end, the HK-ECS stimulation protocol was repeated at distances from the soma of the recorded cell of 20 µm, the base distance used throughout the study, 75 µm and 150 µm, the halfway and maximum distance available for the microscope and camera used, respectively.

Increasing the distance of the puffer pipette from the cell resulted in a marked decrease in the frequency of glycinergic IPSCs at larger distances (**[A]*20 µm*** 0.89±0.19 Hz, **[B]*75 µm*** 0.28±0.11 Hz, **[C]*150 µm*** 0.07±0.03 Hz; One way ANOVA, F(2,12) = 11, **p = 0.002**, n = 5; Tukey test, A-B, p = 0.01, A-C, p = 0.002, B-C, p = 0.52) (Fig. 13).

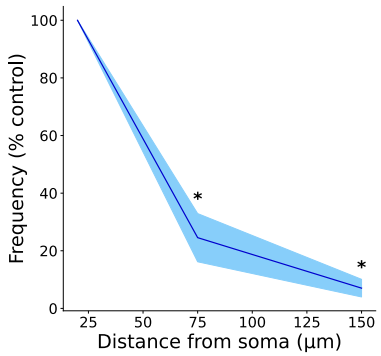

Figure 13. Glycinergic IPSCs recorded on RBCs using HK-ECS stimulation decrease in frequency as the distance from the soma of the stimulation is increased. A sustained 1 min puff of HK-ECS was applied at distances of 20, 75 and 150 µm from the recorded cell, showing a decrease in frequency as the distance is increased. The frequency is expressed as a percentage of the response obtained at a distance of 20 µm. *p < .05.

Additionally, to study the origin of the glycinergic IPSCs observed using HK-ECS, and to rule out a possible origin in the OPL, recordings were performed in axotomized RBCs.

Using the characteristics of the voltage-evoked currents (VEC), it was possible to recognize axotomized cells as RBCs (Fig. 14A), based on the overall kinetics of the currents and the current-voltage (IV) curve, a recognition method previously reported for retinal bipolar cells (Vielma & Schmachtenberg, 2016).

The protocol to obtain these curves consisted in increasing 10 mV voltage steps from -100 mV to 50 mV, with an inter-pulse holding potential of -60 mV. Under these conditions, RBCs displayed a characteristic pattern of VECs (Fig. 14C) and IV curve (Fig. 14B), showing in the first case the current elicited by the feedback response from A17 cells (Fig. 14C) (Elgueta et al., 2018). In the case of axotomized cells, the VECs (Fig. 14D) and IV curve (Fig. 14B) had the same

characteristics (IV curves; ANOVA, F(15) = 1.7, **p = 0.06**, n = 6), but lacked the feedback current from A17 cells (Fig. 14D), as is expected since this synapse occurs in the IPL (Menger & Wässle, 2000).

Unlike the case of the intact RBCs, it was not possible to elicit IPSCs using the HK-ECS stimulation protocol in axotomized RBCs (n=5).

These results support the origin of the observed glycinergic IPSCs as local responses being elicited in the axon terminals of the recorded RBCs and arising from local circuitry.

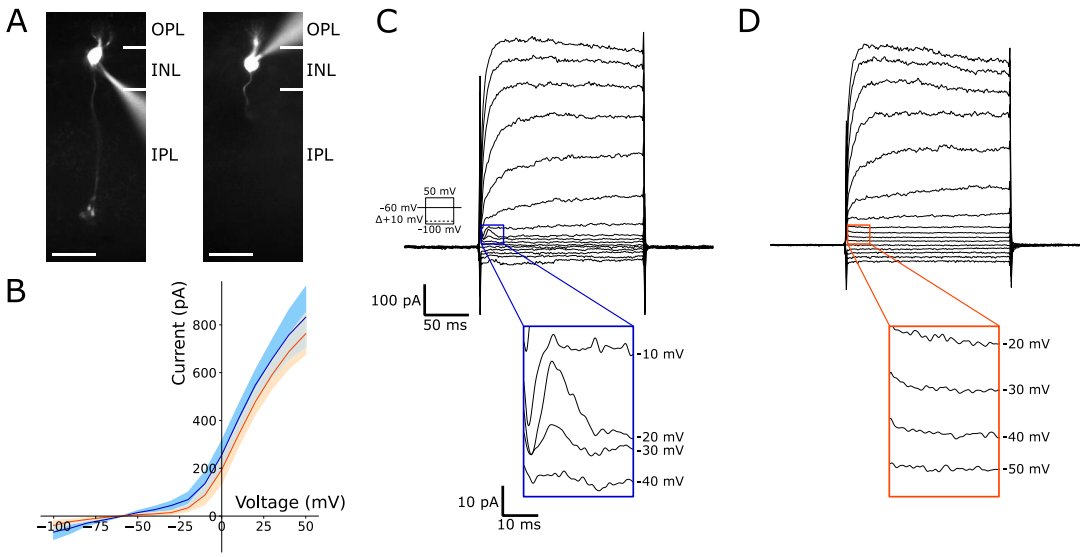

Figure 14. Current-voltage responses of intact and axotomized RBCs. (A) Representative images of lucifer yellow-filled intact (left) and axotomized (right) RBCs. Scale bar = 20 µm, magnification = 40x. **(B)** Current-voltage curves were constructed using currents evoked by multiple 10 mV steps from -100 to 50 mV in intact (blue) and axotomized (orange) RBCs. **(C-D)** The current response families obtained from intact **(C)** and axotomized cells **(D)** for the construction of the I-V curve. The first 25 ms after the pulse are shown as insets to display the feedback inhibitory current from A17 amacrine cells, seen as a positive deflection at -30 and -20 mV in intact cells **(C-inset)** but not in axotomized cells **(D-inset)**.

Glucagon increases the frequency of glycinergic IPSCs in RBCs

To study the effect of glucagon on RBC inhibitory activity, the previous experimental protocols were repeated in the presence of bath application of glucagon.

In the case of glutamate stimulation, bath application of glucagon 1 µM for a period of 5 min produced an increase in the frequency of glycinergic IPSCs (***control*** 1.76±0.28 Hz; ***glucagon*** 2.84±0.63 Hz; paired t test, t(8) = -2.58, **p = 0.03**, n = 9) (Fig. 15B), without a significant change in the average amplitude (***control*** 10.42±1.27 pA; ***glucagon*** 9.98±0.87 pA; paired t test, t(8) = 0.48, **p = 0.65**, n = 9) (Fig. 15D).

When the characteristics of individual events were studied, a modest increase in the average decay time was observed (***control*** 6.28±0.2 ms; ***glucagon*** 6.86±0.15 ms; paired t test, t(8) = -3.43, **p = 0.009**, n = 9) (Fig. 15G), with no changes in the overall distribution of event decay times (Fig. 15H-I). In the case of the amplitude distribution of single events, a shift to higher amplitudes can be observed in the presence of glucagon (Fig. 15E-F), but with no clear multimodality.

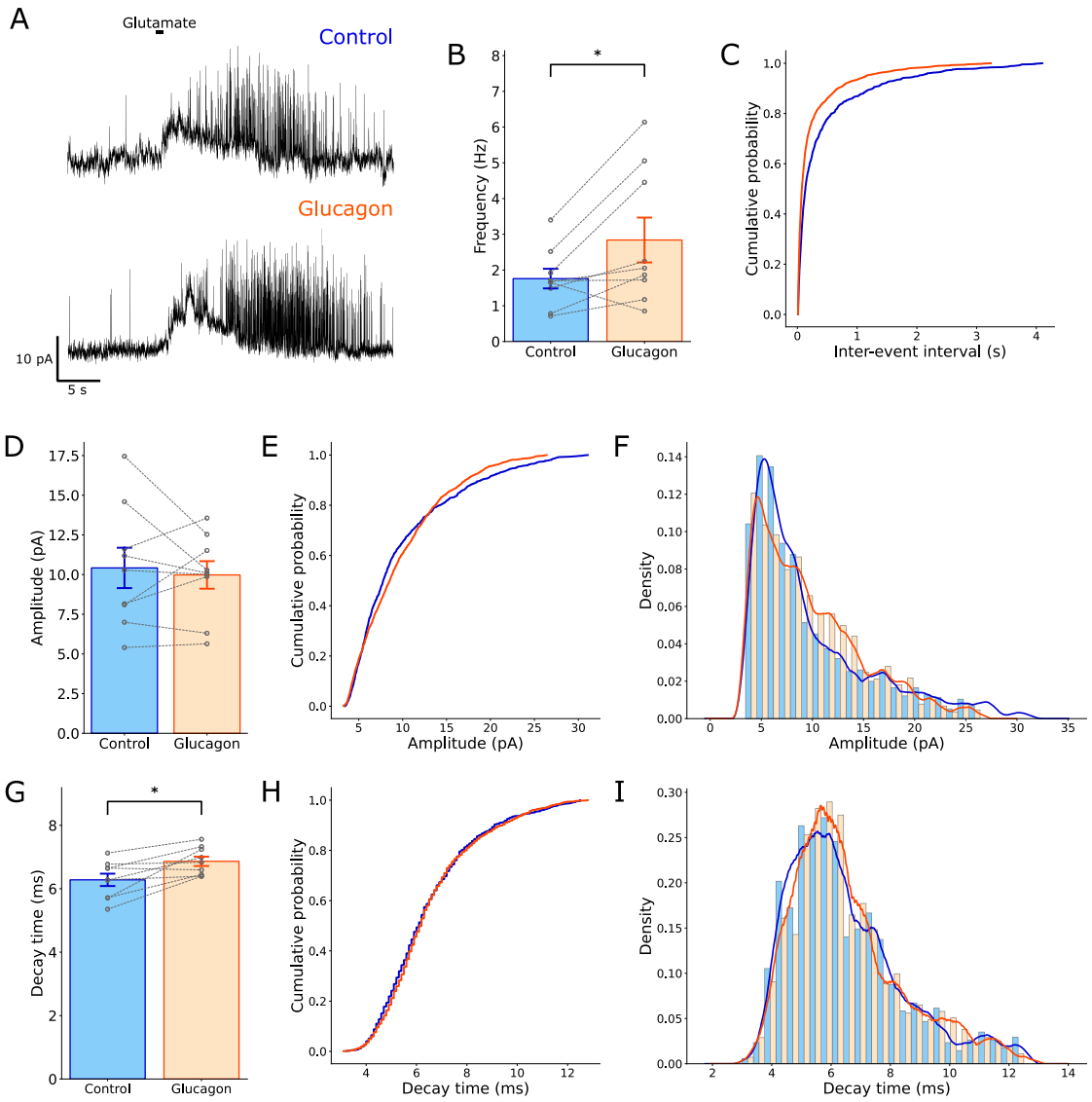

Figure 15. Bath application of glucagon induces an increase in RBC glycinergic IPSC frequency under glutamate stimulation. (A) Representative traces of RBC IPSCs under control conditions (top, blue) and after 5 min of bath application of glucagon 1 µM (bottom, orange). **(B-C)** A decrease was observed in the frequency of glycinergic IPSCs **(B)** with a corresponding shift to the left of the ECDF of the inter-event intervals **(C)**. **(D-F)** No change was observed in the average amplitude **(D)** but a shift to the right was observed around 10-15 pA in the distribution of event amplitudes as shown in the ECDF **(E)** and the histogram with KDE overlay **(F)**. **(G-I)** An increase in average decay time was observed **(G)**, with no overall displacement of the ECDF **(H)** or histogram with KDE overlay **(I)**. * $p < .05$.

There was also a decrease in the decay tau of the sustained response (***control*** 4.48±0.53 s; ***glucagon*** 3.38±0.43 s; Wilcoxon signed-rank test, z = 2.59, **p = 0.008**, n = 18) (Fig. 16C), with no other significant changes in the studied parameters (Fig. 16).

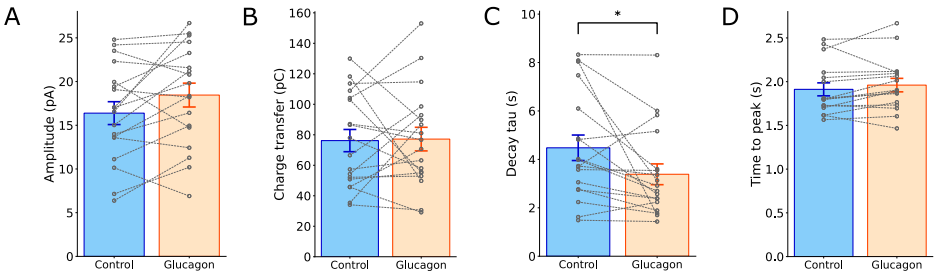

Figure 16. A decrease in the decay tau of the sustained response was observed after bath application of glucagon under glutamate stimulation. (A-D) A decrease in the decay tau of the sustained component of the RBC glutamate response was observed **(C)**, with no changes in the amplitude **(A)**, charge transfer **(B)** or time to peak **(D)** of the sustained component after bath application of glucagon 1 µM.

In the case of HK-ECS stimulation, bath application of glucagon 1 µM produced the same effect seen under glutamate stimulation, increasing the frequency of the glycinergic IPSCs (***control*** 2.14±0.38 Hz; ***glucagon*** 3.05±0.62 Hz; paired t test, t(6) = -2.82, **p = 0.03**, n = 7) (Fig. 17B-C), with no significant changes in the average amplitude (***control*** 13.58±3 pA; ***glucagon*** 15.27±3.12 pA; Wilcoxon signed-rank test, z = -1.35, **p = 0.22**, n = 7) (Fig. 17D).

When individual events were studied, the empirical cumulative distribution function (ECDF) of the amplitude showed a shift to the right in the middle values (Fig. 17E-F), not associated with a change in the average amplitude. As with the case of glutamate stimulation, no multimodality was observed. These results are consistent with a change of the proportion of event amplitudes towards higher amplitude, specifically an increase of events between 15 – 20 pA.

No change was observed in the average decay time (***control*** 7.78±0.49 ms; ***glucagon*** 8.07±0.6 ms; paired t test, t(6) = -0.55, **p = 0.6**, n = 7) (Fig. 17G), or changes in the distribution of the individual values (Fig. 17H-I).

These results support a role of glucagon as a modulator of RBC inhibition, increasing the frequency of glycinergic inhibitory input.

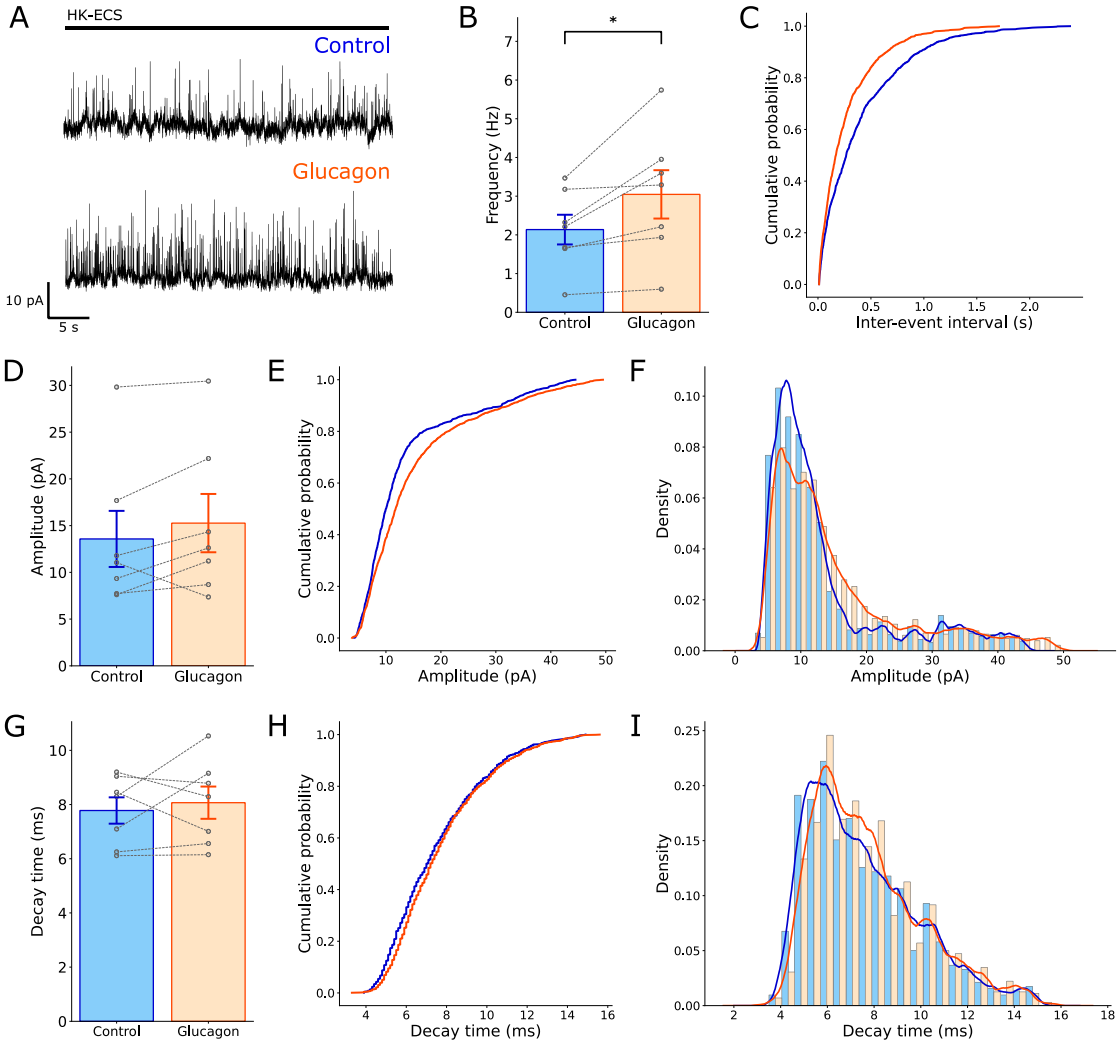

Figure 17. Bath application of glucagon induces an increase in RBC glycinergic IPSC frequency under HK-ECS stimulation. (A) Representative traces of RBC IPSCs under control conditions (top, blue) and after 5 min of bath application of glucagon 1 µM (bottom, orange). **(B-C)** An increase was observed in the frequency of glycinergic IPSCs **(B)** with a shift to the left of the ECDF of the inter-event intervals **(C)**. **(D-F)** No change was evident in the average amplitude **(D)** while the ECDF **(E)** and histogram with KDE overlay **(F)** show a shift to the right in the middle values (around 15-25 pA). **(G-I)** No change was seen in the average decay time **(G)** with no changes in distribution in the ECDF **(H)** and histogram with KDE overlay **(I)**. * $p < .05$.

Glucagon-induced increase in glycinergic IPSC frequency is dose-dependent

To further characterize the effect of glucagon on RBC glycinergic IPSCs, recordings using the HK-ECS protocol were repeated under increasing concentrations of bath application of glucagon, starting from 250 nM up to 2 µM. The ratios of IPSC frequency under control condition and bath application of glucagon were used to construct a dose-response curve.

There was an increase in the ratio of frequency change between the control condition and post bath application of glucagon, which correlated with the concentration of glucagon used, but no statistically significant difference was found (Fig. 18).

This result suggests a possible dose-dependent effect of glucagon on the frequency of glycinergic RBC IPSCs.

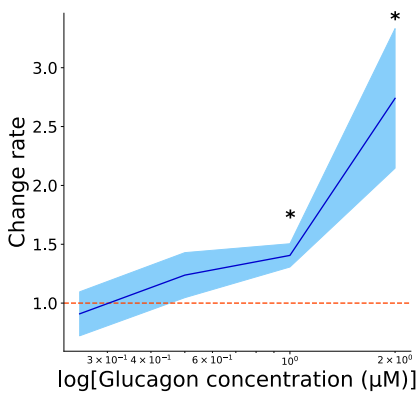

Figure 18. Glucagon-induced change in RBC glycinergic IPSC frequency is dose-dependent. The glucagon-induced change in RBC glycinergic IPSC frequency expressed as the rate between the control condition an after 5 min of bath application of glucagon at different concentrations showed a correlation with the concentration of glucagon used. n = 6.

The effect of glucagon is abolished with the application of the glucagon receptor antagonist L168,049

To study the dependency of the observed effect of glucagon over the frequency of glycinergic RBC IPSCs on glucagon receptor activity, L168,049, a selective non-peptidyl glucagon receptor antagonist was used. Bath application of glucagon 1 μM for 5 min was followed by co-application of glucagon 1 μM and L168,049 500 nM for 10 min.

In line with the previous experiments, bath application of glucagon 1 μM induced an increase in the frequency of glycinergic IPSCs, which was then abolished by the co-application of L168,048 500 nM, returning to a frequency not significantly different from the control (**[A]*control*** 0.95±0.24 Hz; **[B]*glucagon*** 1.41±0.33 Hz; **[C]*glucagon + L168,049*** 0.85±0.31 Hz; Friedman test, $\chi^2(2) = 12.3$, **p = 0.002**, n = 7; Durbin-Conover pairwise comparisons (Bonferroni correction), A-B, p = 0.001, A-C, p = 0.42, B-C, p = < 0.001) (Fig 19B). This change can also be seen in the inter-event interval distribution with a shift of the glucagon condition towards lower values (Fig 19C).

Application of glucagon 1 μM did not change the amplitude of the IPSCs, but the subsequent co-application of L168,049 500 nM produced a decrease in IPSC amplitude (**[A]*control*** 11.8±2.04 pA; **[B]*glucagon*** 10.6±1.97 pA; **[C]*glucagon + L168,049*** 6.35±0.76 pA; repeated measures ANOVA, F(2,12) = 10.2, **p = 0.003**, n = 7; Tukey test, A-B, p = 0.54, A-C, p = 0.02, B-C, p = 0.03) (Fig 19D), this can also be seen in the distribution of event amplitudes, with the co-application of glucagon and L168,049 shifting values towards lower amplitudes (Fig 19E-F).

When the individual events are studied, a shift can be observed to higher decay times when the control is compared to the L168,049 condition, with no other significant differences (**[A]*control*** 6.78±0.33 ms; **[B]*glucagon*** 7.19±0.25 ms; **[C]*glucagon + L168,049*** 8.01±0.31 ms; repeated measures ANOVA, F(2,12) = 6.56, **p = 0.01**, n = 7; Tukey test, A-B, p = 0.61, A-C, p = 0.007, B-C, p = 0.12) (Fig 19G). The decay time distributions show a gradual change towards higher decay times for each subsequent condition (Fig 19H-I).

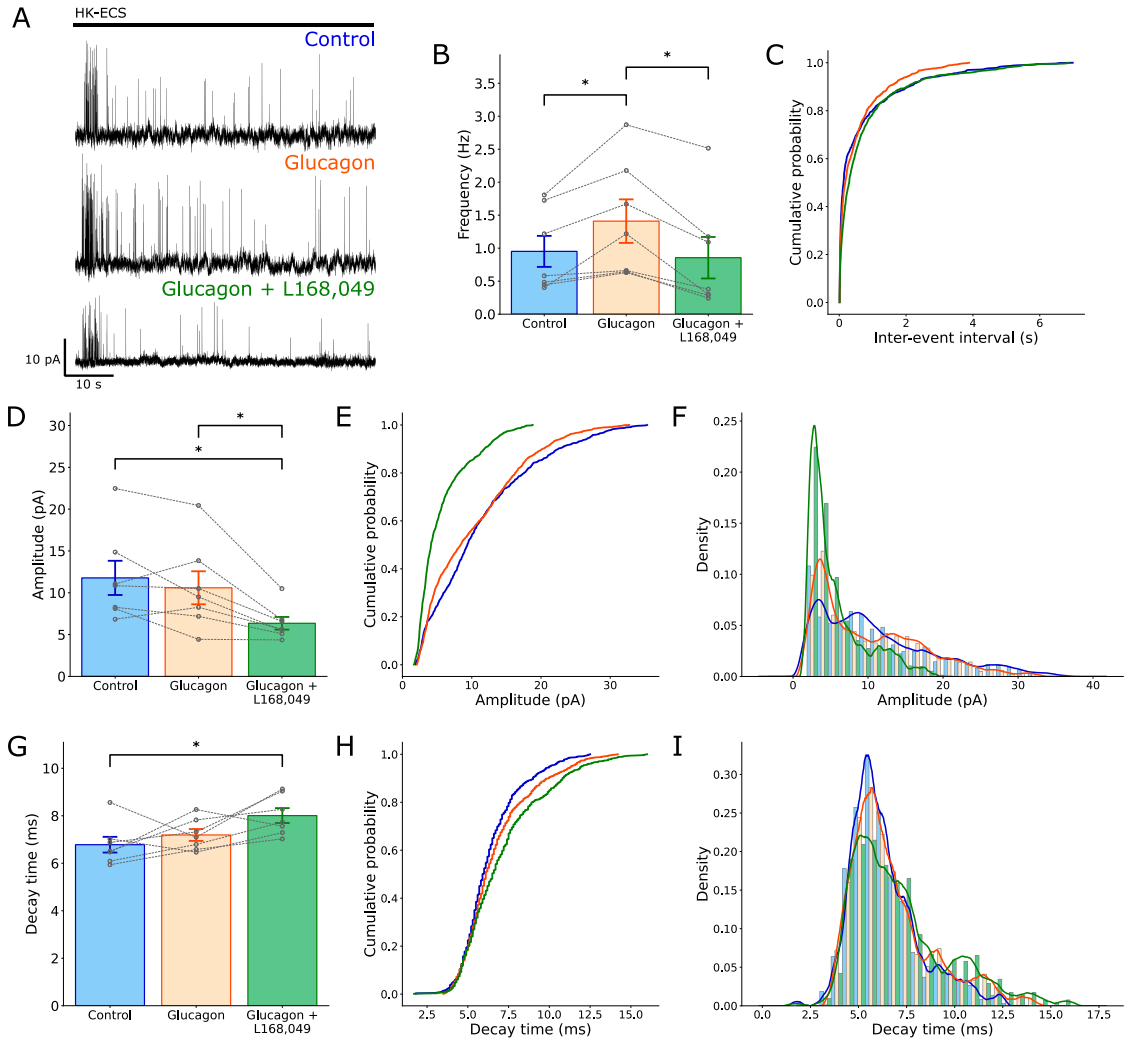

Figure 19. Bath application of L168,049 500 nM abolishes the effect of glucagon under HK-ECS stimulation. (A) Representative traces of RBC IPSCs under control conditions (top, blue), after 5 min of bath application of glucagon 1 µM (middle, orange) and after 10 min of bath application of glucagon 1 µM + L168,049 500 nM (bottom, green). **(B-C)** An increase was observed in the frequency of glycinergic IPSCs **(B)** with a shift to the left of the ECDF of the inter-event intervals **(C)** when glucagon was bath applied, this effect was abolished with the subsequent addition of L168,049. **(D-F)** A decrease was seen in the average amplitude **(D)** with a shift to the left of the ECDF **(E)** and a shift of the distribution to lower values in the histogram with KDE overlay **(F)** when L168,049 was applied. **(G-I)** An increase was observed in the average decay times of IPSCs when L168,049 was added compared to control **(G)**, with the ECDF **(H)** and histogram with KDE overlay **(I)** showing a shift to the right of the decay times. * $p < .05$.

These results show L168,049 blocks the activity of glucagon but also has an unrelated effect on IPSC amplitude.

The glucagon receptor antagonist L168,049 inhibits the effects of glucagon and increases IPSC frequency at high concentrations

To study the effects of L168,049 application by itself and in conjunction with glucagon, and further characterize the observed amplitude change, bath application of L168,049 at different concentrations for 15 min was followed by co-application of L168,049 and glucagon 1 μM for 5 min.

Bath application of L168,049 1 μM induced an increase in the frequency of glycinergic IPSCs (**[A]*control*** 1.81±0.76 Hz; **[B]*L168,049*** 2.67±1.03 Hz; **[C]*L168,049 + glucagon*** 2.86±0.9 Hz; Friedman test, $\chi^2(2) = 9$, **p = 0.01**, n = 6; Durbin-Conover pairwise comparisons (Bonferroni correction), A-B, p = 0.002, A-C, p = 0.002, B-C, p = 1) (Fig. 20B-C) with a decrease in the amplitude (**[A]*control*** 8.86±1.32 pA, **[B]*L168,049*** *6.33*±0.64 pA, **[C]*L168,049 + glucagon*** 5.84±0.77 pA; Friedman test, $\chi^2(2) = 10.3$, **p = 0.006**, n = 6; Durbin-Conover pairwise comparisons (Bonferroni correction), A-B p = 0.002, A-C p < .001, p = 0.05) (Fig. 20D), seen also in the distribution of the events, with a shift to the left of the amplitudes in both conditions (Fig. 20E-F).

When the individual events are studied, no significant change in average decay time was observed (***control*** 8.43±0.98 ms, ***L168,049*** 10.4±0.54 ms, ***L168,049 + glucagon*** 9.54±0.51 ms; repeated measures ANOVA (Greenhouse-Geisser correction), F(1.09,5.44) = 2.78, **p = 0.15**, n = 6) (Fig. 20G), but the overall distribution showed a shift to the right under both L168,049 and L168,049 + glucagon application (Fig. 20H), with a decrease in the proportion of low decay time events, and a shift towards high decay times (Fig. 20I).

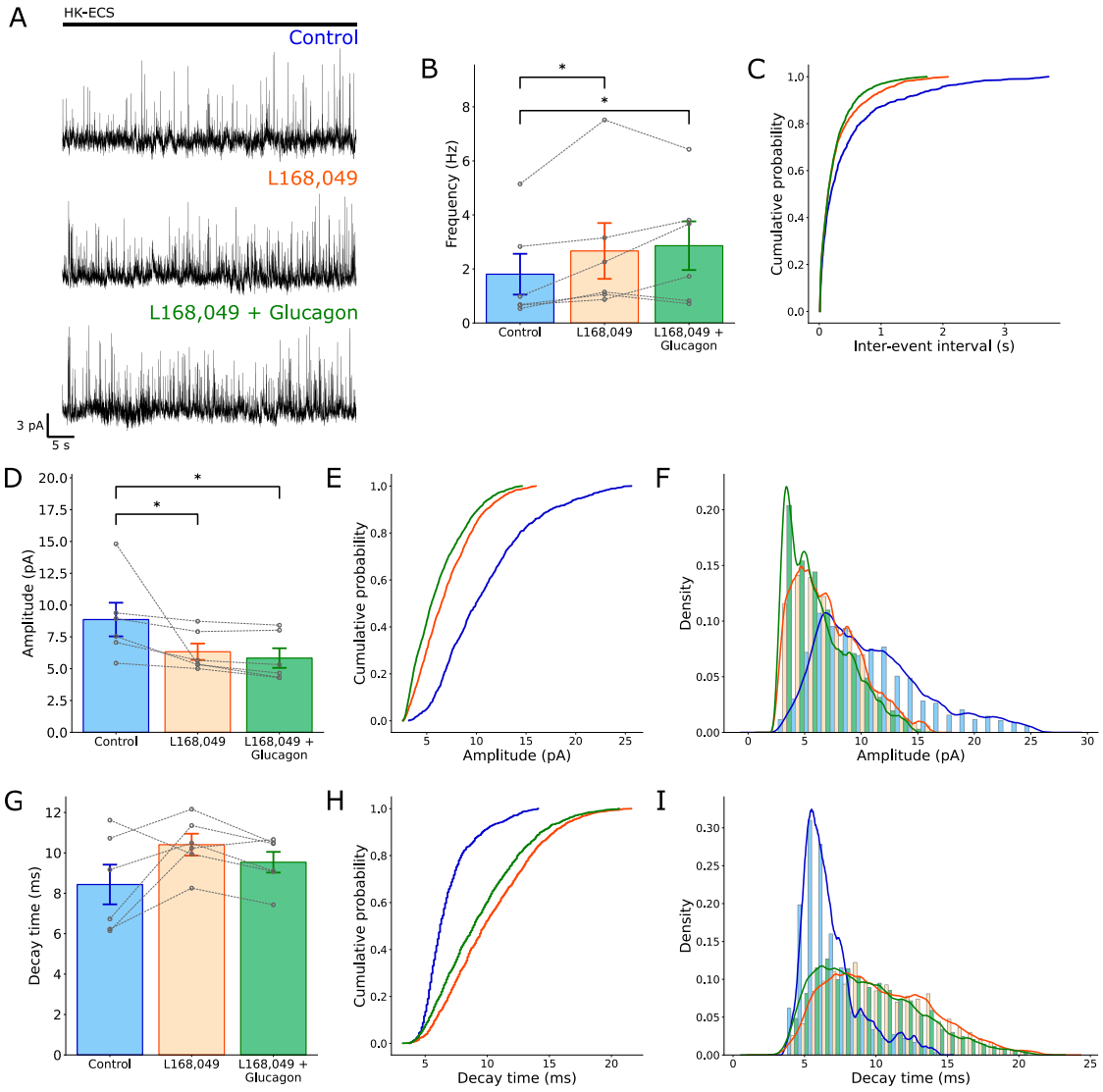

Figure 20. Bath application of L168,049 1 µM induces an increase in RBC glycinergic IPSC frequency and a shift to higher decay times and lower amplitudes under HK-ECS stimulation. (A) Representative traces of RBC IPSCs under control conditions (top, blue), after 15 min of bath application of L168,049 1 µM (middle, orange) and after 5 min of bath application of L168,049 1 µM + glucagon 1 µM (bottom, green). **(B-C)** An increase was observed in the frequency of glycinergic IPSCs **(B)** with a shift to the left of the ECDF of the inter-event intervals **(C)** when L168,049 was bath applied, while no change was observed with the subsequent addition of glucagon. **(D-F)** A decrease was seen in the average amplitude **(D)** with a shift to the left of the ECDF **(E)** and a shift of the distribution to lower values in the histogram with KDE overlay **(F)**. **(G-I)** No change was observed in the average decay times of IPSCs **(G)**, but the ECDF **(H)** and histogram with KDE overlay **(I)** show a shift to the right of the decay times, consistent with a shift to higher values. * $p < .05$.

When bath application of L168,049 at a concentration of 500 nM was used, no significant overall change was observed in the frequency of IPSCs (***control*** 2.34±0.67 Hz, ***L168,049*** 3.36±1.03 Hz, ***L168,049 + glucagon*** 3.59±0.73 Hz; repeated measures ANOVA, F(2,10) = 2.75, **p = 0.11**, n = 6) (Fig 21B), with no significant shift of the ECDFs of inter-event intervals (Fig 21C), but there was a decrease in the amplitude (**[A]*control*** 12.7±1.58 pA, **[B]*L168,049*** 6.41±0.7 pA, **[C]*L168,049 + glucagon*** 6.13±1.08 pA; repeated measures ANOVA, F(2,10) = 18.9, **p < .001**, n = 6; Tukey test, A-B, p = 0.02, A-C, p = 0.01, B-C, p = 0.89) (Fig 21D), with a shift to the left of the ECDF (Fig 21E) and a shift of the proportion of events towards lower amplitudes (Fig 21F).

When individual events are studied, as with the case of L168,049 1 µM concentration, no significant change was observed in average decay times (***control*** 8.2±0.64 ms, ***L168,049*** *9.97*±0.86 ms, ***L168,049 + glucagon*** 9.53±0.7 ms; Friedman test, $\chi^2(2) = 2.33$, **p = 0.31**, n = 6) (Fig 21G), but a shift to the right of the ECDF was observed (Fig 21H), with a decrease in the proportion of low decay time events and a shift towards higher decay times (Fig 21I).

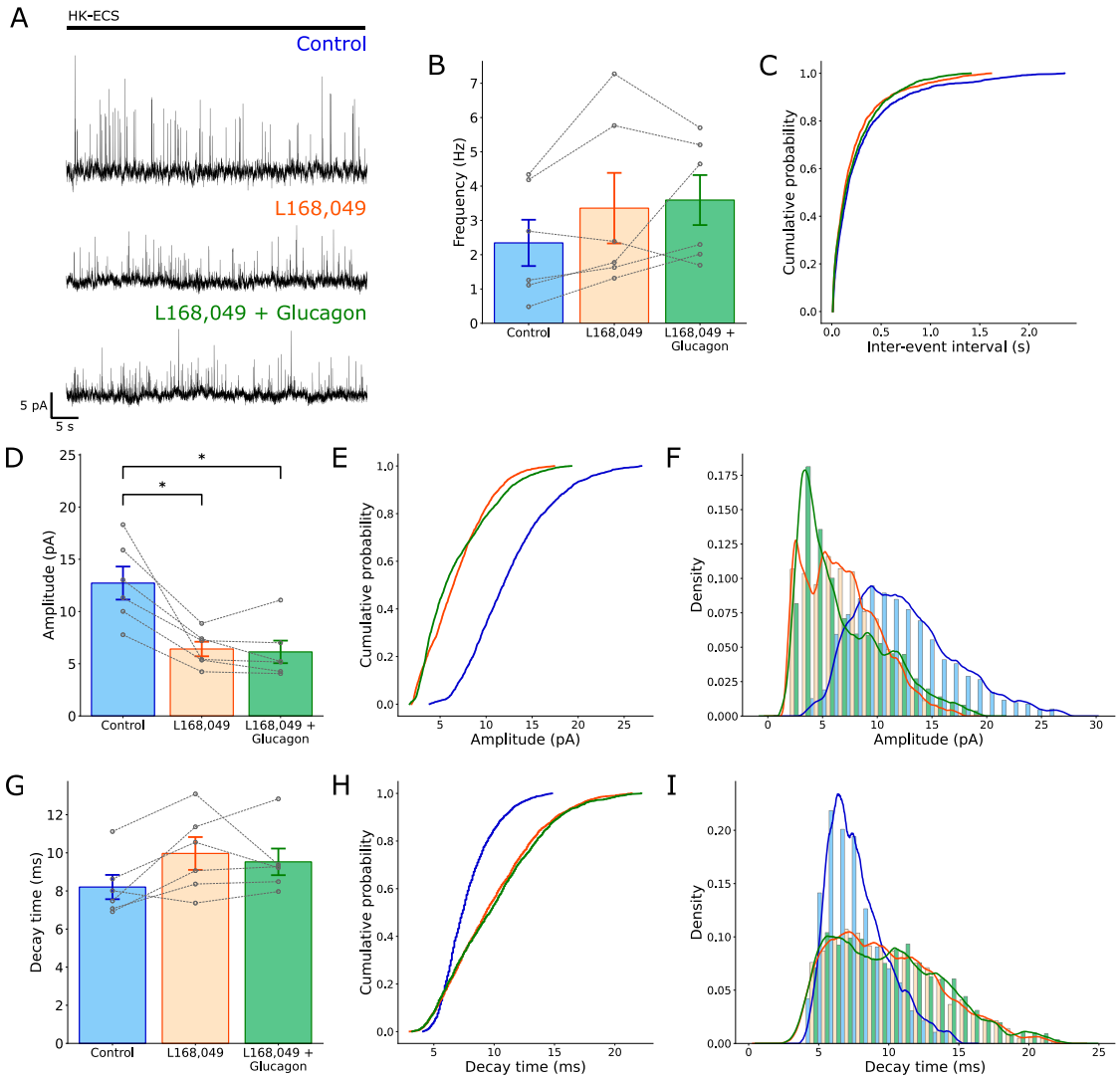

Figure 21. Bath application of L168,049 500 nM induces a decrease in RBC glycinergic IPSC amplitude and a shift to higher decay times under HK-ECS stimulation. (A) Representative traces of RBC IPSCs under control conditions (top, blue), after 15 min of bath application of L168,049 500 nM (middle, orange) and after 5 min of bath application of L168,049 500 nM + glucagon 1 µM (bottom, green). **(B-C)** No significant change was observed in the frequency of glycinergic IPSCs **(B)** with a clumping of the ECDFs of the inter-event intervals **(C)** when L168,049 is bath applied, no change is observed with the subsequent addition of glucagon. **(D-F)** A decrease was observed in the average amplitude **(D)** with a shift to the left of the ECDF **(E)** and a shift of the distribution to lower values in the histogram with KDE overlay **(F)**. **(G-I)** No change was observed in the average decay times of IPSCs **(G)**, but the ECDF **(H)** and histogram with KDE overlay **(I)** show a shift to the right of the decay times, consistent with a shift to higher values. * p < .05.

Further decreasing the bath concentration of L168,049 to 250 nM, produced no significant change in IPSC frequency (***control*** 2.04±0.36 Hz, ***L168,049*** 2.78±0.7 Hz, ***L168,049 + glucagon*** 2.36±0.45 Hz; repeated measures ANOVA, F(2,12) = 1.44, **p = 0.28**, n = 7) (Fig. 22B-C), or amplitude (***control*** 9.48±0.7 pA, ***L168,049*** 6.29±0.67 pA, ***L168,049 + glucagon*** 7.9±1.23 pA; repeated measures ANOVA, F(2,12) = 3.28, **p = 0.07**, n = 7) (Fig. 22D).

When single events were studied, even though the average amplitudes showed no change, a shift towards lower values can still be seen in the ECDF (Fig. 22E), but only under L168,049 application, as addition of glucagon shifts the curve back towards control values; the same can be seen in the histogram with KDE overlay (Fig. 22F). No change was observed in average decay tau at this concentration (***control*** 11.3±0.95 ms, ***L168,049*** 11.2±0.65 ms, ***L168,049 + glucagon*** 11.5±0.58 ms; repeated measures ANOVA, F(2,12) = 0.025, **p = 0.98**, n = 7) (Fig. 22G), with no marked shift in the distribution of individual decay times (Fig. 22H-I).

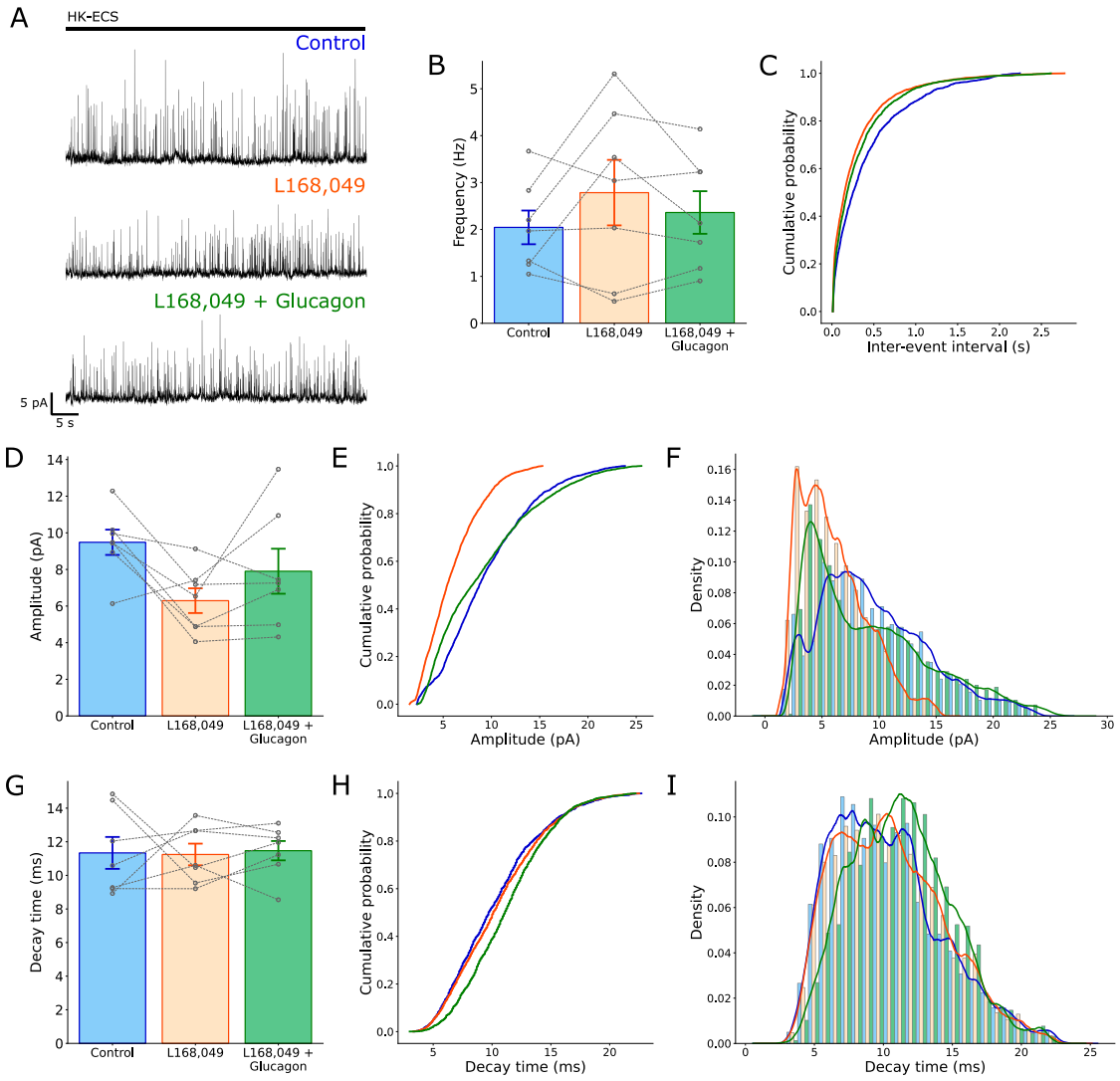

Figure 22. The changes observed at higher concentrations are abolished with application of L168,049 250 nM under HK-ECS stimulation. (A) Representative traces of RBC IPSCs under control conditions (top, blue), after 15 min of bath application of L168,049 250 nM (middle, orange) and after 5 min of bath application of L168,049 250 nM + glucagon 1 µM (bottom, green). **(B-C)** No significant change was observed in the frequency of glycinergic IPSCs **(B)** or the ECDFs of the inter-event intervals **(C)** when L168,049 was bath applied, no change is observed with the subsequent addition of glucagon. **(D-F)** No significant change was observed in the average amplitude of IPSCs **(D)**, but a shift to the right can still be seen in the ECDF **(E)** with a shift of the distribution to lower values in the histogram with KDE overlay **(F)**. **(G-I)** No significant change was observed in the average decay times of IPSCs **(G)**, or their distribution as seen in the ECDF **(H)** and histogram with KDE overlay **(I)**.

These results show an effect of L168,049 application alone, with an increase in the frequency of IPSCs associated with a shift towards events with lower amplitude and slower kinetics at a concentration of 1 µM. Lowering the concentration to 500 nM showed similar characteristics, but the average change in frequency was not significant. In both cases the glucagon-induced increase in IPSC frequency could not be observed. At lower concentrations, although the effect of glucagon on the frequency of IPSCs still cannot be seen, its addition was able to revert the change of the distribution of amplitudes, indicating a loss of the antagonistic functions at this concentration. In all, this suggests L168,049 antagonizes the effect of glucagon on the frequency of IPSCs, while also changing the characteristics of IPSCs at higher concentrations.

Glucagon-induced increase in RBC IPSC frequency is explained by an increase in glycinergic activity

To study the nature of the increase in IPSC frequency and clarify whether the extra activity corresponded to glycinergic activity, sequential application of strychnine 5 µM and strychnine 5 µM combined with glucagon 1 µM was used.

As was the case in the previous experiments, bath application of strychnine produced an abolition of the IPSCs, and subsequent addition of glucagon did not produce significant changes (**[A]*control*** 1.15±0.25 Hz, **[B]*strychnine*** 0.01±0.006 Hz, **[C]*glucagon + strychnine*** 0.03±0.02 Hz; repeated measures ANOVA (Greenhouse-Geisser correction), F(1,4.02) = 19.1, **p = 0.01**, n = 5; Bonferroni correction, A-B, p = 0.03, B-C, p = 0.04, C-D, p = 0.7) (Fig. 23B), the same can be seen in the amplitude of the IPSCs (**[A]*control*** 12.13±1.33 pA, **[B]*strychnine*** 1.82±0.9 pA, **[C]*glucagon + strychnine*** 1.91±0.92 pA; repeated measures ANOVA (Greenhouse-Geisser correction), F(1.06,4.22) = 47.1, **p = 0.002**, n = 5; Bonferroni correction, A-B, p = 0.002, B-C, p = 0.011, C-D, p = 1) (Fig. 23C).

These results support the glucagon-mediated increase in RBC IPSC frequency as being an increase in the frequency of glycinergic activity.

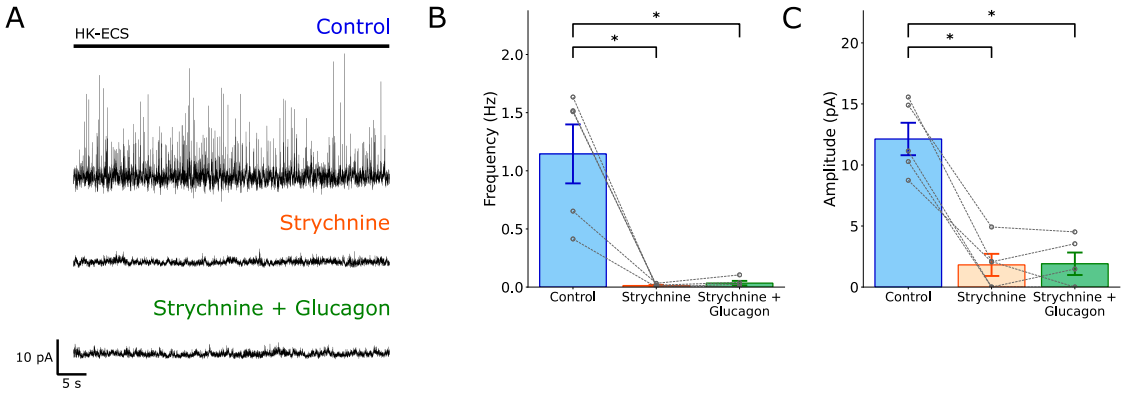

Figure 23. Glucagon-mediated increase in the frequency of IPSCs corresponds to an increase in glycinergic activity. (A) Representative traces of RBC IPSCs under control conditions (top, blue), after 15 min of bath application of strychnine 5 µM (middle, orange) and after 5 min of bath application of strychnine 5 µM + glucagon 1 µM (bottom, green). **(B-C)** Application of strychnine produced an abolition of the glycinergic IPSCs, with a decrease both in frequency **(B)** and amplitude **(C)**. * $p < .05$.

No correlation was found between the change in IPSC frequency induced by glucagon and the morphological characteristics of RBCs

As morphological subtypes of RBC have been described in the literature (Tsukamoto & Omi, 2017), and a variability was observed between the intensities of the responses of RBCs when exposed to glucagon, when expressed as the fold change in IPSC frequency, it was of interest to test whether a correlation existed between morphological characteristics of RBCs and the fold change in IPSC frequency after glucagon application.

The morphological measurements used were the dimensions of the dendritic arbor (width and height), the dimensions of the soma (width and height), the length of the axon, the dimensions of the axon terminal (width and height) and the number of varicosities in the axon terminal (Fig. 24A). These measurements were taken from the pool of control cells used throughout the study.

First, the morphological measurements were contrasted to the fold change in IPSC frequency to see whether there was a correlation or whether clear grouping was observed suggesting

subpopulations. No correlations or groupings were found, with no correlation above with at least $R^2 = 0.7$ (Fig. 24D-F). The correlation coefficients for the comparisons are resumed in Table 1.

To further test associations between the measurements, a principal component analysis followed by principal component correlation was performed. The first 3 components were used as combined they explained 83% (Fig. 24B) of the variance of the original variables. The loadings of the principal components (i.e. the coefficients of the linear combination of the original variables from which the principal components are constructed) show that the first principal component (PC1) was positively correlated with most of the dimensional variables, and weakly inversely correlated with the number of varicosities in the axon terminal, the second principal component (PC2), was strongly inversely correlated with the axon terminal variables (number of varicosities, and terminal dimensions), and the third principal component (PC3) was mainly correlated with the height of the dendritic arbor (Fig. 24C).

When these principal components were plotted against the fold change of IPSC frequency of RBCs, no correlation or grouping was found either, as none of the correlations had an $R^2 \geq 0.7$ (Fig. 24G-I). The correlation coefficients for the comparisons are summarized in Table 1.

Table 1. R^2 correlation coefficients of RBC morphological measurements against the fold-change in IPSC frequency induced by glucagon application

	R^2
Arbor width	0.02
Arbor height	0.05
Soma width	0.04
Soma height	0.03
Axon length	0.007
Terminal width	0.11
Terminal height	0.24
Number of varicosities	0.004

	R^2
PC1	0.08
PC2	0.06
PC3	0.04
PC4	0.02
PC5	0.002
PC6	0.02
PC7	0.11
PC8	0.05

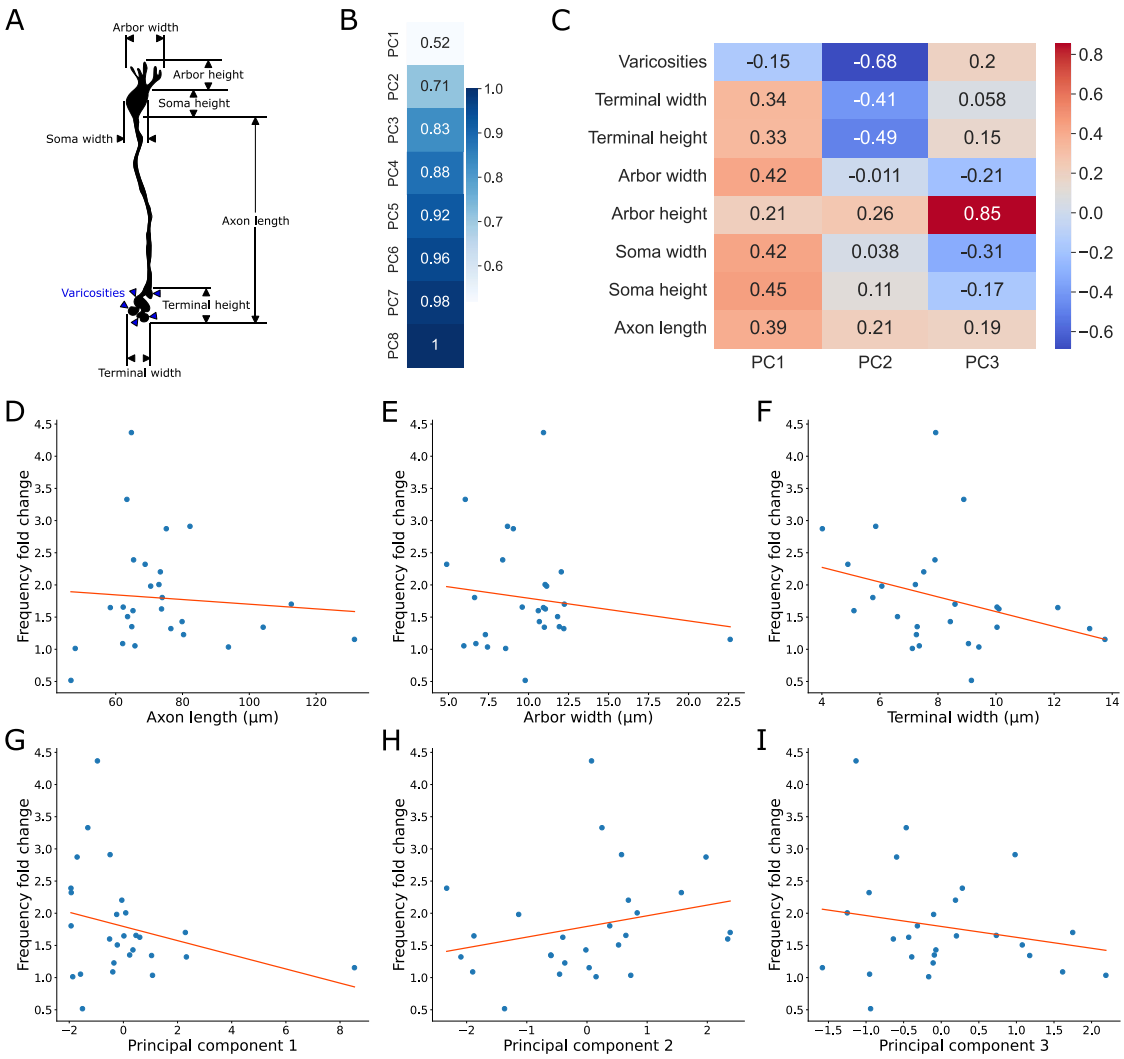

Figure 24. No correlation was found between the morphological characteristics of RBCs and the effect of glucagon on IPSC frequency. (A) Schematic representation of a RBC showing the measurements used in the following analysis. **(B)** Cumulative explained variance for each of the principal components obtained from the principal component analysis. **(C)** Loadings of the first three principal components, showing the relative strength of the contribution of each original variable. **(C-E)** No correlation or grouping was found between the change in frequency and the original variables, including the length of the axon **(C)**, the width of the dendritic arbor **(D)** or the width of the axon terminal **(E)**. **(F-G)** No correlation or grouping was found between the change in frequency and the principal components obtained, the first three of which, PC1 **(F)**, PC2 **(G)** and PC3 **(H)**, are displayed.

Antagonism of D1 receptors inhibits the observed glucagon-mediated increase in RBC IPSC frequency

To study a potential interaction of the observed glucagon-mediated increase in RBC glycinergic IPSC frequency and dopamine receptor activity, SCH 23390 10 µM, a selective dopamine D1 receptor antagonist, was first used to isolate the possible effects of D1 signaling, which have been shown to regulate the activity of inhibitory amacrine cells acting upon RBCs (Flood et al., 2018; Travis et al., 2018).

When glutamate stimulation was used, bath co-application of glucagon 1 µM and SCH 23390 10 µM produced a suppression of the glucagon-mediated increase in IPSC frequency (***control*** 2.97±1.36 Hz; ***glucagon + SCH*** 1.6±0.41 Hz; Wilcoxon signed-rank test, z = 1.15, **p = 0.31**, n = 6) (Fig. 25B), with a shift to higher values of inter-event intervals, suggesting an overall decrease in frequency (Fig. 25C). In the case of the amplitude, no significant change can be seen in the average amplitudes (***control*** 8.36±1.02 pA; ***glucagon + SCH*** 8.87±0.98 pA; Wilcoxon signed-rank test, z = -0.73, **p = 0.56**, n = 6) (Fig. 25D), but a second mode can be seen towards higher values (Fig. 25E-F).

When singular events were studied, there was no significant change in the average decay times (***control*** 7.33±0.69 ms; ***glucagon + SCH*** 8.24±1.17 ms; t test, t(5) = -0.76, **p = 0.48**, n = 6) (Fig. 25G), but a shift towards higher values can be seen in the ECDF (Fig. 25H) and the histogram with KDE overlay (Fig. 25I).

In the case of the sustained component, the glucagon-dependent decrease in decay tau was also abolished (***control*** 3.1±0.68 s; ***glucagon + SCH*** 2.74±0.58 s; Wilcoxon signed-rank test z = 0.84, **p = 0.46**, n = 8) (Fig. 26C), with no significant changes in the rest of the studied parameters (Fig. 26A-B,D).

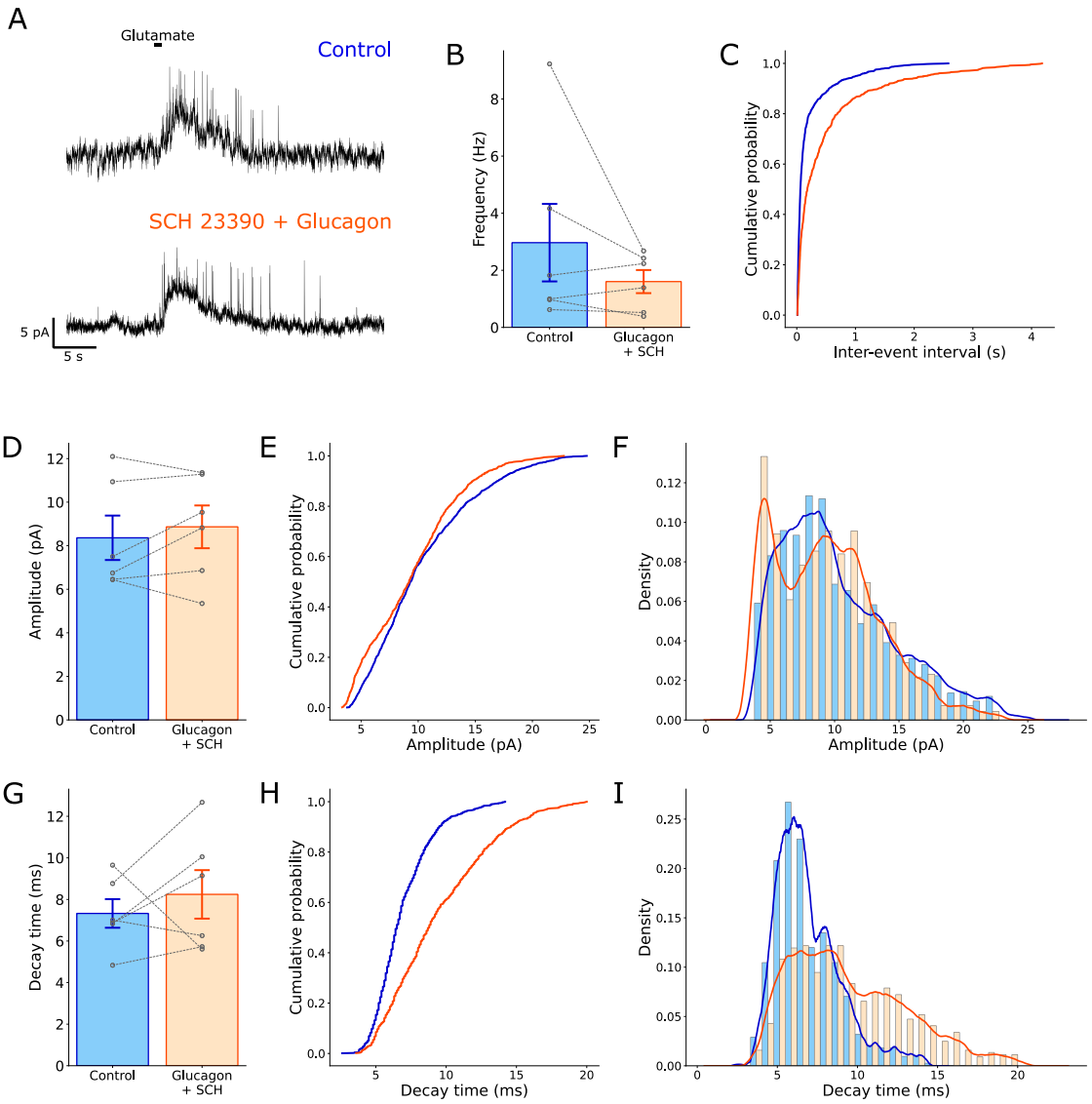

Figure 25. Co-application of SCH 23390 and glucagon abolished glucagon-mediated increase in RBC glycinergic IPSC frequency. (A) Representative traces of RBC IPSCs under control conditions (top, blue) and after 15 min of bath application of SCH 23390 10 + µM glucagon 1 µM (bottom, orange). **(B-C)** No change was observed in the average frequency of glycinergic IPSCs **(B)** with a shift to the right of the ECDF of the inter-event intervals **(C)**. **(D-F)** No change was observed in the average amplitude **(D)** while the ECDF **(E)** and histogram with KDE overlay **(F)** show bimodality. **(G-I)** No change was observed in the average decay time **(G)** with a shift in distribution to the right in the ECDF **(H)** and to higher values in the histogram with KDE overlay **(I)**. * $p < .05$.

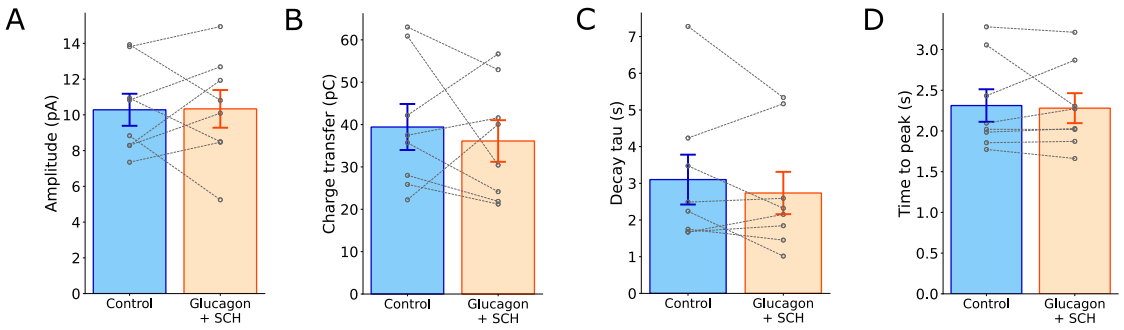

Figure 26. No changes in the sustained response were observed under co-application of SCH 23390 and glucagon under glutamate stimulation. (A-D) No changes in the amplitude **(A)**, charge transfer **(B)**, decay tau **(C)** or time to peak **(D)** of the sustained component were observed.

To isolate effects of SCH 23390 application, sequential bath application first of SCH 23390 10 µM alone followed by co-application of glucagon 1 µM and SCH 23390 10 µM was used. No significant changes were observed with application of SCH 23390 alone or with co-application of glucagon on the average frequency of IPSCs (**[A]control** 3.23±0.41 Hz, **[B]SCH** 3.51±1.06 Hz, **[C]SCH + glucagon** 2.4±0.86 Hz; repeated measures ANOVA, F(2,6) = 1.26, **p = 0.35**, n = 4) (Fig. 27B) or the distribution of inter-event intervals (Fig. 27C). In the case of the amplitude, even though no significant change was observed in the average amplitude (**[A]control** 11.3±2.07 pA, **[B]SCH** 10.3±1.26 pA, **[C]SCH + glucagon** 7.45±1.33 pA; repeated measures ANOVA, F(2,6) = 3.13, **p = 0.11**, n = 4) (Fig. 27D), a shift towards lower values can be observed in the ECDF when glucagon is added (Fig. 27E), also seen in the histogram with KDF overlay (Fig. 27F).

When singular events are studied, the decay times showed no difference in their average values (**[A]control** 6.63±0.46 ms, **[B]SCH** 8.02±0.84 ms, **[C]SCH + glucagon** 7.98±0.74 ms; repeated measures ANOVA, F(2,6) = 4.45, **p = 0.07**, n = 4) (Fig. 27G), but a shift towards higher values can be seen in both SCH application alone and co-application with glucagon in the ECDF (Fig. 27H) and histogram with KDE overlay (Fig. 27I).

No significant changes were observed in the parameters of the sustained response either with SCH 23390 alone or with co-application with glucagon (Fig. 28).

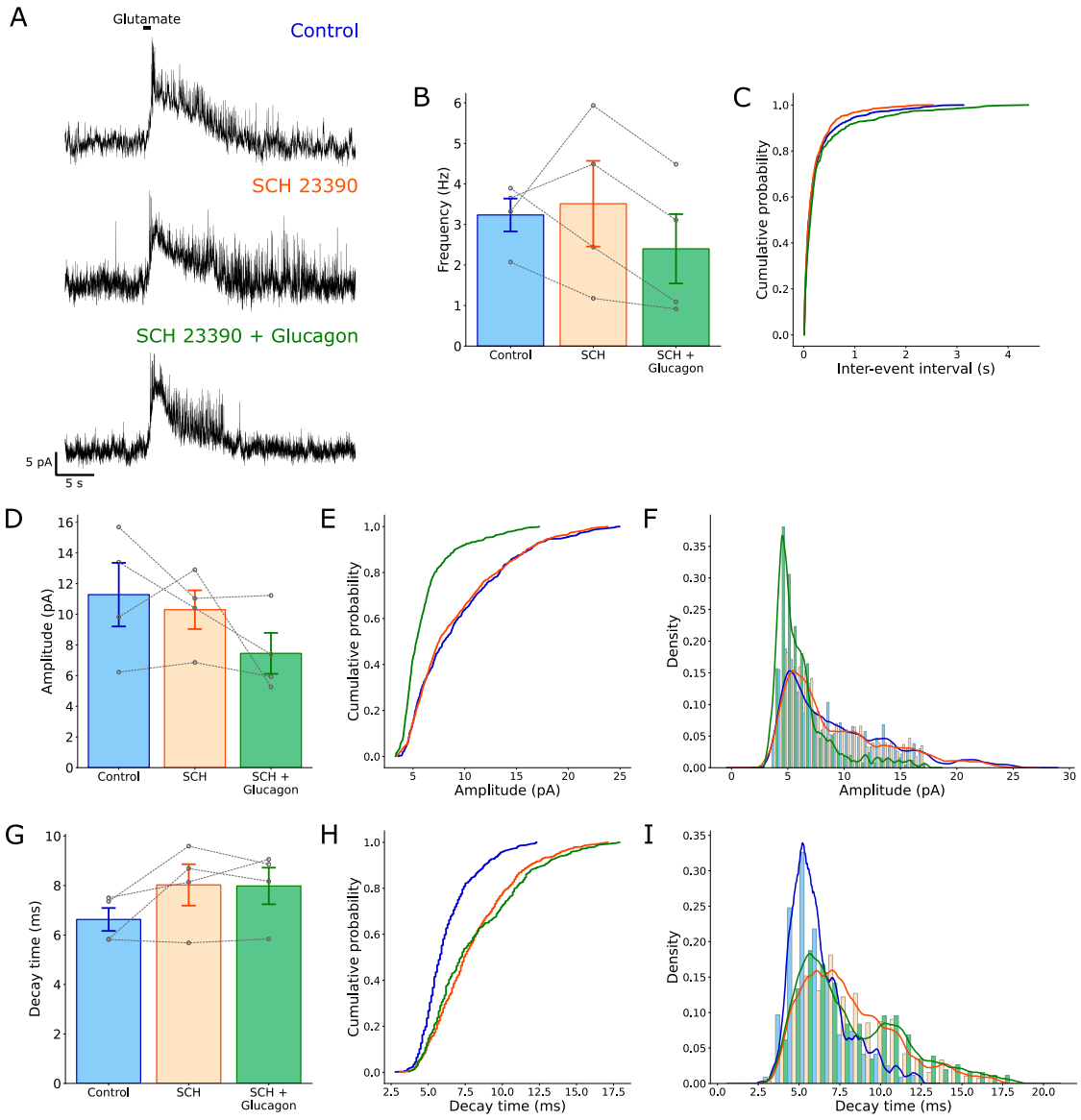

Figure 27. Sequential application of SCH 23390 and SCH 23390 + glucagon produces no significant changes in IPSC frequency under glutamate stimulation. (A) Representative traces of RBC IPSCs under control conditions (top, blue), after 15 min of bath application of SCH 23390 10 µM (middle, orange) and after 5 min of bath application of SCH 23390 10 µM + glucagon 1 µM (bottom, green). **(B-C)** No significant change was observed in the frequency of glycinergic IPSCs **(B)** or the ECDFs of the inter-event intervals **(C)** when SCH 23390 is bath applied, no change is observed with the subsequent addition of glucagon. **(D-F)** No significant change was observed in the average amplitude of IPSCs **(D)**, but a shift to the left can still be seen in the ECDF **(E)** with a shift of the distribution to lower values in the histogram with KDE overlay (F) in the case of SCH 23390 and glucagon co-application. **(G-I)** No significant change was observed in the average decay times of IPSCs **(G)**, but a shift to the right in their distribution as seen in the ECDF **(H)** with a shift to higher values in the histogram with KDE overlay **(I)** can be seen in both SCH 23390 alone and co-application with glucagon.

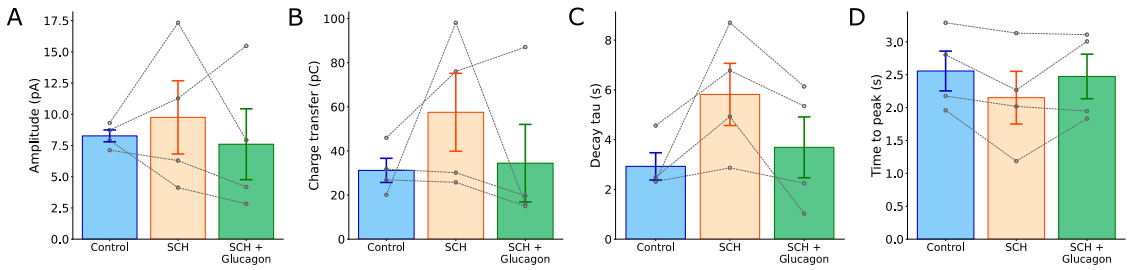

Figure 28. No changes in the sustained response were observed with sequential application of SCH 23390 and SCH 23390 + glucagon under glutamate stimulation. (A-D) No statistically significant changes in the amplitude **(A)**, charge transfer **(B)**, decay tau **(C)** or time to peak **(D)** of the sustained component were observed.

When HK-ECS stimulation was used, the same results were observed, with the sequential application of SCH 23390 10 µM followed by co-application of glucagon 1 µM and SCH 23390 10 µM, producing no significant changes in the frequency of IPSCs (***control*** 2.08±0.46 Hz; ***SCH*** 1.66±0.31 Hz; ***SCH + glucagon*** 2.43±0.47 Hz, repeated measures ANOVA, F(2,18) = 1.81, **p = 0.19**, n = 10) (Fig. 29B). In this case, a decrease in the amplitude of IPSC amplitude was observed with application of SCH 23390, with no difference when it was co-applied with glucagon (**[A]*control*** 9.83±0.87 pA; **[B]*SCH*** 7.07±0.62 pA; **[C]*SCH + glucagon*** 7.29±0.54 pA; Friedman test, $\chi^2(2) = 9.25$, **p = 0.01**, n = 10; Durbin-Conover comparisons (Bonferroni), A-B, p = 0.003, A-C, p = 0.01, B-C, p = 0.72) (Fig. 29D). This was associated with a shift to the left of the ECDFs (Fig. 29E) and a shift of the overall distribution of event amplitudes toward lower values (Fig. 29F).

When the characteristics of single events were analyzed, no significant change in the average decay times was observed (***control*** 9.85±0.64 ms; ***SCH*** 10.7±0.55 ms; ***SCH + glucagon*** 10.5±0.54 ms, repeated measures ANOVA, F(2,18) = 3.15, **p = 0.07**, n = 10) (Fig. 29G), or changes in their overall distributions (Fig. 29H-I).

These results suggest a dependency on D1R activity of the glucagon-mediated increase on RBC glycinergic IPSC activity.

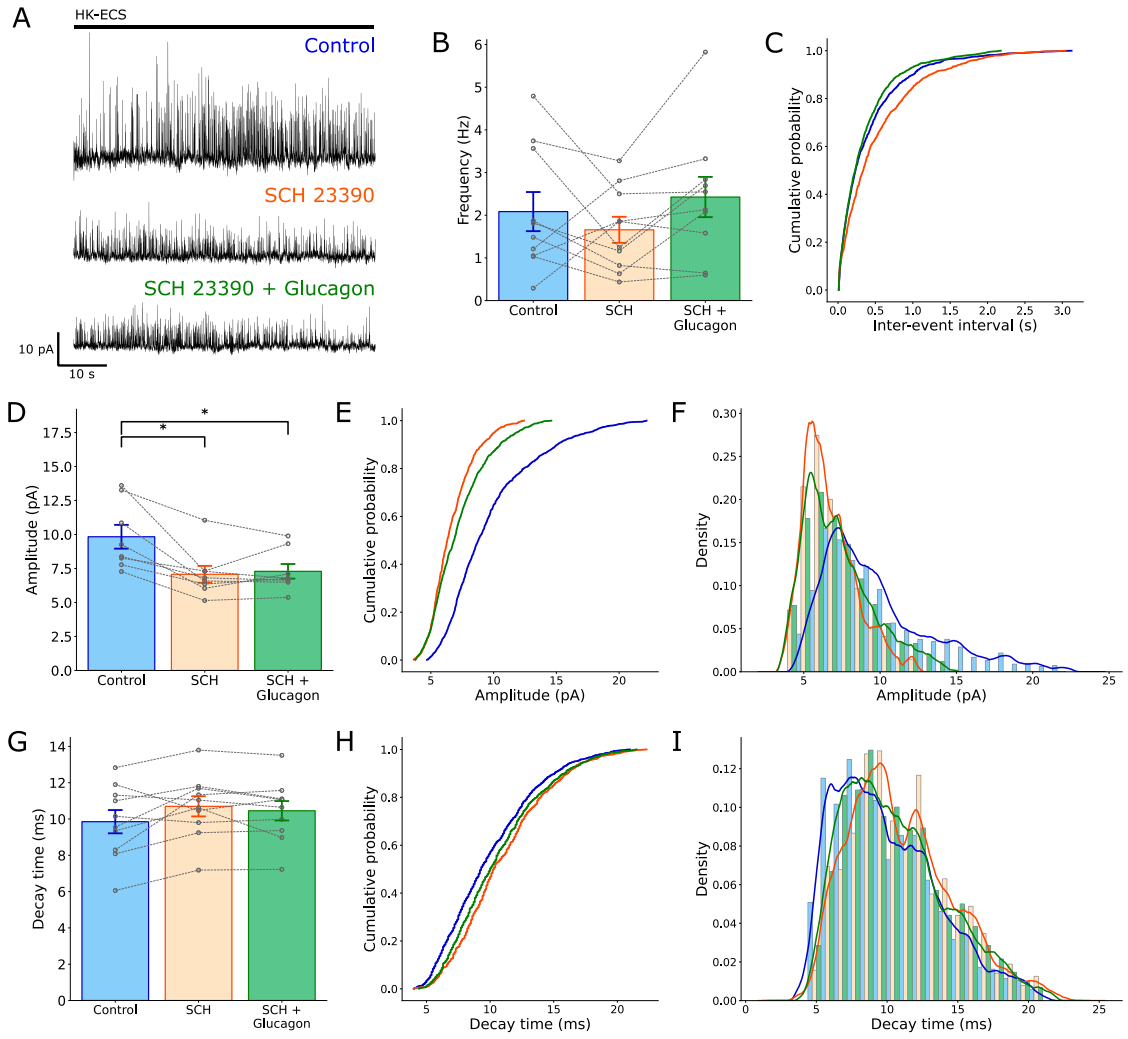

Figure 29. Antagonism of D1 receptors prevents the glucagon-mediated increase in RBC glycinergic IPSC frequency and decreases event amplitude. (A) Representative traces of RBC IPSCs under control conditions (top, blue), after 15 min of bath application of SCH 23390 10 µM (middle, orange) and after 5 min of bath application of SCH 23390 10 µM + glucagon 1 µM (bottom, green). **(B-C)** Application of SCH 23390 alone or co-application with glucagon did not produce changes in average IPSC frequency **(B)** or the distribution of inter-event intervals **(C)**. **(D-F)** Application of SCH-23390 alone produced a decrease in average IPSC amplitude that persisted after glucagon addition **(D)**, visible as a left shift of the amplitude distribution curves **(E)** and a change towards lower values in the histogram with KDF overlay (F). **(G-I)** No significant change was observed in the average decay times of IPSCs **(G)**, or their distribution as seen in the ECDF **(H)** and histogram with KDE overlay **(I)**. * $p < .05$.

D2 dopamine receptor activity is not required for glucagon modulation of glycinergic IPSC frequency

To complete the study of the effects of dopaminergic activity on the glucagon-mediated increase of glycinergic IPSC frequency, sulpiride, a selective antagonist of D2 dopamine receptors was used. Sulpiride was bath applied first at a concentration of 10 μM for 15 min and followed by a co-application of sulpiride 10 μM and glucagon 1 μM.

Application of sulpiride alone did not produce a significant change in frequency compared to baseline, while addition of glucagon produced an increase when compared to the baseline (**[A]control** 1.26±0.33 Hz, **[B]*sulpiride*** 1.4±0.42 Hz, **[C]*sulpiride* + *glucagon*** 2.09±0.52 Hz; Friedman test, $\chi^2(2) = 6.89$, **p = 0.03**, n = 9; Durbin-Conover comparisons (Bonferroni), A-B, p = 0.83, A-C, p = 0.02, B-C, p = 0.2) (Fig. 30B-C). No significant changes were found in the amplitude of the events (**[A]*control*** 8.9±0.98 pA, **[B]*sulpiride*** 7.1±0.62 pA, **[C]*sulpiride* + *glucagon*** 7.22±0.61 pA; repeated measures ANOVA (Greenhouse-Geisser correction), F(1.18, 8.23) = 4.14, **p = 0.07**, n = 9) (Fig. 30D).

When single events are studied, despite not observing a change in average amplitudes, a shift towards lower amplitudes can be observed in the ECDF (Fig. 30E) and histogram with KDE overlay (Fig. 30F), with no difference between sulpiride alone and co-application with glucagon. In the case of the decay times, there was a significant increase in average decay times when sulpiride was added (**[A]*control*** 9.82±1.22 ms, **[B]*sulpiride*** 12.1±1.18 ms, **[C]*sulpiride* + *glucagon*** 12.1±1.09 ms; repeated measures ANOVA, F(2, 16) = 12.3, **p < .001**, n = 9; Tukey test, A-B, p = 0.017, A-C, p = 0.007, B-C, p = 1) (Fig. 30G), with a shift to higher values in the ECDF and histogram with KDE overlay (Fig. 30H-I), again with no difference between sulpiride alone and co-application with glucagon.

These results are inconsistent with a role of D2 receptor signaling in the modulation of the glucagon-mediated increase in RBC glycinergic IPSC frequency, but show an effect of D2 receptor antagonism over the kinetics of glycinergic RBC IPSCs.

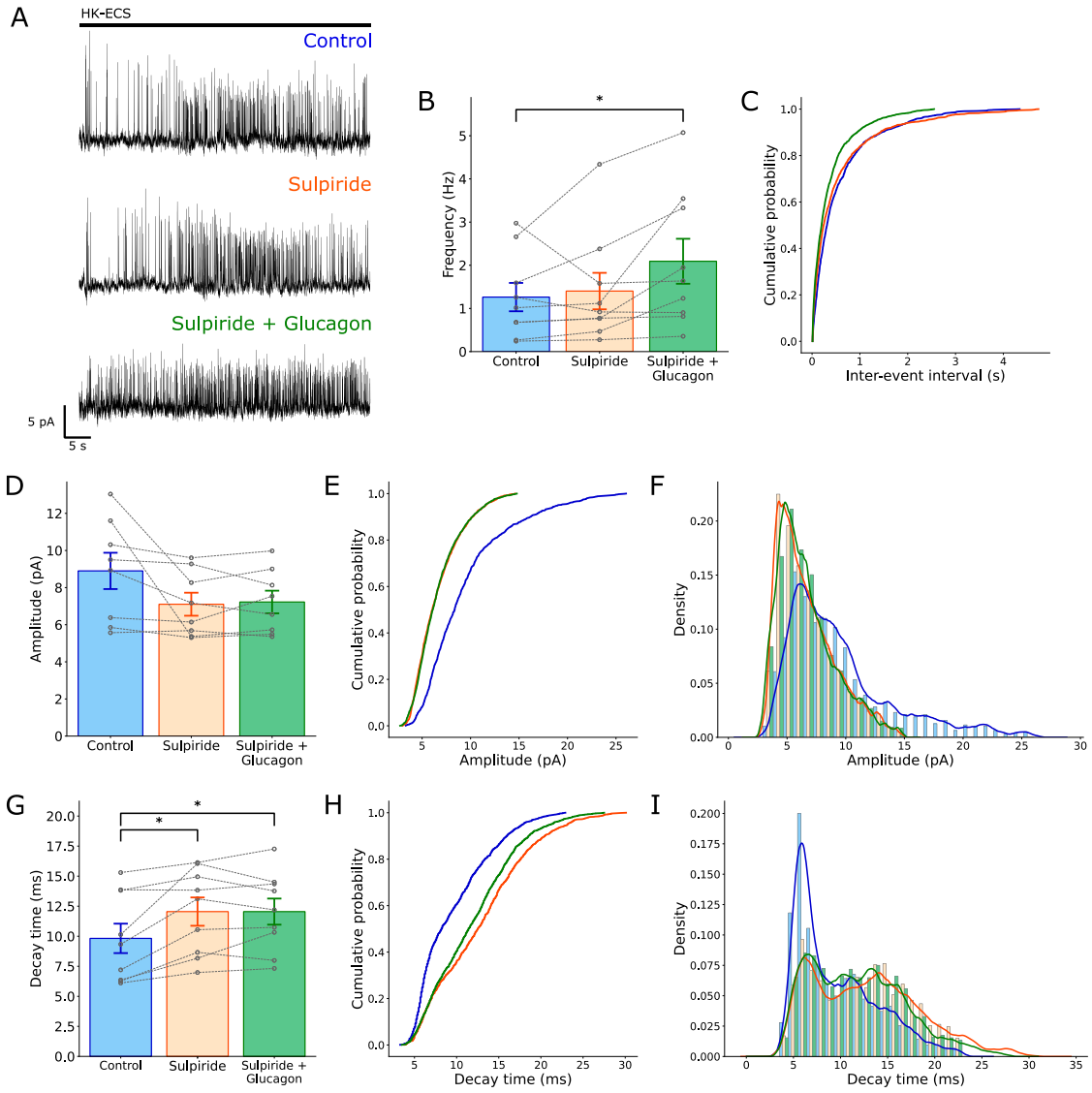

Figure 30. Glucagon-mediated increase of RBC glycinergic IPSC frequency persists under D2 receptor blockage. (A) Representative traces of RBC IPSCs under control conditions (top, blue), after 15 min of bath application of sulpiride 10 µM (middle, orange) and after 5 min of bath application of sulpiride 10 µM + glucagon 1 µM (bottom, green). **(B-C)** Application of sulpiride alone did not produce changes in IPSC frequency and co-application with glucagon increased it compared to control **(B).** This can also be seen in the distribution of inter-event intervals, with a shift to the left when glucagon is added **(C)**. **(D-E)** Sulpiride did not produce a significant change in the average amplitude of IPSCs **(D)**, even though a left shift of the amplitude can be observed under sulpiride and sulpiride + glucagon application in the ECDF **(E)** and the histogram with KDE overlay **(F)**. **(G-I)** Application of sulpiride produced an increase in the average decay time of glycinergic IPSCs **(G)**, with no change when glucagon was added, this can be observed as a shift to the right in the ECDF **(H)** and a decrease in the low decay time component observed in the histogram with KDE overlay **(I)**. * $p < .05$.

Glucagon induced changes in IPSC frequency are abolished in scotopic conditions

To further study the effects of lowered dopaminergic activity on the glucagon-mediated increase in RBC glycinergic IPSC frequency, recordings of RBC inhibitory activity were performed in scotopic conditions after a period of 2 h of dark adaptation, as scotopic conditions are associated with a decrease in dopamine release in the retina (Doyle et al., 2002; Roy & Field, 2019).

In these conditions, bath application of glucagon did not produce an increase in frequency of IPSCs (***control*** 1.49±0.43 Hz, ***glucagon*** 1.66±0.4 Hz; paired t test, t(7) = -0.58, **p = 0.58**, n = 8) (Fig. 31B) with no shift in the EPSC of inter-event intervals (Fig. 31C). On the other hand, a decrease in IPSC amplitude was observed (***control*** 13.6±1.44 pA, ***glucagon*** 9.21±0.73 pA; paired t test, t(7) = 2.9, **p = 0.02**, n = 8) (Fig. 31D), with a shift to the left of the distribution of event amplitudes (Fig. 31E-F).

No significant change was observed in the average decay time of IPSCs (***control*** 8.86±0.64 ms, ***glucagon*** 10.3±0.95 ms; paired t test, t(7) = -2.15, **p = 0.07**, n = 8) (Fig. 31G), with no clear shift in their overall distribution (Fig. 31H-I).

These results are in line with the ones observed under dopaminergic antagonism, suggesting it is associated with a suppression of the glucagon-mediated increase in RBC IPSC frequency.

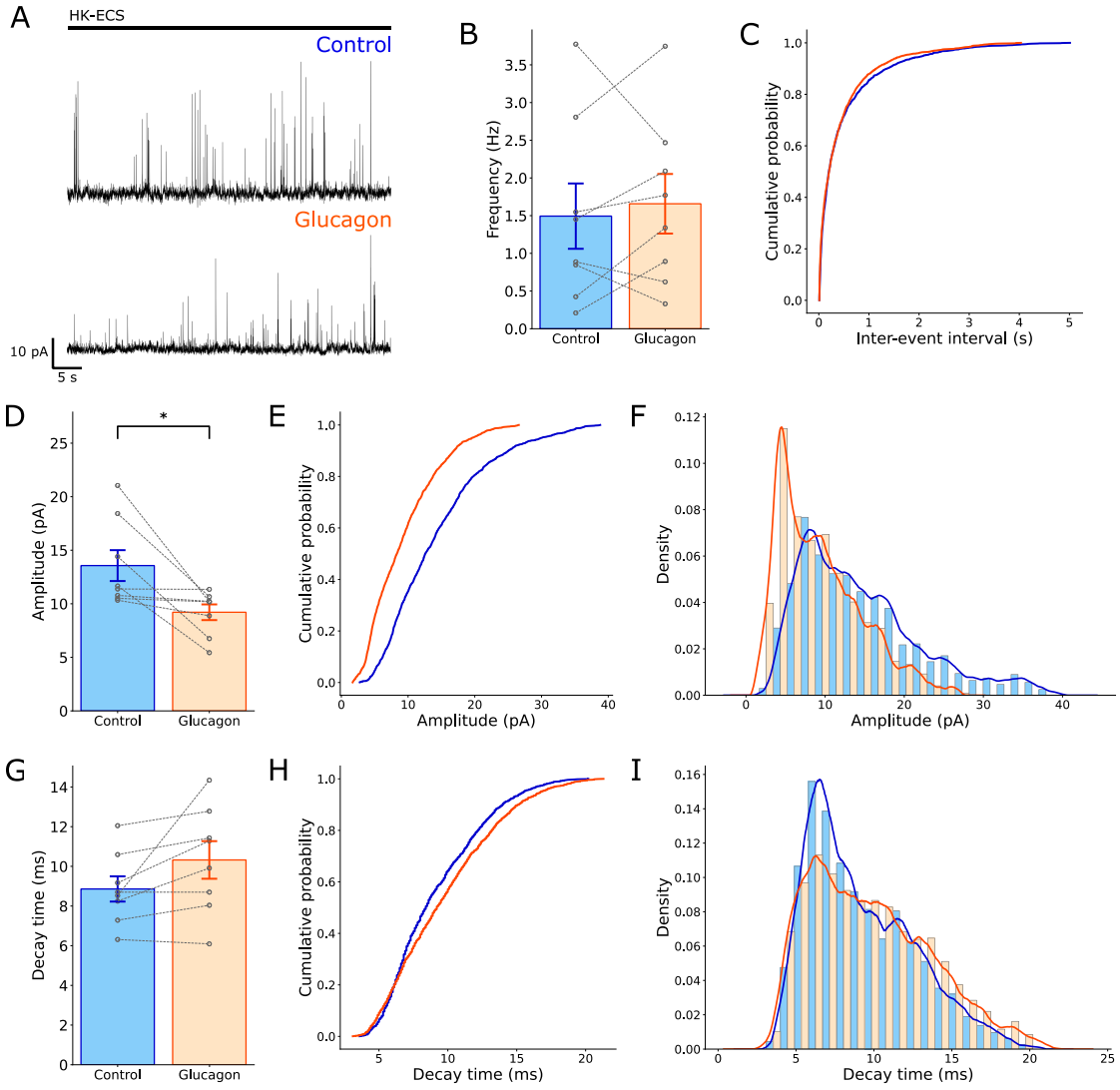

Figure 31. Glucagon-mediated increase in RBC glycinergic IPSC frequency is abolished in scotopic conditions. (A) Representative traces of RBC IPSCs under control conditions (top, blue) and after 5 min of bath application of glucagon 1 µM (bottom, orange). **(B-C)** No change was observed in the frequency of glycinergic IPSCs **(B)** or the ECDF of the inter-event intervals **(C)**. **(D-F)** A decrease was observed in the average amplitude **(D)** while the ECDF **(E)** and histogram with KDE overlay **(F)** show a corresponding shift to the left. **(G-I)** No change was observed in the average decay time **(G)** with no changes in distribution in the ECDF **(H)** and histogram with KDE overlay **(I)**. * $p < .05$.

No changes of the glucagon-mediated increase in RBC IPSC frequency are observed in a 2-week murine myopia model

To study the effects of myopia induction on the observed role of glucagon signaling in the regulation of RBC glycinergic IPSC frequency, a myopia murine model was used. The intervention consisted in the placement of a -10 D lens over one of the eyes of the animal for a period of 2 to 3 weeks, leaving the opposite eye uncovered as a control.

In the animals exposed to a -10 D lens for a period of 2 weeks, the glucagon-mediated increase of IPSC frequency, as seen in previously in wild-type animals, was present in the treated eye (***control*** 1.29±0.21 Hz, ***glucagon*** 2.3±0.56 Hz; paired t test, t(7) = -2.55, **p = 0.04**, n = 8) (Fig. 32B), as well as the control eye (***control*** 1.64±0.46 Hz, ***glucagon*** 3.24±0.88 Hz; Wilcoxon signed rank test, z = -2.2, **p = 0.03**, n = 6) (Fig. 33B), with a shift to the left of the inter-event interval ECDFs in both the treated (Fig. 32C) and control eyes (Fig. 33C).

In the case of the amplitude, the treated eye showed a decrease in average amplitude (***control*** 12.2±1.11 pA, ***glucagon*** 8.32±1.12 pA; paired t test, t(9) = 2.61, **p = 0.03**, n = 8) (Fig. 32D) and a shift of amplitude event distribution towards the left in the ECDF (Fig. 32E) and the histogram with KDE overlay (Fig. 32F), not seen in the control eye (***control*** 13.8±2.97 pA, ***glucagon*** 12.2±2.81 pA; paired t test, t(6) = 1.14, **p = 0.3**, n = 7) (Fig. 33C-E).

When individual IPSCs were analyzed, the treated eye (***control*** 9.23±1 ms, ***glucagon*** 9.3±0.85 ms; paired t test, t(7) = -0.18, **p = 0.86**, n = 8) (Fig. 32G) and the control eye (***control*** 6.58±0.43 ms, ***glucagon*** 6.66±0.26 ms; paired t test, t(5) = -0.21, **p = 0.84**, n = 6) (Fig. 33G) showed no change in average decay time. In the case of the treated eye, the distribution of decay times showed bimodality in the control condition, with the modes ubicated at 5.41 pA and 11.85 pA (Fig. 32H-I), the control eye showed no differences (Fig. 33H-I).

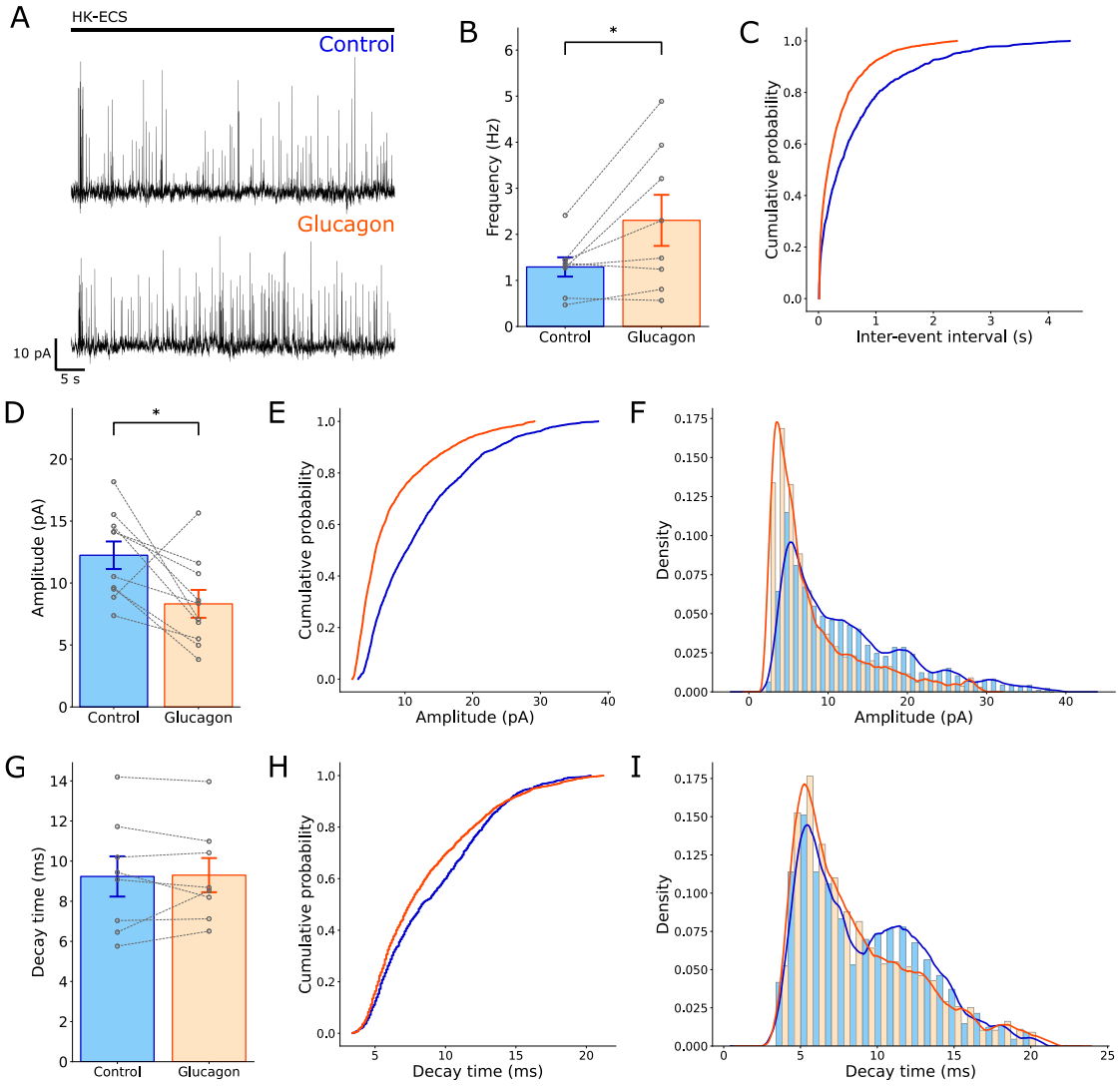

Figure 32. The glucagon-mediated increase in RBC glycinergic IPSC frequency is maintained in a 2-week murine myopia model, which however displays a decrease in IPSC amplitude. (A) Representative traces of RBC IPSCs under control conditions (top, blue) and after 5 min of bath application of glucagon 1 µM (bottom, orange), in the treated eye of a 2-week murine myopia model. **(B-C)** An increase was observed in the frequency of glycinergic IPSCs **(B)** with a shift to the left of the ECDF of the inter-event intervals **(C)**. **(D-F)** A decrease was observed in the average amplitude of IPSCs **(D)** with a shift to the left of the ECDF **(E)** and to lower values in histogram with KDE overlay **(F)**. **(G-I)** No change was observed in the average decay time **(G)** with no changes in distribution in the ECDF **(H)**, the histogram with KDE overlay showed two modes in the control condition **(I)** at 5.41 pA and 11.85 pA. * $p < .05$.

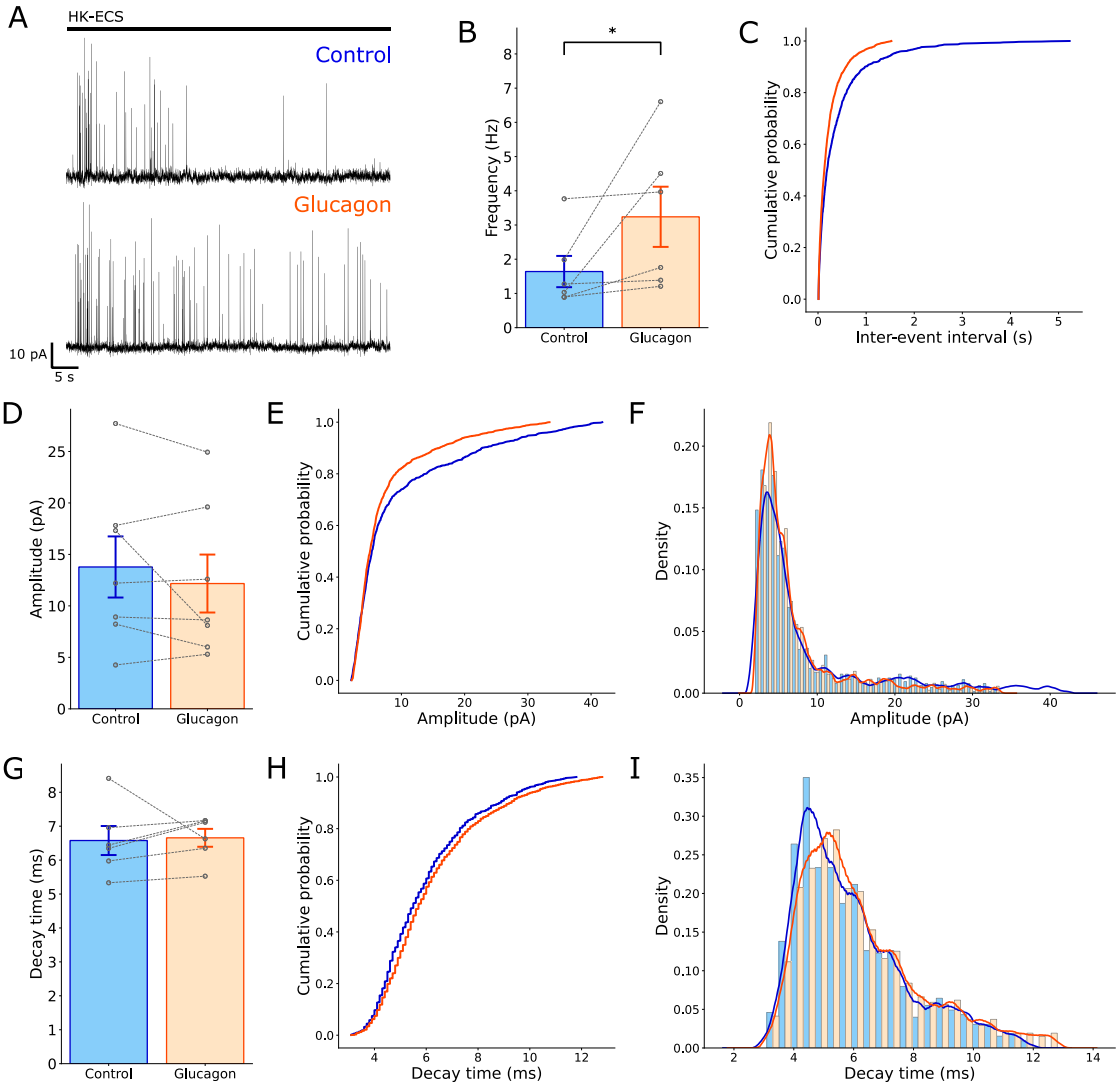

Figure 33. The control eye of a 2-week myopia model shows the same characteristics as a wild-type animal when glucagon 1 µM is bath-applied. (A) Representative traces of RBC IPSCs under control conditions (top, blue) and after 5 min of bath application of glucagon 1 µM (bottom, orange), in the control eye of a 2-week murine myopia model. **(B-C)** An increase was observed in the frequency of glycinergic IPSCs **(B)** with a shift to the left of the ECDF of the inter-event intervals **(C)**. **(D-F)** No change was observed in the average amplitude **(D)** or the distribution as seen in the ECDF **(E)** and histogram with KDE overlay **(F)**. **(G-I)** No change was observed in the average decay time **(G)** with no changes in distribution in the ECDF **(H)** and histogram with KDE overlay **(I)**. * $p < .05$.

The glucagon-mediated increase in RBC IPSC frequency is abolished in a 3-week murine myopia model

In the animals in which one of the eyes was exposed to a -10 D lens for a period of 3 weeks, the glucagon mediated increase in IPSC frequency was abolished, with no change of the average frequencies (***control*** 1.41±0.28 Hz, ***glucagon*** 1.51±0.57 Hz, paired t test, t(4) = -0.24, **p = 0.82**, n = 5) (Fig. 34B) or the distribution of inter-event intervals (Fig. 34C), as opposed to the control eye where the frequency increase (***control*** 1.24±0.31 Hz, ***glucagon*** 2.63±0.57 Hz, paired t test, t(4) = -3.43, **p = 0.03**, n = 5) (Fig. 35B) and inter-event interval ECDF shift to the left (Fig. 35C) can be observed. The decrease in amplitude seen at 2 weeks was also seen in these animals in the treated eye (***control*** 17.5±1.7 pA, ***glucagon*** 7.98±0.56 pA, paired t test, t(4) = 5.24, **p = 0.01**, n = 5) (Fig. 34D), but not in the control eye (***control*** 20.6±3.62 pA, ***glucagon*** 18.8±2.83 pA, paired t test, t(4) = 1.08, **p = 0.34**, n = 5) (Fig. 35D-F). This is associated with a shift of the ECDF to the left and a shift in the density of events towards lower values (Fig. 34E-F).

When the individual events are studied, no change is observed in the average decay times in the treated eye (***control*** 10.3±0.72 ms, ***glucagon*** 10.7±1.23 ms; paired t test, t(4) = -0.88, **p = 0.43**, n = 5) (Fig. 34G) or the control eye (***control*** 7.68±0.29 ms, ***glucagon*** 8.03±0.68 ms; paired t test, t(4) = -0.64, **p = 0.56**, n = 5) (Fig. 35G). But when the ECDF (Fig. 34H) and histogram with KDE overlay (Fig. 34I) of the treated eye are studied, a shift to the right can be observed in the decay times, with a decrease in the density of lower decay time events. This was not seen in the control eye (Fig. 35H-I).

These results are consistent with myopic induction using a -10 D lens abolishing the effect of glucagon on glycinergic IPSC frequency, in an exposure-time-dependent manner, with significant changes starting later than two weeks of myopic induction.

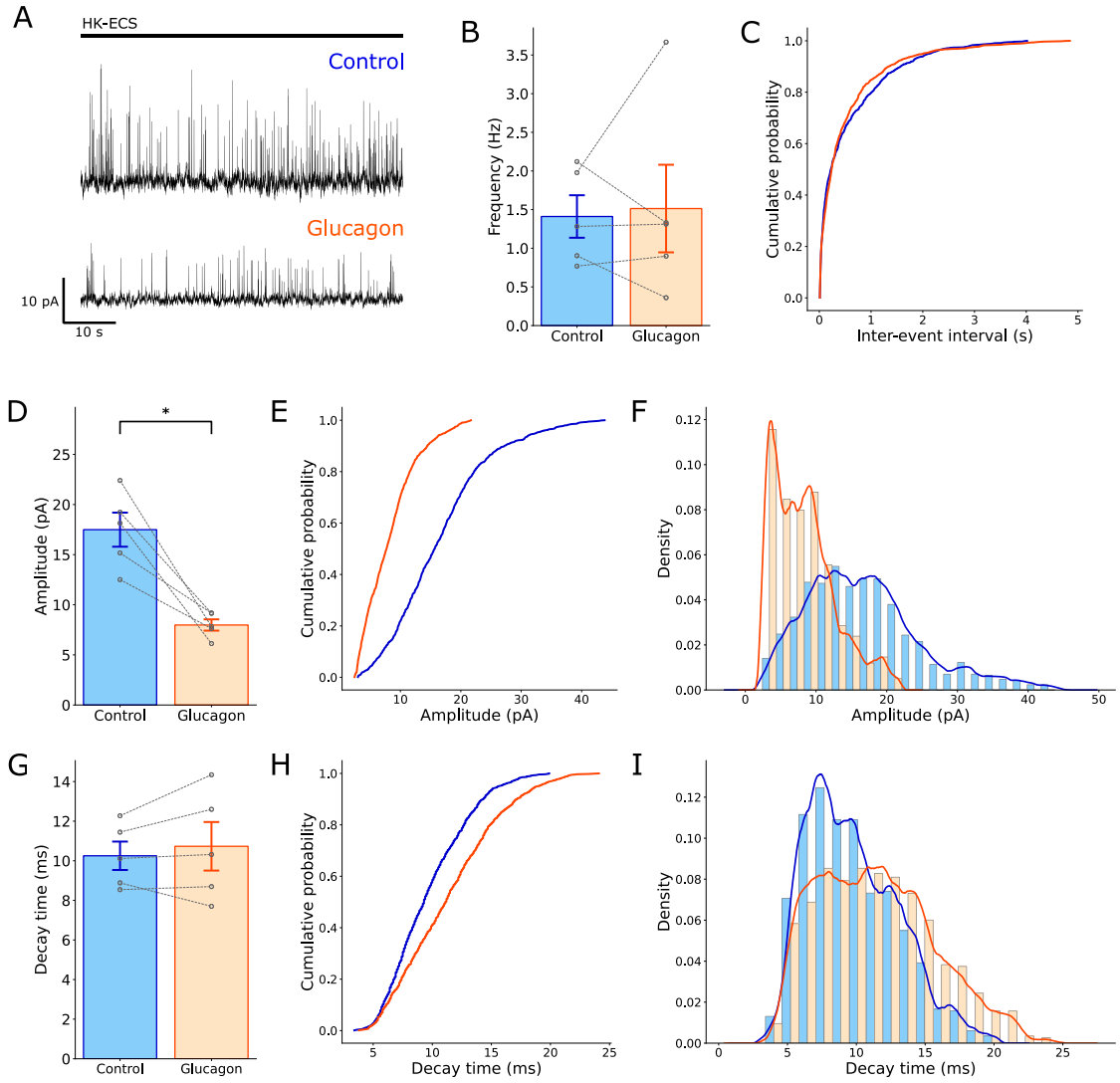

Figure 34. The glucagon-mediated increase in RBC glycinergic IPSC frequency is abolished in a 3-week murine myopia model and is associated with a decrease in IPSC amplitude. (A) Representative traces of RBC IPSCs under control conditions (top, blue) and after 5 min of bath application of glucagon 1 µM (bottom, orange), in the treated eye of a 3-week murine myopia model. **(B-C)** No significant change was observed in the average frequency of glycinergic IPSCs **(B)** or the ECDF of the inter-event intervals **(C)**. **(D-F)** A decrease was observed in the average amplitude of IPSCs **(D)** with a shift to the left of the ECDF **(E)** and to lower values in the histogram with KDE overlay **(F)**. **(G-I)** No change was observed in the average decay time **(G)** with a shift in distribution to the right in the ECDF **(H)**, and a shift toward higher values in the histogram with KDE overlay **(I)**. * $p < .05$.

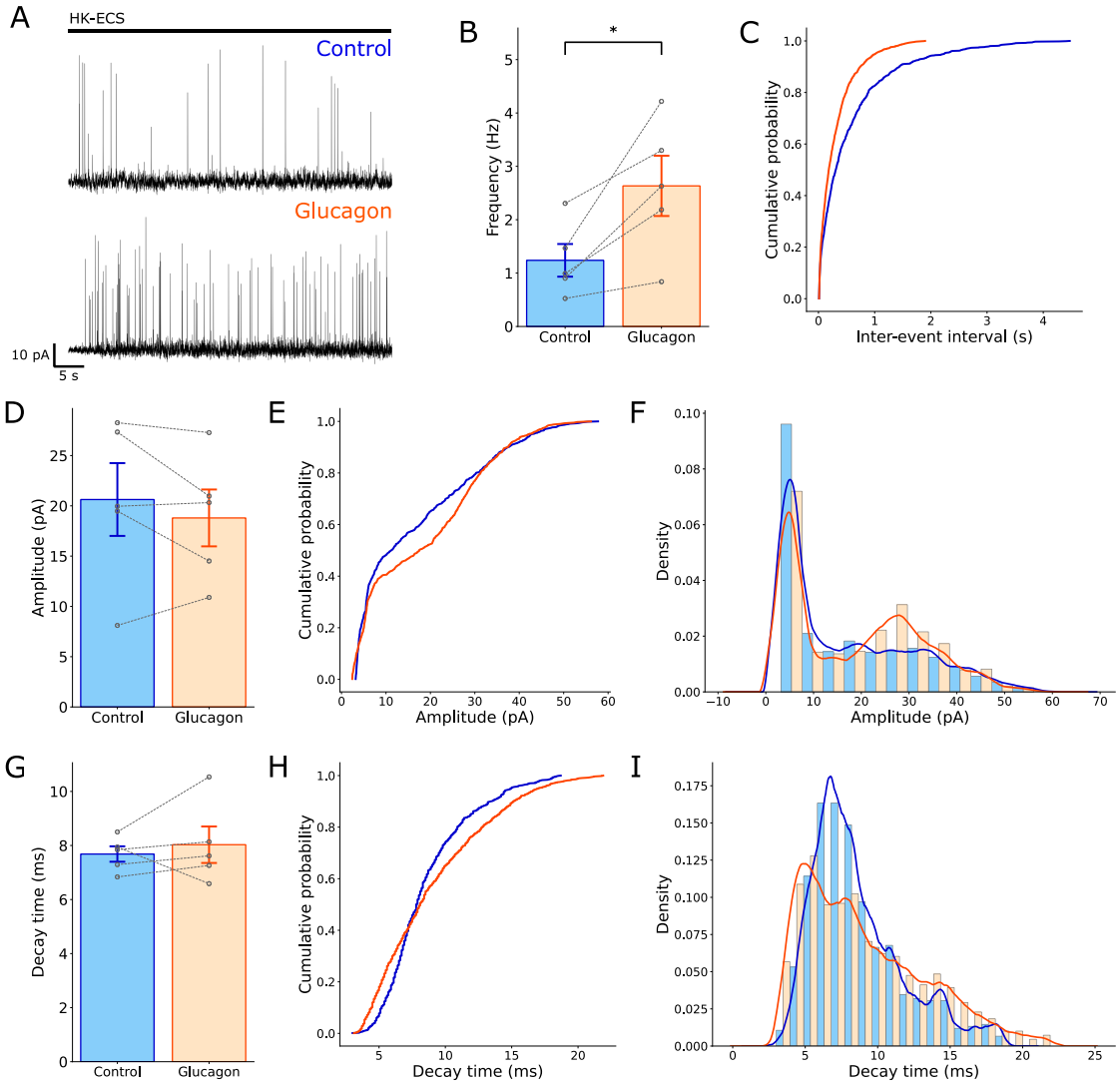

Figure 35. The control eye of a 3-week myopia model shows the same characteristics as a wild-type animal when glucagon 1 µM is bath-applied. (A) Representative traces of RBC IPSCs under control conditions (top, blue) and after 5 min of bath application of glucagon 1 µM (bottom, orange), in the control eye of a 3-week murine myopia model. **(B-C)** An increase was observed in the frequency of glycinergic IPSCs **(B)** with a shift to the left of the ECDF of the inter-event intervals **(C)**. **(D-F)** No change was observed in the average amplitude **(D)** or the distribution as seen in the ECDF **(E)** and histogram with KDE overlay **(F)**. **(G-I)** No change was observed in the average decay time **(G)** with no changes in distribution in the ECDF **(H)** and histogram with KDE overlay **(I)**. * $p < .05$.

Dopamine D1 receptor agonism increases RBC glycinergic IPSC frequency in a murine myopia model

To test whether the lower dopamine levels observed in myopia animal models (Carr & Stell, 1995; M. Feldkaemper & Schaeffel, 2013) were a factor in the abolition of the regulatory effect of glucagon on glycinergic IPSCs, a selective D1 receptor agonist, SKF 81297, was bath applied at a concentration of 10 µM for 15 min followed by co-application with glucagon 1 µM for 5 min.

In animals with an eye exposed to a -10 D lens for a period of 2 weeks, bath application of SKF 81297 by itself produced an increase in the frequency of glycinergic IPSCs, with no significant difference when glucagon was added (**[A]*control*** 1.96±0.53 Hz, **[B]*SKF*** 2.62±0.63 Hz, **[C]*SKF + glucagon*** 2.65±0.62 Hz; repeated measures ANOVA, F(2,8) = 13, **p = 0.003**, n = 5; Tukey test, A-B, p = 0.04, A-C, p = 0.01, B-C, p = 0.98) (Fig. 36B), this was associated with a shift to the left of the ECDFs of both conditions (Fig. 36C).

When individual events were analyzed, no change was observed in the average decay time (**[A]*control*** 10.4±0.59 ms, **[B]*SKF*** 11.3±1.08 ms, **[C]*SKF + glucagon*** 11.1±1.67 ms; repeated measures ANOVA (Greenhouse-Geisser correction), F(1.1,5.49) = 0.45, **p = 0.55**, n = 5) (Fig. 36G). In the case of the distribution of decay times, a shift towards lower values can be observed in the ECDF (Fig. 36H) and histogram with KDE overlay (Fig. 36I), in the SKF 81297 + glucagon condition.

In animals with an eye exposed for 3 weeks to the treatment with a -10 D lens, the same effects were observed, with an increase in IPSC frequency in the presence of SKF 81297 alone, and no significant change when glucagon was added (**[A]*control*** 1.42±0.22 Hz, **[B]*SKF*** 2.54±0.33 Hz, **[C]*SKF + glucagon*** 2.93±0.43 Hz; repeated measures ANOVA F(2,12) = 9.99, **p = 0.003**, n = 7; Tukey test, A-B, p = 0.02, A-C, p = 0.04, B-C, p = 0.34) (Fig. 37B), the ECDFs showing a more marked shift to the left (Fig. 37C).

When individual events were analyzed, again, no change was observed in the decay time (***control*** 12±1.22 ms, ***SKF*** 10.7±0.95 ms, ***SKF + glucagon*** 10.7±0.94 ms; repeated measures ANOVA F(2,14) = 1.2, **p = 0.33**, n = 7) (Fig. 37G), but the distribution shift towards lower values was observed on both SKF 81297 alone and SKF 81297 + glucagon conditions (Fig. 37H-I).

Dopamine D1 receptor agonism restores RBC glycinergic IPSC amplitude up to 2 weeks of myopia induction in a murine myopia model

In the case of the average amplitude decrease of RBC glycinergic IPSC observed after bath application of glucagon in the treated eyes of myopia model animals, bath application of SKF 81297 10 µM abolished this decrease in the animal with an eye exposed to a -10 D lens for 2 weeks (***control*** 11.1±1.05 pA, ***SKF*** 10.7±1.01 pA, ***SKF + glucagon*** 10.2±1.22 pA, repeated measures ANOVA (Greenhouse-Geisser correction), F(1.04,4.15) = 0.54, **p = 0.51**, n = 5) (Fig. 36D-F). But in the case of animals with an eye exposed for 3 weeks to myopia induction, the amplitude decrease was still present (**[A]*control*** 8.97±0.86 pA, **[B]*SKF*** 6.08±0.64 pA, **[C]*SKF + glucagon*** 5.02±0.65 pA; repeated measures ANOVA (Greenhouse-Geisser correction), F(1.15,6.9) = 10.9, **p = 0.01**, n = 7; Bonferroni correction, A-B, p = 0.1, A-C, p = 0.03, B-C, p = 0.05) (Fig. 37D-F).

These results are consistent with a regulatory role of dopamine through D1 receptor activity over RBC glycinergic IPSCs, with D1R agonism producing an increase in IPSC frequency and abolishing the amplitude decrease associated with glucagon application.

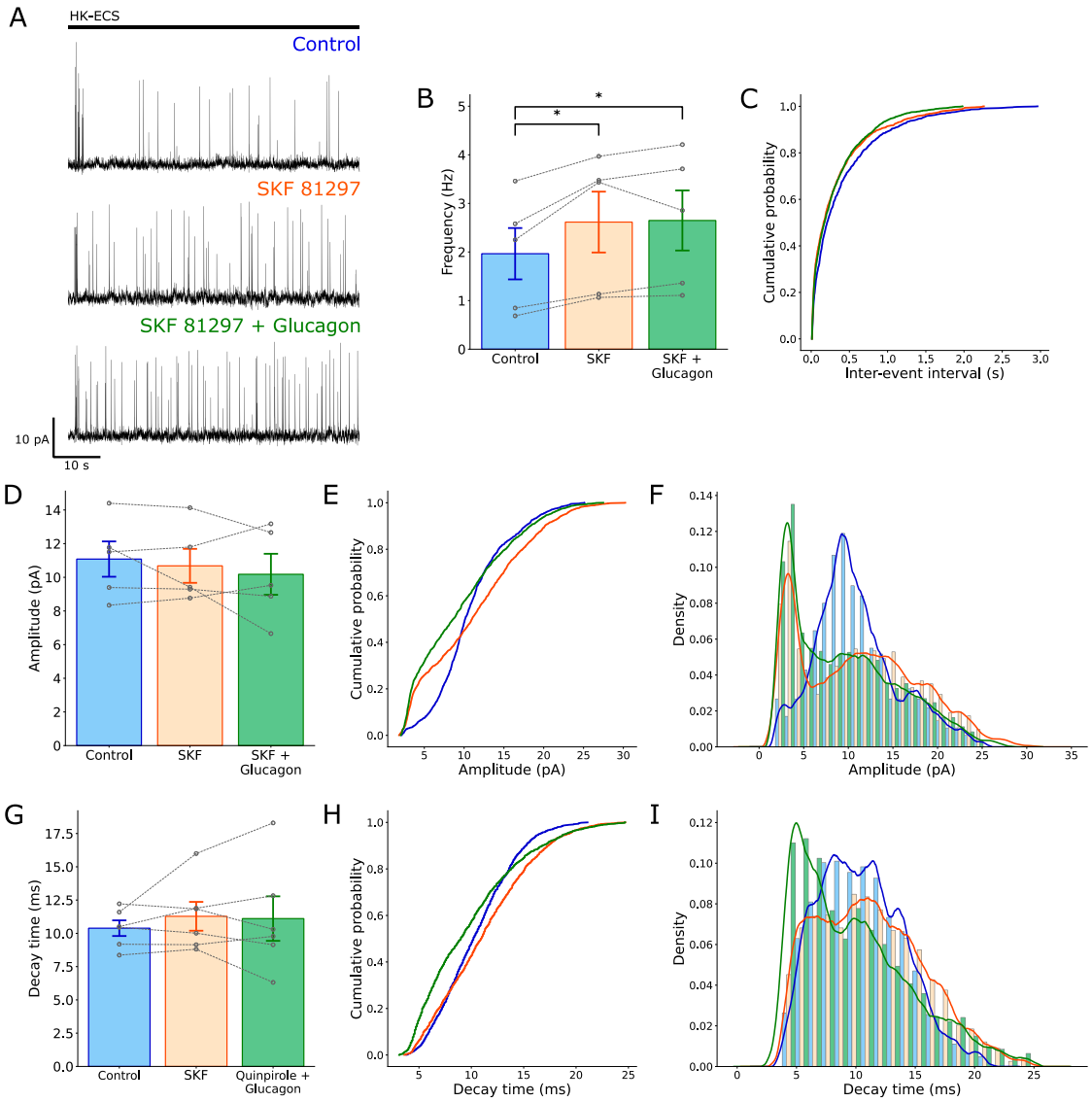

Figure 36. Dopamine D1 receptor agonism increases the frequency of RBC glycinergic IPSCs and abolishes the amplitude decrease previously seen in a 2-week murine myopia model. (A) Representative traces of RBC IPSCs under control conditions (top, blue), after 15 min of bath application of SKF 81297 10 µM (middle, orange) and after 5 min of bath application of SKF 81297 10 µM + glucagon 1 µM (bottom, green), in the treated eye of a 2-week murine myopia model. **(B-C)** Application of SKF 81297 alone increased average IPSC frequency, with no change when glucagon was added **(B),** a corresponding shift to the left can be seen in the inter-event interval ECDFs **(C)**. **(D-E)** SKF 81297 did not produce a significant change in the average amplitude of IPSCs **(D)**, even though a preponderant second mode with lower amplitude can be seen appear in the density distribution of IPSC amplitude under SKF 81297 and SKF 81297 + glucagon application in the ECDF **(E)** and the histogram with KDE overlay **(F)**. **(G-I)** No change was observed in the average decay time **(G)** with a shift towards lower values seen only when glucagon was added both in the ECDF **(H)** and histogram with KDE overlay **(I)**. * $p < .05$.

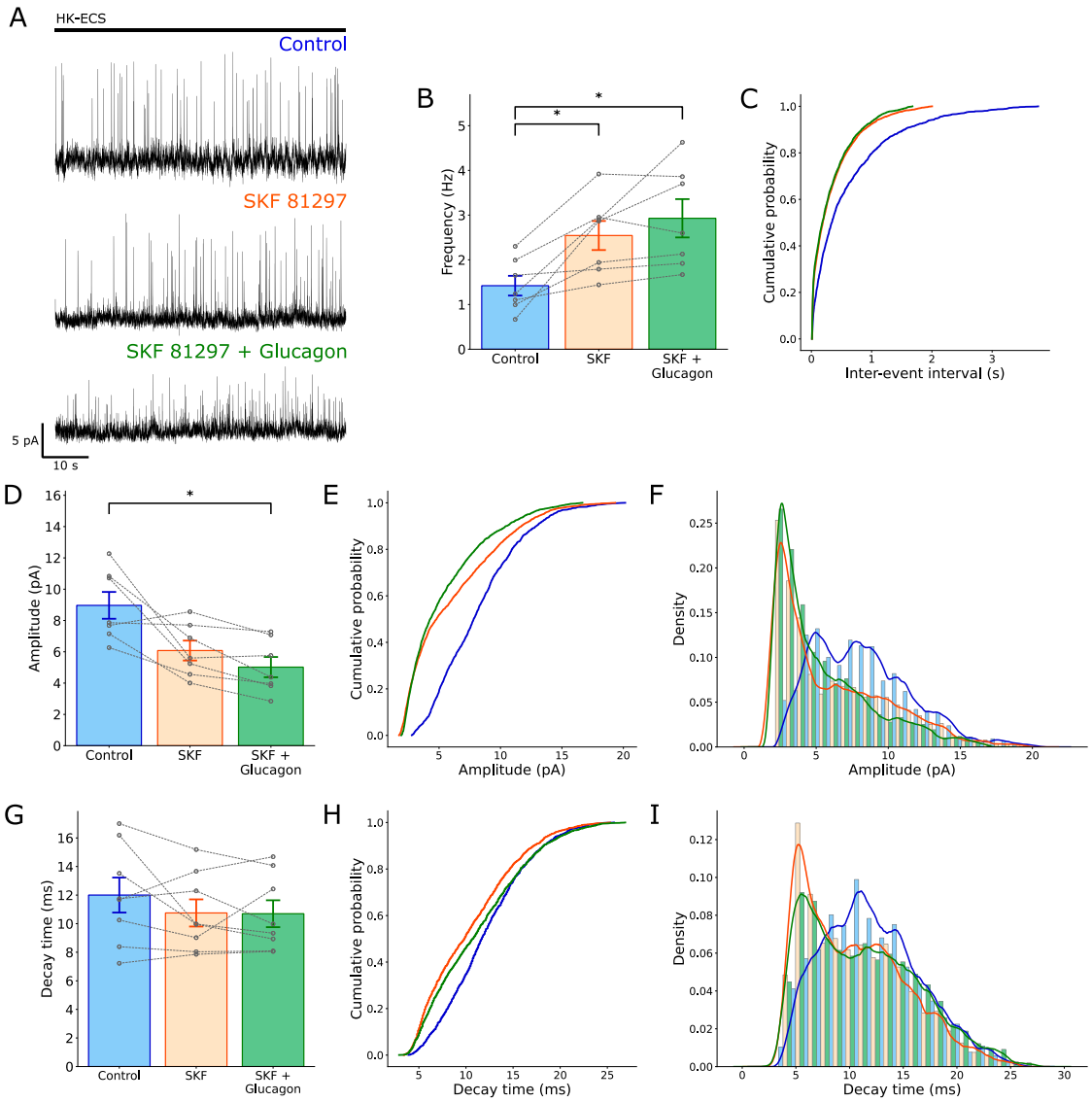

Figure 37. Dopamine D1 receptor agonism increases the frequency of RBC glycinergic IPSCs but does not abolish the amplitude decrease previously seen in a 3-week murine myopia model. (A) Representative traces of RBC IPSCs under control conditions (top, blue), after 15 min of bath application of SKF 81297 10 µM (middle, orange) and after 5 min of bath application of SKF 81297 10 µM + glucagon 1 µM (bottom, green), in the treated eye of a 3-week murine myopia model. **(B-C)** Application of SKF 81297 alone increased average IPSC frequency, with no change when glucagon was added **(B),** a corresponding shift to the left can be seen in the inter-event interval ECDFs **(C)**. **(D-E)** SKF 81297 alone did not produce a significant change in the average amplitude of IPSCs, but subsequent addition of glucagon decreased it **(D)**, a shift towards lower values can be observed in the ECDF **(E)** and the histogram with KDE overlay **(F)** for both conditions. **(G-I)** No change was observed in the average decay time **(G)** with a shift towards lower values in the ECDF **(H)** and histogram with KDE overlay **(I)** for both SKF 81297 alone and co-application with glucagon. * $p < .05$.

Dopamine D2 receptor agonism had no effects on the changes observed in the 2-week murine myopia model

To complement the previous results under D1 receptor agonism and to test the effects of D2 agonism on the changes seen in the murine myopia model, quinpirole, a selective D2 receptor agonist, was used at a concentration of 10 µM for 15 min, followed by co-application with glucagon 1 µM for 5 min.

In animals exposed for 2 weeks to treatment with a -10 D lens, bath application of quinpirole was not associated with significant changes in IPSC frequency (***control*** 2.18±0.31 Hz, ***quinpirole*** 2.14±0.23 Hz, ***quinpirole + glucagon*** 1.93±0.24 Hz, repeated measures ANOVA, F(2,8) = 0.46, **p = 0.65**, n = 5) (Fig. 38B), which can also be noticed in the grouping of inter-event interval ECDF curves (Fig. 38C), and with a decrease in amplitude (**[A]*control*** 24.5±2.55 pA, **[B]*quinpirole*** 14.4±2.63 pA, **[C]*quinpirole + glucagon*** 9.61±0.89 pA; repeated measures ANOVA, F(2,8) = 41.9, **p < .001**, n = 5; Tukey test, A-B, p = 0.004, A-C, p = 0.003, B-C, p = 0.11) (Fig. 38D), seen as a shift towards the left in the ECDF (Fig. 38E) and histogram with KDE overlay (Fig. 38F), becoming more prominent with the addition of glucagon.

When individual events are analyzed, no change was observed in the average decay time (***control*** 8.9±1.05 ms, ***quinpirole*** 9.91±0.86 ms, ***quinpirole + glucagon*** 9.28±1.05 ms, repeated measures ANOVA, F(2,8) = 0.91, **p = 0.44**, n = 5) (Fig. 38G), which is also noted by the lack of change of their distributions (Fig. 38H-I).

These results argue against a role of dopamine D2 receptor signaling in the glucagon-mediated regulation of RBC glycinergic IPSCs in the myopia murine model.

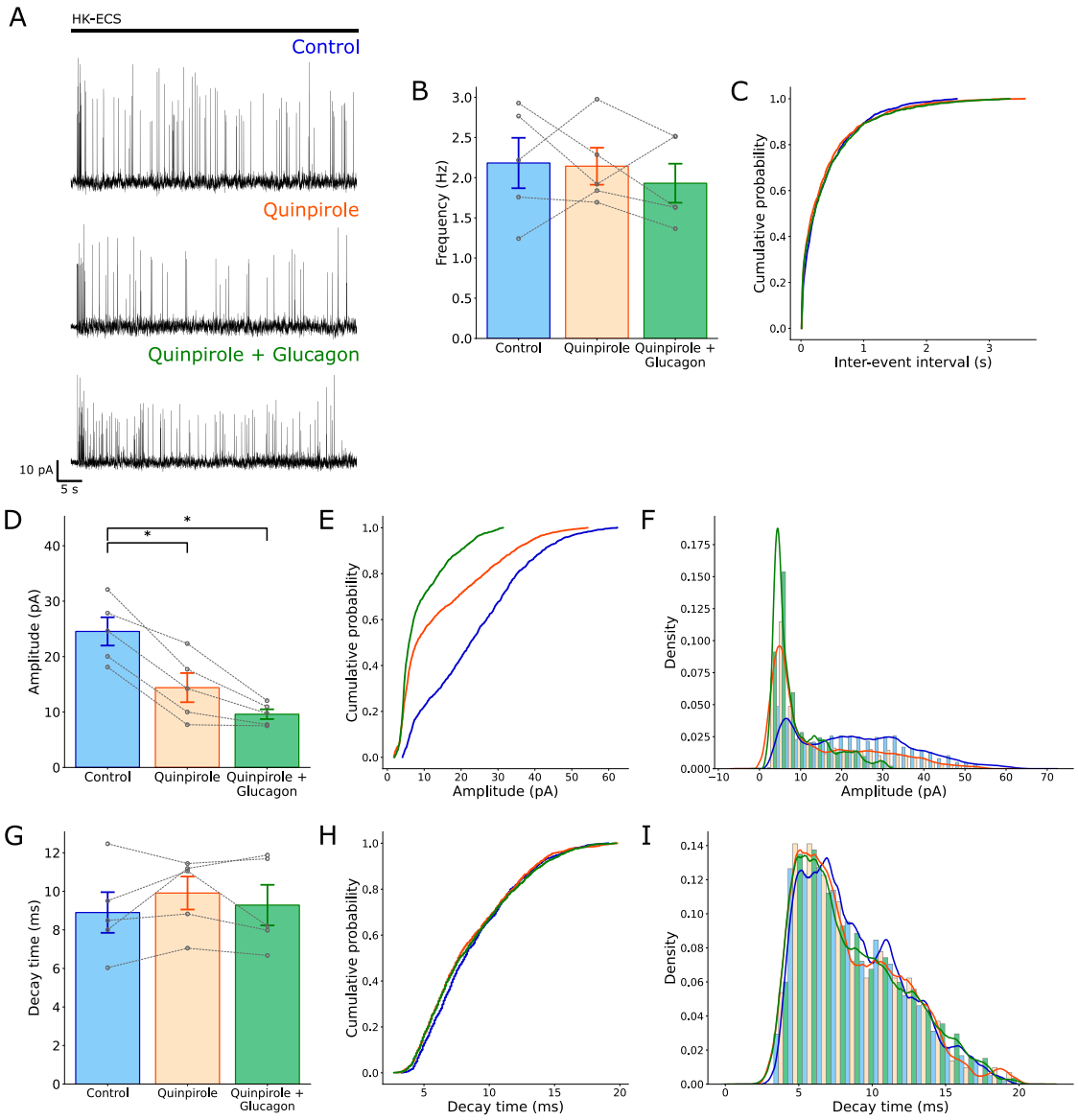

Figure 38. Dopamine D2 receptor agonism does not restore the glucagon-mediated increase of RBC IPSC frequency, or the amplitude decrease previously seen in a 2-week murine myopia model. (A) Representative traces of RBC IPSCs under control conditions (top, blue), after 15 min of bath application of quinpirole 10 µM (middle, orange) and after 5 min of bath application of quinpirole 10 µM + glucagon 1 µM (bottom, green), in the treated eye of a 2-week murine myopia model. **(B-C)** No significant change was observed in the average frequency of glycinergic IPSCs **(B)** or the ECDF of the inter-event intervals **(C)**. **(D-E)** Quinpirole alone and co-applied with glucagon produced a significant decrease in the average amplitude of IPSCs **(D)**, with a shift towards lower values observed in the ECDF **(E)** and the histogram with KDE overlay **(F)** for both conditions. **(G-I)** No change was observed in the average decay time **(G)** with no changes in distribution in the ECDF **(H)** and histogram with KDE overlay **(I)**. * $p < .05$.

The decrease in IPSC amplitude observed in murine myopia model animals corresponds to a pre-synaptic change

To study the nature of the decrease of RBC glycinergic IPSC amplitude observed in scotopic conditions, dopamine receptor antagonism and in the treated eyes of myopia model animals after the application of glucagon, current responses to the application of glycine over the axon terminal at a concentration of 300 µM, a saturating dose for murine RBCs (Ivanova et al., 2006), were recorded under bath application of a cocktail of blockers to prevent ON and OFF signaling and GABA receptor activity, in order to chemically isolate the recorded cell and prevent pre-synaptic effects from affecting it. The experiments were performed in myopia model animals exposed to a -10 D lens for 2 weeks.

Under these conditions, and when comparing the control condition and after bath application of glucagon for a period of 5 min, the addition of glucagon did not produce a significant change in the characteristics of the glycine-evoked current, including the amplitude (***control*** 63.9±14.7 pA, ***glucagon*** 43.2±6.63 pA; paired t test, t(6) = 1.81, **p = 0.12**, n = 7) (Fig. 39B), charge transfer (***control*** 144±38.6 pC, ***glucagon*** 88.2±19 pC; paired t test, t(6) = 2, **p = 0.09**, n = 7), time to peak (***control*** 1.19±0.2 s, ***glucagon*** 1.16±0.16 s; paired t test, t(6) = 0.33, **p = 0.75**, n = 7) and the decay tau (***control*** 1.3±0.19 s, ***glucagon*** 1.19±0.19 s; paired t test, t(6) = 1.3, **p = 0.24**, n = 7) (Fig. 39E).

These results suggest the change in amplitude observed when glucagon is applied in a murine myopia model to be a pre-synaptic effect.

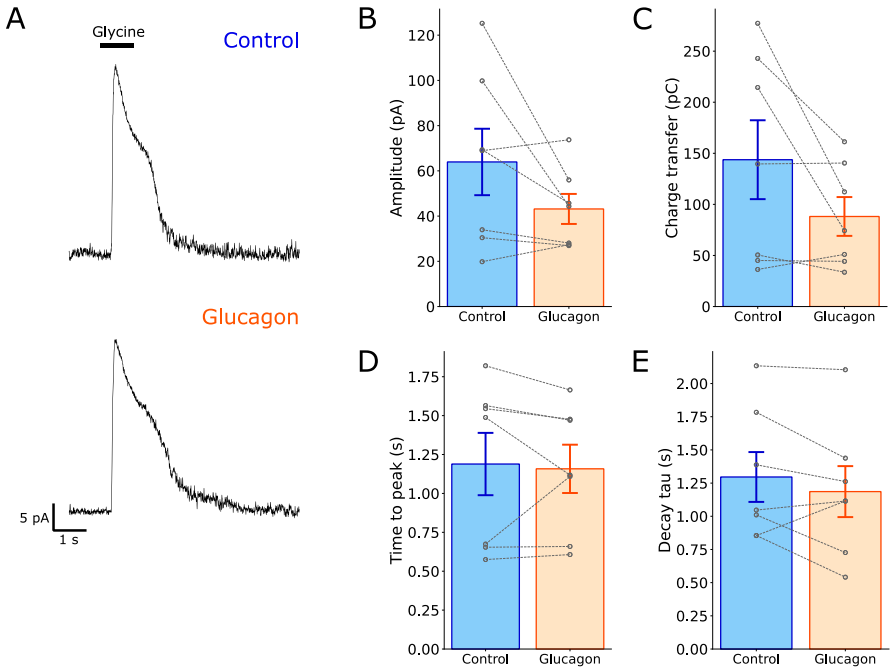

Figure 39. The glucagon-mediated decrease in RBC IPSC amplitude observed in myopia model animals is a pre-synaptic effect. (A) Representative traces of RBC IPSC evoked via puff application of glycine 300 µM in the axon terminal under control conditions (top, blue) and after 5 min of bath application of quinpirole 10 µM + glucagon 1 µM (bottom, orange), in the treated eye of a 2-week murine myopia model. The bath solution for both conditions contained a cocktail of blockers to prevent ON pathway, OFF pathway and GABAergic signaling. **(B-E)** No significant changes were observed in the amplitude **(B)**, charge transfer **(C)**, time to peak **(D)** or decay tau **(E)** of the response when comparing control and glucagon bath-application conditions.

The decrease in IPSC amplitude observed with glucagon application in scotopic conditions is not dependent on GABAergic inhibitory activity

To study the possible mechanism underlying the decrease in amplitude observed in scotopic conditions when glucagon is added, recordings were performed under either $GABA_A$ or $GABA_{A\text{-}\rho}$ receptor blockade, as evidence exists of crosstalk between GABA and glycine receptors in the central nervous system of mammals (Tang et al., 2020; Trombley et al., 1999).

Application of TPMPA 50 µM for 10 minutes to block $GABA_{A\text{-}\rho}$ receptors in scotopic conditions produced an increase in ISPC frequency by itself, with no change when glucagon 1 µM was added (**[A]*control*** 1.19±0.62 Hz; **[B]*TPMPA*** 1.73±0.54 Hz; **[C]*TPMPA + glucagon*** 2.04±0.62 Hz;

Friedman test, $\chi^2(2) = 7.6$, **p = 0.02**, n = 5; Durbin-Conover pairwise comparisons (Bonferroni correction), A-B, p = 0.01, A-C, p = 0.004, B-C, p = 1) (Fig 40B) with a shift to the right of the inter-event intervals (Fig 40C). The decrease in IPSC amplitude associated with glucagon application persisted (**[A]*control*** 16.7±3.15 pA, **[B]*TPMPA*** 10.6±1.88 pA, **[C]*TPMPA + glucagon*** 7.36±1.35 pA; repeated measures ANOVA, F(2,8) = 11.1, **p < .005**, n = 5; Tukey test, A-B, p = 0.14, A-C, p = 0.02, B-C, p = 0.19) (Fig 40D), with a clear shift of the distribution of single event amplitudes towards lower values as seen in the ECDF (Fig 40E) and histogram with KDE overlay (Fig 40F).

When individual events are analyzed, a change was observed in the average decay time, but was too close to the statistical significance limit for a post-hoc test (**[A]*control*** 6.91±0.26 ms, **[B]*TPMPA*** 8.07±0.52 ms, **[C]*TPMPA + glucagon*** 7.05±0.37 ms, repeated measures ANOVA, F(2,8) = 4.85, **p = 0.04**, n = 5; Tukey test, A-B, p = 0.14, A-C, p = 0.8, B-C, p = 0.2) (Fig. 40G). When the single event distribution is analyzed, a shift toward higher values can be observed for both TPMPA and TPMPA + glucagon conditions (Fig. 40H-I).

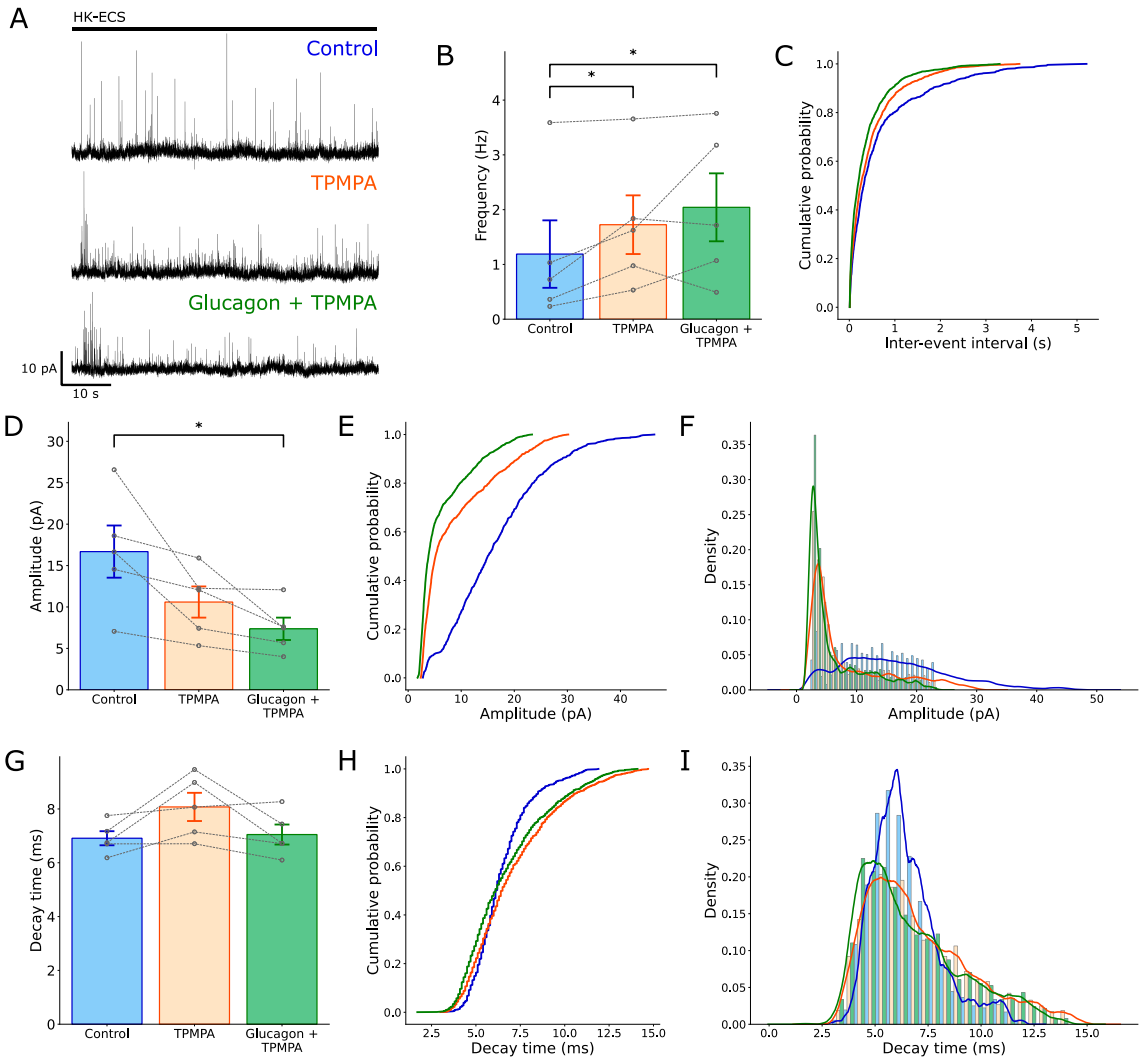

Figure 40. Blockade of $GABA_{A-\rho}$ receptors under scotopic conditions does not reverse the glucagon-induced decrease in IPSC amplitude and induces an increase in IPSC frequency. **(A)** Representative traces of RBC IPSCs under control conditions (top, blue), after 10 min of bath application of TPMPA 50 µM (middle, orange) and after 5 min of bath application of TPMPA 50 µM + glucagon 1 µM (bottom, green), under scotopic conditions. **(B-C)** An increase was observed in the average frequency of glycinergic IPSCs when TPMPA was added with no change with the subsequent addition of glucagon **(B)**, this can also be observed as a shift to the left of the ECDF of the inter-event intervals **(C)**. **(D-F)** TPMPA alone did not produce a significant change in IPSC amplitude, but subsequent addition of glucagon produced a significant decrease in the average amplitude of IPSCs when compared to the control condition **(D)**, with a shift towards lower values observed in the ECDF **(E)** and the histogram with KDE overlay **(F)**. **(G-I)** No significant change was observed in the average decay time **(G)** with a shift toward higher values in the ECDF **(H)** and histogram with KDE overlay **(I)**. * $p < .05$.

On the other hand, application of SR-95531 10 μM for 10 minutes to block $GABA_A$ receptors under scotopic conditions produced no significant change in IPSC frequency (**[A]*control*** 1.83±0.65 Hz, **[B]*SR-95531*** 2.05±0.43 Hz, **[C]*SR-95531 + glucagon*** 1.8±0.58 Hz; repeated measures ANOVA, F(2,10) = 0.18, **p = 0.84**, n = 6) (Fig 41B) or observable changes in the distribution of inter-event intervals (Fig 41C). Subsequent addition of glucagon 1 μM did not produce any significant change either. Application of SR-95531 and subsequent addition of glucagon were associated with a decrease in IPSC amplitude compared to the control condition (**[A]*control*** 9.4±1.66 pA, **[B] *SR-95531*** 6.91±1.52 pA, **[C] *SR-95531 + glucagon*** 4.36±0.44 pA; repeated measures ANOVA, F(2,10) = 11.6, **p = .002**, n = 6; Tukey test, A-B, p = 0.01, A-C, p = 0.02, B-C, p = 0.18) (Fig 41D). This change can also be seen in the ECDF of event amplitudes, with a shift to the right (Fig 41E), and a shift toward higher values in the histogram with KDE overlay (Fig 41F).

When individual events are analyzed, no change was observed in the average decay time (**[A]*control*** 7.59±0.69 ms, **[B]*SR-95531*** 7.81±0.64 ms, **[C]*SR-95531 + glucagon*** 8.42±0.73 ms; repeated measures ANOVA, F(2,10) = 2.25, **p = 0.16**, n = 6) (Fig. 41G), which is also noted by the lack of change of their distributions (Fig. 41H-I).

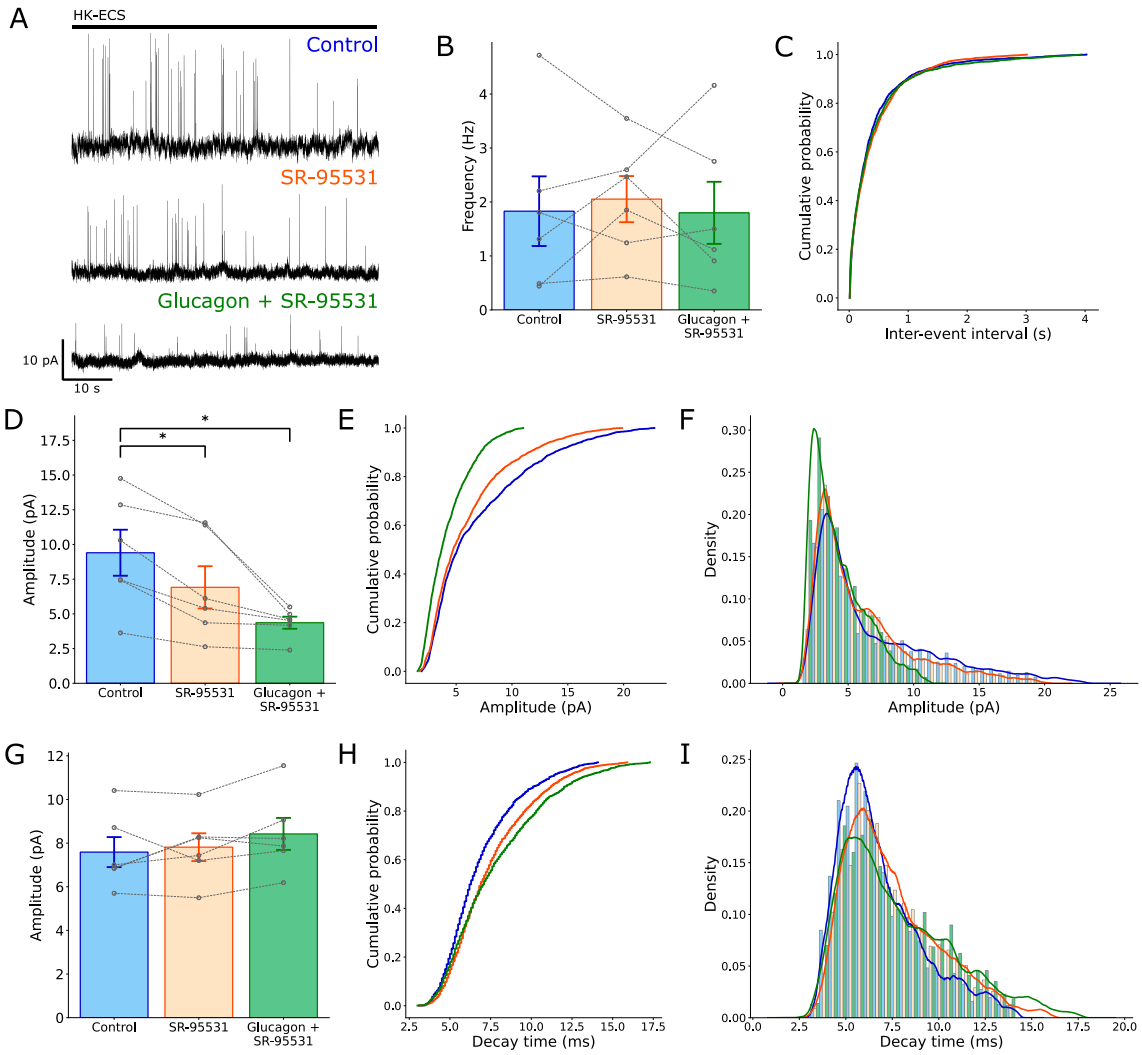

Figure 41. Blockade of $GABA_A$ receptors under scotopic conditions does not reverse the glucagon-induced decrease in IPSC amplitude. (A) Representative traces of RBC IPSCs under control conditions (top, blue), after 10 min of bath application of SR-95531 10 µM (middle, orange) and after 5 min of bath application of SR-95531 10 µM + glucagon 1 µM (bottom, green), under scotopic conditions. **(B-C)** No change was observed in the average frequency of glycinergic IPSCs when SR-95531 was added alone or co-applied with glucagon **(B)**, and no change was observed either in the ECDF of the inter-event intervals **(C)**. **(D-F)** SR-95531 alone and co-application with glucagon produced a significant decrease in the average amplitude of IPSCs when compared to the control condition **(D)**, with a shift towards lower values observed in the ECDF **(E)** and the histogram with KDE overlay **(F)**. **(G-I)** No significant change was observed in the average decay time **(G)**, with no changes in either the ECDF **(H)** or the histogram with KDE overlay **(I)**. * $p < .05$.

No overall changes in retinal activity are observed with glucagon application using calcium imaging

To find possible overall changes in retinal activity produced by the application of glucagon, retinal slices where incubated in fluo-4 to study the calcium dynamics of the different layers. For quantification, the retina was subdivided into the ONL, OPL, INL, IPL and GLC (Fig. 42A). The INL was further subdivided into the first two thirds (INL_A) and the last third (INL_B) to differentiate the lower part of the INL where the somata of amacrine cells are located (Remington, 2012) (Fig. 42A). The IPL was subdivided into the sublamina a (IPL_A) and the sublamina b (IPL_B) to differentiate the OFF and ON synaptic layers, respectively (Fig. 42A).

The recording consisted of 3 min of baseline recording with standard bath solution, 5 min of bath solution including glucagon 1 µM and 9 min of washing control bath solution.

When the data was corrected for photobleaching, no significant change was observed for any of the studied layers compared to the baseline (Fig. 42B).

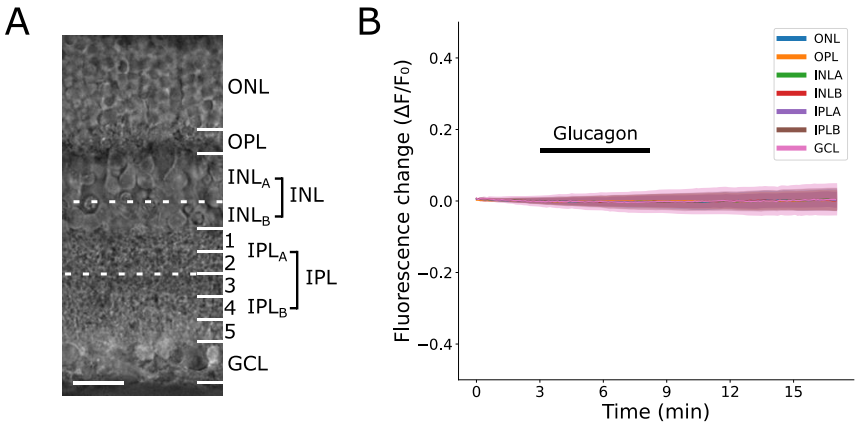

Figure 42. No overall changes in fluorescence are observed after application of glucagon using calcium imaging. (A) For quantification of fluorescence, the retina was divided in areas following the standard layer subdivision, in the case of the INL, it was further subdivided into the first two thirds (INLA) and the last third (INLB) and the IPL was subdivided into the sublamina a (IPLA) and the sublamina b (IPLB). Scale bar = 20 µm, magnification = 40x. **(B)** Average fluorescence change traces of the different layers, no significant overall change was seen.

DISCUSSION

Glucagon as a novel neuromodulator of retinal activity in the mouse

The data obtained in the present study supports glucagon as a neuromodulator in the mouse retina, playing a role in the regulation of the glycinergic activity received by RBCs. To date, no electrophysiological or other functional studies have reported an effect of glucagon on the mammalian retina, the literature being limited to contradictory immunohistochemical reports (M. Feldkaemper et al., 2004; Mathis & Schaeffel, 2007). This positions the results obtained (summarized in Table 2) as a novel approach to the study of retinal glucagonergic activity.

The effect observed, an increase in RBC glycinergic IPSC frequency, was abolished under dopaminergic antagonism, specifically of D1R. The same effect was seen on a murine LIM model, and were reversed by D1R agonism, showing a possible interaction between these two pathways and a putative role in myopia development.

Table 2. Overview of the changes over the characteristics of RBC glycinergic IPSCs observed under the different studied conditions

Photopic conditions

	Frequency	Amplitude
$GABA_A$ antagonism	↑	–
$GABA_{A\text{-}\rho}$ antagonism	–	–
Glycine antagonism	✕	✕
Glucagon	↑	–
└ +L168,049	–	↓
└ +Strychnine	✕	✕
└ +D1R antagonism	–	↓
└ +D2R antagonism	↑	–
D1R antagonism	–	↓
D2R antagonism	–	↓

Scotopic conditions

	Frequency	Amplitude
Glucagon	–	↓
└ +$GABA_A$ antagonism	–	↓
└ +$GABA_{A\text{-}\rho}$ antagonism	↑	↓
$GABA_A$ antagonism	–	↓
$GABA_{A\text{-}\rho}$ antagonism	↑	↓

Myopia model

	Frequency	Amplitude
2 weeks		
Glucagon	↑	↓
└ +D1R agonism	↑	–
└ +D2R agonism	–	↓
D1R agonism	↑	–
D2R agonism	–	↓
3 weeks		
Glucagon	–	↓
└ +D1R agonism	↑	↓
D1R agonism	↑	↓

↑: Increase, ↓: Decrease, −: No change, ✕: Abolition.

Glycinergic inhibition of RBCs appears as a transient component

RBCs receive multiple inhibitory inputs from amacrine cells in the IPL, which can be mainly divided into GABAergic and glycinergic. In general, GABAergic input arises from wide field amacrine cells and glycinergic input from small field amacrine cells (Long et al., 2020; MacNeil & Masland, 1998; Menger et al., 1998). Application of either glutamate or HK-ECS, while holding the cell at 0 mV, was able to elicit IPSCs, showing both a transient and a sustained component. The sustained component is compatible with what has been shown in previous studies to be a component dependent on glutamate transporter activity, specifically excitatory amino acid transporter 5 (EAAT 5) (Wersinger et al., 2006). This explains why the component was not abolished with the use of either GABAergic or glycinergic inhibitors.

In the case of the transient component, pharmacological antagonism revealed it to be of glycinergic origin under both glutamate and HK-ECS stimulation, consistent with previous reports (Ivanova et al., 2006; Wersinger et al., 2006). This glycinergic activity arises in the axon terminal of RBCs since axotomized cells lacked the response and has a topological profile similar to those previously reported for glycinergic activity (Chávez & Diamond, 2008). Coincident with these facts, its origin is most likely small field amacrine cells (Long et al., 2020). It was also found that this glycinergic activity was regulated by GABAergic activity via $GABA_AR$. The possible circuit involved in this interaction will be discussed further below.

Glucagon increases the frequency of RBC glycinergic IPSCs

The main and most consistent effect of the addition of glucagon to the bath solution was an increase in the frequency of RBC glycinergic IPSCs.

As previously mentioned, the role of glucagon in the CNS has been mostly studied in regard to its metabolic effects (Abraham & Lam, 2016), but GLP-1, the molecule sharing the most homology to glucagon in the secretin/glucagon family (Adelhorst et al., 1994), has been shown able to

depolarize hypocretin neurons and increase their spike frequency, in a process dependent on modulation of pre-synaptic glutamate release in mouse lateral hypothalamus (Acuna-Goycolea, 2004), and to increase the release of glutamate in rat basal ganglia (Mora et al., 1992). Also through the use of multiple GLP-1 analogues, GLP-1R agonism was shown to enhance LTP in rat hippocampus (McClean et al., 2010). These results support GLP-1 as a pre-synaptic modulator of neuronal activity, acting most likely through modulation of cAMP levels and activation of exocytotic mechanisms (Green et al., 2004). This represents a precedent for a role of members of the secretin/glucagon family as neuromodulators in the brain.

The observed effect of glucagon was also seen to be dose-dependent, with an increase over the dose used of 1 µM producing a significant increase in RBC glycinergic IPSC frequency, and lower doses not generating any significant change. The obtained dose-response curve is however limited to few values and requires more study, as evidence suggests dose-response curves for GCR spanning at least 6 logarithmic units (Jorgensen et al., 2007).

The increase in activity is not related with the addition of a different source of activity, as the profiles of event amplitude and decay time do not show a significant shift or a change in modality. Still, it is of note that glucagon addition produced a moderate increase in events around 15-20 pA; for this reason, the experiments were repeated in the presence of strychnine, to test whether the increase in IPSC frequency elicited by glucagon was indeed glycinergic in origin. As the co-application of glucagon and strychnine abolished the glucagon-induced increase in IPSC frequency, the effect of glucagon on IPSC frequency is most likely limited to an increase in glycinergic activity.

It is also of note that the observation of different levels of response to glucagon addition was not related to the morphological characteristics of the studied cells. Previous reports classify at least two RBC subtypes based on morphology, specifically the extent of RBC axon terminal stratification into the GCL (Tsukamoto & Omi, 2017). As these subclassifications could be related to functional differences, the possible correlation with the fold-change of glycinergic IPSC frequency was

studied, but none was found either when using the original measurements or when using them as a whole via principal component analysis, a method also useful for finding hidden variables. This indicates that the effect of glucagon and its intensity are not related with a specific morphological subtype of RBC, nor do they define one.

The use of calcium imaging allowed an overview of the retinal activity, to study the possible extent of the effects glucagon addition. The analysis was separated by retinal layers in order to broadly target specific cell subtypes and signaling pathways, but no significant difference was observed when glucagon was added. This is in line with the antecedent that studies looking for glucagon in the retina have had mixed results (M. Feldkaemper et al., 2004; Mathis & Schaeffel, 2007), possibly due to the fact that it is not broadly distributed and only low levels play a role in retinal function (M. Feldkaemper et al., 2004). This is also in line with the overall subtle nature of the changes observed in the current study.

A more directed study using transgenic mice to target specifically glucagon or GCR-containing cells for recording would be of great utility to elucidate the particular characteristics of this signaling pathway and determine its real extent within the mammalian retina.

The glucagon antagonist L168,049 inhibits the effect of glucagon but also elicits a second type of activity

The application of the glucagon receptor antagonist L168,049 at a concentration of 500 nM produced the abolition of the glucagon-mediated increase in IPSC frequency, suggesting that this specific effect is mediated by glucagon acting through its canonical receptor. This was also associated with a decrease in the amplitude of the IPSCs, and a shift towards slower kinetics.

To further characterize this secondary effect, L168,049 was applied at different concentrations, showing a combination of different responses. At a concentration of 1 µM, the highest concentration tested, there was an increase in the frequency of RBC glycinergic IPSCs when

L168,049 alone was added to the bath solution, accompanied by a shift in the amplitude of the events towards lower values and to higher decay times. As none of these changes were seen when glucagon was used alone, this suggests the events elicited by L168,049 correspond to a different source of activity than those seen with glucagon. Subsequent addition of glucagon to the bath solution did not produce any significant changes, suggesting blockage of the effect of glucagon, as the profile of glucagon-related events did not appear over the profile of L168,049-related events.

The increase in IPSC frequency with a particular profile observed with L168,049 alone could be related to off-target effects, due to the high similarity of the receptors in the secretin/glucagon family (Tam et al., 2014). Glucagon receptor shows high similarity with GLP-1 receptor (Runge et al., 2003), making it a likely target. The studies available about L168,049 specificity are limited, showing a much lower affinity to the GLP-1 receptor (Cascieri et al., 1999), with no studies testing other members of the secretin/glucagon family. The receptors in this family show high selectivity for their ligands (Runge et al., 2003), but since L168,049 is an allosteric antagonist, off-target effects cannot be ruled out and should be subject to further study.

When the concentration of L168,049 was decreased to 500 nM, the same tendencies of frequency and amplitude change could be seen in the distributions of the events, but only the average amplitude suffered a significant alteration. The fact that the changes in amplitude and decay time of the events can still be seen in the overall event distributions suggests the effect of L168,049 is maintained, but as the change in IPSC frequency is no longer significant, it suggests it still retains antagonistic effects on glucagon receptors.

Finally, using a concentration of 250 nM produced no change in the frequency or decay times of events, even with the addition of glucagon. However, a change in the distribution of the amplitudes to lower values was seen, that was normalized when glucagon was added to the bath solution, suggesting that, at this concentration, L168,049 no longer fully abolished glucagon activity.

It will be of interest to test other types of GCR antagonists such as the peptidyl antagonists [des-His[1],des-*Phe*[6],Glu[9]]-glucagon-NH_2 and [des-His[1], Glu[9]]-glucagon-NH_2, as these have been previously used in the study of the effects of glucagon on myopia (M. P. Feldkaemper & Schaeffel, 2002; Vessey, Lencses, et al., 2005).

The glucagon-mediated increase in RBC glycinergic IPSC frequency is dependent on dopaminergic activity

Dopamine has been shown to control the inhibitory activity of RBCs, but the available studies are limited to GABAergic activity (Flood et al., 2018; Travis et al., 2018). The current study was designed to study the role of dopaminergic neuromodulation of RBC glycinergic activity and of its regulation by glucagon, as this interaction could give hints about the physiopathology of myopia.

In the case of D1R, antagonism of this receptor family produced the abolition of the glucagon-mediated increase in glycinergic IPSC frequency, with no changes on the average frequency when added alone. This suggests an involvement of D1R activity, as it is necessary for the effect of glucagon on glycinergic IPSCs. The IPSC frequency change was associated with an amplitude decrease seen with the addition of the D1R antagonist alone, that persisted when glucagon was added, suggesting an effect of D1R activity on RBC glycinergic IPSC amplitude. A similar effect has been reported, for example in rat prefrontal cortex, where dopamine application reduced IPSC amplitude in pyramidal neurons, in a D1R dependent and pre-synaptic manner (Gonzalez-Islas & Hablitz, 2001). On the other hand, prior evidence also shows that dopamine can decrease IPSC amplitude by directly modulating post-synaptic $GABA_A$ receptors in rat neostriatal neurons (Flores-Hernandez et al., 2000). It is of interest that the addition of the D1R antagonist produced a shift in the decay times of the events to higher values, but this was only seen when using glutamate stimulation. As this stimulation is closer to a physiological response, this could be due to different cellular groups being recruited.

In the case of D2R antagonism, the glucagon-mediated increase in glycinergic IPSC frequency was preserved, with no change in the average frequency when the antagonist was added by itself, effectively discarding a role of D2R activity in the regulation of the effect of glucagon on glycinergic activity. A shift in amplitude to lower values was also observed in this case, but it is also associated with a shift in the decay times to higher values when the antagonist is added alone, and persists with the addition of glucagon, suggesting these D2R-related effects on amplitude depend on a different circuit within the retina.

As dopamine levels are regulated by light levels (Iuvone et al., 1978; Landis et al., 2021) and its concentration in the retina decreases in scotopic conditions (Doyle et al., 2002; Goel & Mangel, 2021), recordings were performed in dark-adapted mice under scotopic conditions, to compare the results with those observed in the pharmacologic antagonism experiments. The effects of the scotopic condition were comparable with those seen under D1R antagonism, with an abolition of the glucagon-mediated increase in glycinergic IPSC frequency and a decrease in IPSC amplitude, but not associated with a change in the decay times.

These results suggests that retinal low dopamine conditions are associated with an abolition of the effect of glucagon, and with a decrease in the amplitude of glycinergic IPSCs, and this effect is mediated by decreased D1R activity. Further study is necessary to determine how the amacrine cells involved in this pathway are connected and if they correspond to any specific known subtype.

The glucagon-mediated increase in RBC glycinergic IPSC frequency is abolished, and the glucagon effect profile shifted, in a murine myopia model

To study how the observed effect of glucagon on glycinergic activity is affected in myopic conditions, a murine LIM model was used. The model involves the placement of a -10 D lens over one of the eyes of the animal, which has been shown to induce the development of myopia in the

affected eye (Barathi et al., 2008; Jiang et al., 2018). The lens was kept for a period of 2 or 3 weeks, and experiments were conducted at these two time points.

After a period of 2 weeks of exposure to the lens, the effect of glucagon on RBC glycinergic IPSC frequency is still present, but a decrease in IPSC amplitude can be seen. After 3 weeks, the glucagon-mediated increase in glycinergic IPSC frequency is abolished, and a marked decrease in amplitude can be observed. This profile is compatible with the one seen under D1R antagonism and in scotopic conditions, which can be related to the fact that dopamine activity is decreased in myopic conditions (M. Feldkaemper & Schaeffel, 2013; Zhou et al., 2017). In addition, after 3 weeks, a shift to higher decay times is associated with the application of glucagon, which combined with the change in amplitude can be considered a shift of the effect of glucagon, as it recruits a different set of events under myopic conditions.

The changes of the glucagon effect on RBC glycinergic IPSCs in a myopia model are mediated by D1R activity

To study the dependency of the changes in the glucagon effect on dopaminergic activity, the effect of the addition of dopamine receptor agonists was studied.

When a D1R agonist was used, there was an increase in glycinergic IPSC frequency when it was added alone, and the increase persisted when glucagon was added. There was also an effect on the IPSC amplitude, with an increase of the average amplitude when the agonist was added, this increase being related with the presence of a second, high amplitude mode in the event distribution.

At 3 weeks, the increase in IPSC frequency with the addition of the agonist can still be seen, but the amplitude decrease reappears, and the second high-amplitude mode is absent.

The results thus far suggest that the increase in RBC glycinergic activity produced by glucagon is dependent on D1R activity, and this activity is decreased in low dopamine contexts, such as

scotopic and myopic conditions, abolishing said effect. Agonism of D1R recovers the effect in the case of the myopic animal model, for at least up to 3 weeks of induction.

When a D2R agonist is used in a 2-week myopia model, the abolition of the glucagon-mediated increase in glycinergic IPSC frequency persists, also associated with a decrease in IPSC amplitude. Taking this and the previous results into consideration, D2R activity seems to not be related to the effects of glucagon on glycinergic activity.

The decrease in amplitude seems to be caused by a more complex circuitry, as it can be seen in both D1R and D2R antagonism, and the agonism of either family is not enough to recover baseline levels. Both cases are also associated with a consistent pattern of shift to higher decay time values under D2R antagonism, with no change under D1R antagonism alone, suggesting D2R activity is related to the maintenance of a subset of low decay time glycinergic events in RBCs.

When a cocktail of receptor blockers is used to isolate the activity acting on RBCs and glycine is administered on the axon terminal in a myopia murine model, it can be seen that glucagon addition does not produce a significant change in the glycine-evoked response, suggesting the effect on IPSC amplitude is of pre-synaptic origin.

A cross-talk between GABA and glycine receptors has been shown in different neurons of the CNS (Tang et al., 2020; Trombley et al., 1999), so the effect of GABA receptor blockade over IPSC amplitude was tested on scotopic conditions. Neither $GABA_A$ nor $GABA_{A\text{-}\rho}$ receptor antagonism abolished the decrease in amplitude observed, ruling out these pathways as the possible mechanism for the effect of glucagon on IPSC amplitude observed under these conditions. Further tests focusing on other possible receptors modulating glycinergic transmission, such as $GABA_B$ (O'Brien et al., 2004), are necessary.

The possible circuit involved in glucagonergic modulation of RBC glycinergic activity

The most probable source of glucagon in the retina are glucagonergic amacrine cells; these have been described in the chicken retina as wide-field cells with processes extending into the IPL (Fischer et al., 2006a), however, no data are available about these cells in the mammalian retina.

Since the data shown here suggests that the effect of glucagon is dependent on the activity of dopamine receptors, specifically D1R, and glucagon application does not revert the effect of D1R antagonism, D1R seems to be downstream of glucagonergic signaling. This could indicate that glucagonergic amacrine cells regulate the activity of DACs, and direct recording of these cells would be a useful tool to determine whether this is the case.

At the other end of this pathway are RBCs, which receive glycinergic input from small-field glycinergic amacrine cells. These cells comprise more than 10 different morphological types (Wässle, 2009), and innervate RBCs primarily on their axon terminals (Cui et al., 2003; Haverkamp et al., 2003, 2004), which is consistent with the observation in the current study that axotomized RBCs do not display glycinergic IPSCs.

The question of how these two sides of the glucagonergic-glycinergic regulation pathway interact with each other remains difficult to explain with the data available from this study. GABAergic activity seems to play a role, as both $GABA_A$ and $GABA_{A\text{-}\rho}$ signaling change glycinergic IPSC frequency in photopic and scotopic conditions respectively, but the available evidence shows that the glycinergic amacrine cells making synapses with RBCs do not receive regulation from GABAergic pathways (Chen et al., 2011; Eggers & Lukasiewicz, 2006), and that $GABA_{A\text{-}\rho}$ is specific to RBC terminals, with serial inhibition between amacrine cells being mediated via $GABA_A$ receptors (Eggers & Lukasiewicz, 2006). This rules out the possibility of the glycinergic amacrine cell directly innervating the recorded RBC being the direct target of glucagon/dopamine-induced GABAergic modulation.

Another possibility is that the GABAergic signaling acts upon cone BCs, as these cells express both $GABA_A$ and $GABA_{A\text{-}\rho}$ receptors (Wässle, 2009). The available evidence suggests that the glycinergic amacrine cells innervating RBCs receive glutamatergic input from both ON and OFF BCs, primarily via NMDA and AMPA receptors (Chávez & Diamond, 2008), and both types of BCs express both $GABA_A$ and $GABA_{A\text{-}\rho}$, with inhibitory activity in ON BC corresponding predominantly to $GABA_{A\text{-}\rho}$ signaling and OFF BC inhibitory activity to $GABA_A$ signaling (Popova, 2014). Thus, GABA acting differentially on ON and OFF BCs can regulate the subsequent level of activation of glycinergic amacrine cells.

This is also related to the difference in the effect of selective GABAergic antagonism under photopic and scotopic conditions, as evidence shows a role of a sustained $GABA_{A\text{-}\rho}$ input in the regulation of ON BCs under scotopic conditions (Herrmann et al., 2011; B. J. Smith et al., 2013). This higher dependency of scotopic BC inhibitory signaling on $GABA_{A\text{-}\rho}$ activity could explain why its antagonism has an effect primarily under scotopic conditions. An overview of the possible pathways is presented in Fig. 43.

Selective blockade of ON/OFF pathways and direct recordings of ON BCs to study the effects of glucagonergic activity will be useful first steps to get a better understanding of this complex signaling pathway.

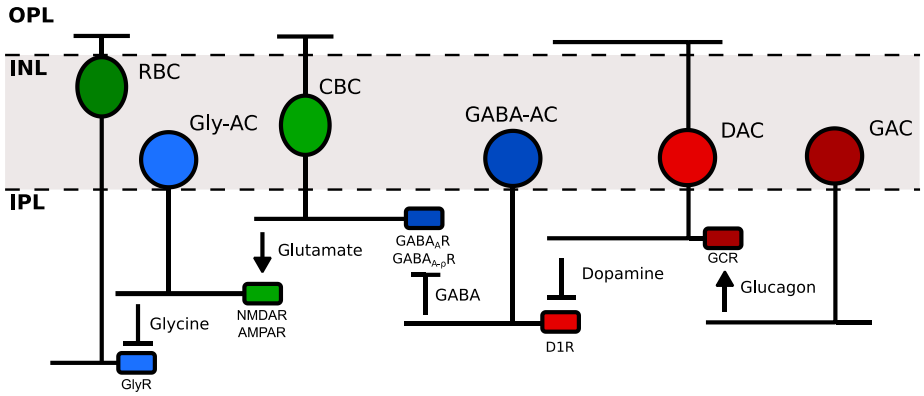

Figure 43. Possible pathways involved in glucagonergic signaling. Glucagonergic amacrine cells (GAC) are the most probable source for glucagon within the retina, with dopaminergic signaling from dopaminergic amacrine cells (DAC) acting downstream and modulating the activity of the glycinergic amacrine cells (Gly-AC) innervating RBCs. This modulation acts through GABAergic signaling, originating from GABAergic amacrine cells (GABA-AC) and acting upon cone bipolar cells (CBC), which are the cells in charge of regulating Gly-AC activity.

Glucagon as a novel neuromodulator of RBC glycinergic activity

Taking all these results together, glucagon emerges as a novel neuromodulator in the retina of mice and possibly other mammals, with a role in the regulation of the inhibitory activity received by RBCs. Glucagonergic activity increases the frequency of glycinergic IPSCs in these cells, in a D1R receptor-dependent manner. The latter result goes against the initial hypothesis that glucagon is in charge of dopamine release and suggests it works in the opposite way, with dopamine being necessary for glucagon to exert its role. This is also related to the fact that myopia produced the abolition of the effect of glucagon on glycinergic IPSCs, which was restored with D1R agonism, confirming once again dopamine as a central molecule in the development of myopia.

As there are no data available about the types of amacrine cells in charge of glucagon production in the mammalian retina, whose detection has proven to be difficult (M. Feldkaemper et al., 2004), and the limitations associated with the approach centered on RBCs, it is difficult to achieve a complete picture of the circuitry involved in glucagonergic signaling. Although GCR has been detected in the retina of mice (M. Feldkaemper et al., 2004), the cells in which it is expressed have

not been specified. The results obtained suggest a pre-synaptic effect of glucagon, which rules out RBCs a priori, leaving amacrine cells as the likely candidates. Whether the amacrine cell expressing the GCR is the same cell as the glycinergic amacrine cell acting directly on RBCs or it is a secondary amacrine cell regulating the glycinergic cell via serial inhibition cannot be conclusively answered with the data obtained in this study. Another question left open regarding the circuitry involved is the location of the D1Rs as these could either be located on the glucagonergic amacrine cells, the glycinergic amacrine cells or on an intermediate amacrine cell, making further research in this topic necessary.

Another important question that arises is the functional role of glucagon during normal vision. Glycinergic activity is linked to the lateral feedback received by RBCs during light stimulation (Bligard et al., 2020) and overall glycinergic activity is related to ON-OFF cross-talk, which plays a role in functions such as contrast sensitivity (Popova, 2015). How glucagonergic activity modulates these functions and what the implications of its alteration in myopic conditions are remains to be uncovered. In addition, how the role of glucagon relates to the levels of Egr-1 expression and to the sensing of the sign of image defocus, and how this information is passed on to the glucagonergic system could not be answered here.

Conclusion

Overall, the physiological data and pharmacological manipulations of the present study support a role of glucagon as a neuromodulator in the mouse retina, specifically increasing the frequency of the glycinergic inhibitory activity received by the axon terminals of RBCs under photopic conditions, this is the first description of such a function of glucagon in the CNS.

This glucagonergic activity is in turn dependent on dopaminergic signaling through dopamine D1 receptors, as its specific antagonism and conditions associated with low dopamine levels, such as scotopic conditions, abolish the effect of glucagon. Moreover, this interaction is disrupted in a

murine myopia model, with an abolition of the effect of glucagon over RBC glycinergic activity that can be rescued using dopamine D1R agonism. These results show an also novel interaction pathway between glucagon and dopamine in the inner retina.

The glucagonergic retinal pathway, and its interaction with retinal dopaminergic signaling opens new research targets that could help further the understanding of complex retinal functions such as contrast sensitivity, and also, as the dysfunction of this system is associated with the pathogenesis of myopia, it could be useful to shed light on the processes behind this pathology and be a future target for the development of new options for myopia prevention and treatment.

More research is clearly needed to elucidate a full picture of the role of glucagon as a neuromodulator in the mammalian retina, its functions under normal and pathological conditions and the possible utility it may present as a therapeutic target candidate.

REFERENCES

Abraham, M. A., & Lam, T. K. T. (2016). Glucagon action in the brain. *Diabetologia*, *59*(7), 1367–1371. https://doi.org/10.1007/s00125-016-3950-3

Acuna-Goycolea, C. (2004). Glucagon-Like Peptide 1 Excites Hypocretin/Orexin Neurons by Direct and Indirect Mechanisms: Implications for Viscera-Mediated Arousal. *Journal of Neuroscience*, *24*(37), 8141–8152. https://doi.org/10.1523/JNEUROSCI.1607-04.2004

Adelhorst, K., Hedegaard, B. B., Knudsen, L. B., & Kirk, O. (1994). Structure-activity studies of glucagon-like peptide-1. *Journal of Biological Chemistry*, *269*(9), 6275–6278. https://doi.org/10.1016/s0021-9258(17)37366-0

Ashby, R., Kozulin, P., Megaw, P. L., & Morgan, I. G. (2010). Alterations in ZENK and glucagon RNA transcript expression during increased ocular growth in chickens. *Molecular Vision*, *16*(April), 639–649.

Ashby, R., McCarthy, C. S., Maleszka, R., Megaw, P., & Morgan, I. G. (2007). A muscarinic cholinergic antagonist and a dopamine agonist rapidly increase ZENK mRNA expression in the form-deprived chicken retina. *Experimental Eye Research*, *85*(1), 15–22. https://doi.org/10.1016/j.exer.2007.02.019

Barathi, V. A., Boopathi, V. G., Yap, E. P. H., & Beuerman, R. W. (2008). Two models of experimental myopia in the mouse. *Vision Research*, *48*(7), 904–916. https://doi.org/10.1016/j.visres.2008.01.004

Beaulieu, J.-M., & Gainetdinov, R. R. (2011). The Physiology, Signaling, and Pharmacology of Dopamine Receptors. *Pharmacological Reviews*, *63*(1), 182–217. https://doi.org/10.1124/pr.110.002642

Bitzer, M., & Schaeffel, F. (2002). Defocus-induced changes in ZENK expression in the chicken retina. *Investigative Ophthalmology and Visual Science*, *43*(1), 246–252.

Bjelke, B., Goldstein, M., Tinner, B., Andersson, C., Sesack, S. R., Steinbusch, H. W. M., Lew, J. Y., He, X., Watson, S., Tengroth, B., & Fuxe, K. (1996). Dopaminergic transmission in the rat retina: Evidence for volume transmission. *Journal of Chemical Neuroanatomy*, *12*(1), 37–50. https://doi.org/10.1016/S0891-0618(96)00176-7

Bligard, G. W., DeBrecht, J., Smith, R. G., & Lukasiewicz, P. D. (2020). Light-evoked glutamate transporter EAAT5 activation coordinates with conventional feedback inhibition to control rod bipolar cell output. *Journal of Neurophysiology*, *123*(5), 1828–1837. https://doi.org/10.1152/jn.00527.2019

Cakmak, A. I., Basmak, H., Gursoy, H., Ozkurt, M., Yildirim, N., Erkasap, N., Bilgec, M. D.,

Tuncel, N., & Colak, E. (2017). Vasoactive intestinal peptide, a promising agent for myopia? *International Journal of Ophthalmology*, *10*(2), 211–216. https://doi.org/10.18240/ijo.2017.02.05

Carr, B. J., & Stell, W. K. (1995). The Science Behind Myopia. In *Webvision: The Organization of the Retina and Visual System* (Issue 4). http://www.ncbi.nlm.nih.gov/pubmed/29266913

Carr, B. J., & Stell, W. K. (2017). The Science Behind Myopia. In *Webvision: The Organization of the Retina and Visual System*. http://www.ncbi.nlm.nih.gov/pubmed/29266913

Cascieri, M. A., Koch, G. E., Ber, E., Sadowski, S. J., Louizides, D., De Laszlo, S. E., Hacker, C., Hagmann, W. K., MacCoss, M., Chicchi, G. G., & Vicario, P. P. (1999). Characterization of a novel, non-peptidyl antagonist of the human glucagon receptor. *Journal of Biological Chemistry*, *274*(13), 8694–8697. https://doi.org/10.1074/jbc.274.13.8694

Chávez, A. E., & Diamond, J. S. (2008). Diverse mechanisms underlie glycinergic feedback transmission onto rod bipolar cells in rat retina. *Journal of Neuroscience*, *28*(31), 7919–7928. https://doi.org/10.1523/JNEUROSCI.0784-08.2008

Chen, X., HSUEH, H. A., & WERBLIN, F. S. (2011). Amacrine-to-amacrine cell inhibition: Spatiotemporal properties of GABA and glycine pathways. *Visual Neuroscience*, *28*(3), 193–204. https://doi.org/10.1017/S0952523811000137

Cui, J., Ma, Y., Lipton, S. A., & Pan, Z. (2003). Glycine Receptors and Glycinergic Synaptic Input at the Axon Terminals of Mammalian Retinal Rod Bipolar Cells. *The Journal of Physiology*, *553*(3), 895–909. https://doi.org/10.1113/jphysiol.2003.052092

Das, A., Pansky, B., & Budd, G. C. (1985). Glucagon-like immunoreactivity in mouse and rat retina. *Neuroscience Letters*, *60*(2), 215–218. https://doi.org/10.1016/0304-3940(85)90246-0

De Laszlo, S. E., Hacker, C., Li, B., Kim, D., MacCoss, M., Mantlo, N., Pivnichny, J. V., Colwell, L., Koch, G. E., Cascieri, M. A., & Hagmann, W. K. (1999). Potent, orally absorbed glucagon receptor antagonists. *Bioorganic and Medicinal Chemistry Letters*, *9*(5), 641–646. https://doi.org/10.1016/S0960-894X(99)00081-5

Diether, S., & Schaeffel, F. (1997). Local Changes in Eye Growth Induced by Imposed Local Refractive Error Depite Active Accomodation. *Vision Research*, *37*(6), 659–668.

Djamgoz, M. B. A., & Wagner, H. J. (1992). Localization and function of dopamine in the adult vertebrate retina. *Neurochemistry International*, *20*(2), 139–191. https://doi.org/10.1016/0197-0186(92)90166-O

Dolgin, E. (2015). The myopia boom. *Nature*, *519*(7543), 276–278. https://doi.org/10.1038/519276a

Dong, F., Zhi, Z., Pan, M., Xie, R., Qin, X., Lu, R., Mao, X., Chen, J. F., Willcox, M. D. P., Qu, J., & Zhou, X. (2011). Inhibition of experimental myopia by a dopamine agonist: Different effectiveness between form deprivation and hyperopic defocus in guinea pigs. *Molecular Vision*, *17*(August), 2824–2834.

Doyle, S. E., McIvor, W. E., & Menaker, M. (2002). Circadian rhythmicity in dopamine content of mammalian retina: Role of the photoreceptors. *Journal of Neurochemistry*, *83*(1), 211–219. https://doi.org/10.1046/j.1471-4159.2002.01149.x

Eggers, E. D., & Lukasiewicz, P. D. (2006). GABAA, GABAC and glycine receptor-mediated inhibition differentially affects light-evoked signalling from mouse retinal rod bipolar cells. *Journal of Physiology*, *572*(1), 215–225. https://doi.org/10.1113/jphysiol.2005.103648

Eggers, E. D., & Lukasiewicz, P. D. (2011). Multiple pathways of inhibition shape bipolar cell responses in the retina. *Visual Neuroscience*, *28*(1), 95–108. https://doi.org/10.1017/S0952523810000209

Eggers, E. D., Mazade, R. E., & Klein, J. S. (2013). Inhibition to retinal rod bipolar cells is regulated by light levels. *Journal of Neurophysiology*, *110*(1), 153–161. https://doi.org/10.1152/jn.00872.2012

Elgueta, C., Leroy, F., Vielma, A. H., Schmachtenberg, O., & Palacios, A. G. (2018). Electrical coupling between A17 cells enhances reciprocal inhibitory feedback to rod bipolar cells. *Scientific Reports*, *8*(1), 3123. https://doi.org/10.1038/s41598-018-21119-0

Feldkaemper, M., Burkhardt, E., & Schaeffel, F. (2004). Localization and regulation of glucagon receptors in the chick eye and preproglucagon and glucagon receptor expression in the mouse eye. *Experimental Eye Research*, *79*(3), 321–329. https://doi.org/10.1016/j.exer.2004.04.009

Feldkaemper, M. P., & Schaeffel, F. (2002). Evidence for a potential role of glucagon during eye growth regulation in chicks. *Visual Neuroscience*, *19*(6), 755–766. https://doi.org/10.1017/S0952523802196064

Feldkaemper, M., & Schaeffel, F. (2013). An updated view on the role of dopamine in myopia. *Experimental Eye Research*, *114*, 106–119. https://doi.org/10.1016/j.exer.2013.02.007

Fernandez-Durango, R., Sanchez, D., & Fernandez-Cruz, A. (1990). Identification of Glucagon Receptors in Rat Retina. *Journal of Neurochemistry*, *54*(4), 1233–1237. https://doi.org/10.1111/j.1471-4159.1990.tb01953.x

Fischer, A. J., McGuire, J. J., Schaeffel, F., & Stell, W. K. (1999). Light-and focus-dependent expression of the transcription factor ZENK in the chick retina. *Nature Neuroscience*, *2*(8), 705–712. https://doi.org/10.1038/11167

Fischer, A. J., Skorupa, D., Schonberg, D. L., & Walton, N. A. (2006a). Characterization of glucagon-expressing neurons in the chicken retina. *The Journal of Comparative Neurology*, *496*(4), 479–494. https://doi.org/10.1002/cne.20937

Fischer, A. J., Skorupa, D., Schonberg, D. L., & Walton, N. A. (2006b). Characterization of glucagon-expressing neurons in the chicken retina. *The Journal of Comparative Neurology*, *496*(4), 479–494. https://doi.org/10.1002/cne.20937

Flitcroft, D. I., He, M., Jonas, J. B., Jong, M., Naidoo, K., Ohno-Matsui, K., Rahi, J., Resnikoff, S., Vitale, S., & Yannuzzi, L. (2019). IMI – Defining and Classifying Myopia: A Proposed Set of Standards for Clinical and Epidemiologic Studies. *Investigative Opthalmology & Visual Science*, *60*(3), M20. https://doi.org/10.1167/iovs.18-25957

Flood, M. D., Moore-Dotson, J. M., & Eggers, E. D. (2018). Dopamine D1 receptor activation contributes to light-adapted changes in retinal inhibition to rod bipolar cells. *Journal of Neurophysiology*, *120*(2), 867–879. https://doi.org/10.1152/jn.00855.2017

Flores-Hernandez, J., Hernandez, S., Snyder, G. L., Yan, Z., Fienberg, A. A., Moss, S. J., Greengard, P., & Surmeier, D. J. (2000). D 1 Dopamine Receptor Activation Reduces GABA A Receptor Currents in Neostriatal Neurons Through a PKA/DARPP-32/PP1 Signaling Cascade. *Journal of Neurophysiology*, *83*(5), 2996–3004. https://doi.org/10.1152/jn.2000.83.5.2996

Fortin, S. M., Lipsky, R. K., Lhamo, R., Chen, J., Kim, E., Borner, T., Schmidt, H. D., & Hayes, M. R. (2020). GABA neurons in the nucleus tractus solitarius express GLP-1 receptors and mediate anorectic effects of liraglutide in rats. *Science Translational Medicine*, *12*(533).

https://doi.org/10.1126/scitranslmed.aay8071

Frederick, J. M., Rayborn, M. E., Laties, A. M., Lam, D. M., & Hollyfield, J. G. (1982). Dopaminergic neurons in the human retina. *J Comp Neurol*, *210*(1), 65–79. https://doi.org/10.1002/cne.902100108

Gao, Q., Liu, Q., Ma, P., Zhong, X. W., Wu, J., & Ge, J. (2006). Effects of direct intravitreal dopamine injections on the development of lid-suture induced myopia in rabbits. *Graefe's Archive for Clinical and Experimental Ophthalmology*, *244*(10), 1329–1335. https://doi.org/10.1007/s00417-006-0254-1

Ghosh, K. K., Bujan, S., Haverkamp, S., Feigenspan, A., & Wässle, H. (2004). Types of Bipolar Cells in the Mouse Retina. *Journal of Comparative Neurology*, *469*(1), 70–82. https://doi.org/10.1002/cne.10985

Goel, M., & Mangel, S. C. (2021). Dopamine-Mediated Circadian and Light/Dark-Adaptive Modulation of Chemical and Electrical Synapses in the Outer Retina. *Frontiers in Cellular Neuroscience*, *15*(May), 1–18. https://doi.org/10.3389/fncel.2021.647541

Gonzalez-Islas, C., & Hablitz, J. J. (2001). Dopamine Inhibition of Evoked IPSCs in Rat Prefrontal Cortex. *Journal of Neurophysiology*, *86*(6), 2911–2918. https://doi.org/10.1152/jn.2001.86.6.2911

Green, B. D., Gault, V. A., Flatt, P. R., Harriott, P., Greer, B., & O'Harte, F. P. M. (2004). Comparative effects of GLP-1 and GIP on cAMP production, insulin secretion, and in vivo antidiabetic actions following substitution of Ala 8/Ala2 with 2-aminobutyric acid. *Archives of Biochemistry and Biophysics*, *428*(2), 136–143. https://doi.org/10.1016/j.abb.2004.05.005

Haverkamp, S., Müller, U., Harvey, K., Harvey, R. J., Betz, H., & Wässle, H. (2003). Diversity of glycine receptors in the mouse retina: Localization of the α3 subunit. *Journal of Comparative Neurology*, *465*(4), 524–539. https://doi.org/10.1002/cne.10852

Haverkamp, S., Müller, U., Zeilhofer, H. U., Harvey, R. J., & Wässle, H. (2004). Diversity of glycine receptors in the mouse retina: Localization of the α2 subunit. *Journal of Comparative Neurology*, *477*(4), 399–411. https://doi.org/10.1002/cne.20267

Herrmann, R., Heflin, S. J., Hammond, T., Lee, B., Wang, J., Gainetdinov, R. R., Caron, M. G., Eggers, E. D., Frishman, L. J., McCall, M. A., & Arshavsky, V. Y. (2011). Rod Vision Is Controlled by Dopamine-Dependent Sensitization of Rod Bipolar Cells by GABA. *Neuron*, *72*(1), 101–110. https://doi.org/10.1016/j.neuron.2011.07.030

Holden, B. A., Fricke, T. R., Wilson, D. A., Jong, M., Naidoo, K. S., Sankaridurg, P., Wong, T. Y., Naduvilath, T. J., & Resnikoff, S. (2016). Global Prevalence of Myopia and High Myopia and Temporal Trends from 2000 through 2050. *Ophthalmology*, *123*(5), 1036–1042. https://doi.org/10.1016/j.ophtha.2016.01.006

Huang, F., Huang, F., Yan, T., Yan, T., Shi, F., Shi, F., An, J., An, J., Xie, R., Xie, R., Zheng, F., Zheng, F., Li, Y., Li, Y., Chen, J., Chen, J., Qu, J., Qu, J., Zhou, X., & Zhou, X. (2014). Activation of dopamine d2 receptor is critical for the development of form-deprivation myopia in the c57bl/6 mouse. *Investigative Ophthalmology and Visual Science*, *55*(9), 5537–5544. https://doi.org/10.1167/iovs.13-13211

Huang, F., Zhang, L., Wang, Q., Yang, Y., Li, Q., Wu, Y., Chen, J., Qu, J., & Zhou, X. (2018). Dopamine D1 receptors contribute critically to the apomorphine-induced inhibition of form-deprivation myopia in mice. *Investigative Ophthalmology and Visual Science*, *59*(6), 2623–2634. https://doi.org/10.1167/iovs.17-22578

Iuvone, P., Galli, C., Garrison-Gund, C., & Neff, N. (1978). Light stimulates tyrosine hydroxylase activity and dopamine synthesis in retinal amacrine neurons. *Science*, *202*(4370), 901–902. https://doi.org/10.1126/science.30997

Ivanova, E., Müller, U., & Wässle, H. (2006). Characterization of the glycinergic input to bipolar cells of the mouse retina. *European Journal of Neuroscience*, *23*(2), 350–364. https://doi.org/10.1111/j.1460-9568.2005.04557.x

Jelinek, L. J., Lok, S., Rosenberg, G. B., Smith, R. A., Grant, F. J., Biggs, S., Bensch, P. A., Kuijper, J. L., Sheppard, P. O., Sprecher, C. A., O'Hara, P. J., Foster, D., Walker, K. M., Chen, L. H. J., McKernan, P. A., & Kindsvogel, W. (1993). Expression cloning and signaling properties of the rat glucagon receptor. *Science*, *259*(5101), 1614–1616. https://doi.org/10.1126/science.8384375

Jiang, X., Kurihara, T., Kunimi, H., Miyauchi, M., Ikeda, S. I., Mori, K., Tsubota, K., Torii, H., & Tsubota, K. (2018). A highly efficient murine model of experimental myopia. *Scientific Reports*, *8*(1), 1–12. https://doi.org/10.1038/s41598-018-20272-w

Jonas, J. B., Holbach, L., & Panda-Jonas, S. (2014). Bruch′s membrane thickness in high myopia. *Acta Ophthalmologica*, *92*(6), e470–e474. https://doi.org/10.1111/aos.12372

Jonas, J. B., Holbach, L., & Panda-Jonas, S. (2016). Histologic differences between primary high myopia and secondary high myopia due to congenital glaucoma. *Acta Ophthalmologica*, *94*(2), 147–153. https://doi.org/10.1111/aos.12937

Jorgensen, R., Kubale, V., Vrecl, M., Schwartz, T. W., & Elling, C. E. (2007). Oxyntomodulin differentially affects glucagon-like peptide-1 receptor β-arrestin recruitment and signaling through Gαs. *Journal of Pharmacology and Experimental Therapeutics*, *322*(1), 148–154. https://doi.org/10.1124/jpet.107.120006

Jung, S. K., Lee, J. H., Kakizaki, H., & Jee, D. (2012). Prevalence of myopia and its association with body stature and educational level in 19-year-old male conscripts in Seoul, South Korea. *Investigative Ophthalmology and Visual Science*, *53*(9), 5579–5583. https://doi.org/10.1167/iovs.12-10106

Kim, Y. C., Jung, K. I., Park, H. Y. L., & Park, C. K. (2017). Three-Dimensional Evaluation of Posterior Pole and Optic Nerve Head in Myopes with Glaucoma. *Scientific Reports*, *7*(1), 1–12. https://doi.org/10.1038/s41598-017-18297-8

Korol, S. V., Jin, Z., Babateen, O., & Birnir, B. (2015). GLP-1 and Exendin-4 Transiently Enhance GABAA Receptor–Mediated Synaptic and Tonic Currents in Rat Hippocampal CA3 Pyramidal Neurons. *Diabetes*, *64*(1), 79–89. https://doi.org/10.2337/db14-0668

Landis, E. G., Park, H. N., Chrenek, M., He, L., Sidhu, C., Chakraborty, R., Strickland, R., Iuvone, P. M., & Pardue, M. T. (2021). Ambient Light Regulates Retinal Dopamine Signaling and Myopia Susceptibility. *Investigative Opthalmology & Visual Science*, *62*(1), 28. https://doi.org/10.1167/iovs.62.1.28

Long, Y., Seilheimer, R. L., & Wu, S. M. (2020). Glycinergic and GABAergic interneurons shift the location and differentially alter the size of ganglion cell receptive field centers in the mammalian retina. *Vision Research*, *170*(March), 18–24. https://doi.org/10.1016/j.visres.2020.03.002

Ma, M., Xiong, S., Zhao, S., Zheng, Z., Sun, T., & Li, C. (2021). COVID-19 Home Quarantine Accelerated the Progression of Myopia in Children Aged 7 to 12 Years in China. *Investigative Opthalmology & Visual Science*, *62*(10), 37. https://doi.org/10.1167/iovs.62.10.37

MacNeil, M. A., & Masland, R. H. (1998). Extreme diversity among amacrine cells: Implications for function. *Neuron*, *20*(5), 971–982. https://doi.org/10.1016/S0896-6273(00)80478-X

Mathis, U., & Schaeffel, F. (2007). Glucagon-related peptides in the mouse retina and the effects of deprivation of form vision. *Graefe's Archive for Clinical and Experimental Ophthalmology*, *245*(2), 267–275. https://doi.org/10.1007/s00417-006-0282-x

Matsumura, S., Ching-Yu, C., & Saw, S.-M. (2020). Global Epidemiology of Myopia. In *Updates on Myopia* (pp. 27–51). Springer Singapore. https://doi.org/10.1007/978-981-13-8491-2_2

McBrien, N. A., & Millodot, M. (1987). A biometric investigation of late onset myopic eyes. *Acta Ophthalmologica*, *65*(4), 461–468. https://doi.org/10.1111/j.1755-3768.1987.tb07024.x

Mcbrien, N. A., Moghaddam, H. O., Cottriall, C. L., Leech, E. M., & Cornell, L. M. (1995). The effects of blockade of retinal cell action potentials on ocular growth, emmetropization and form deprivation myopia in young chicks. *Vision Research*, *35*(9), 1141–1152. https://doi.org/10.1016/0042-6989(94)00237-G

McCarthy, C. S., Megaw, P., Devadas, M., & Morgan, I. G. (2007). Dopaminergic agents affect the ability of brief periods of normal vision to prevent form-deprivation myopia. *Experimental Eye Research*, *84*(1), 100–107. https://doi.org/10.1016/j.exer.2006.09.018

McClean, P. L., Gault, V. A., Harriott, P., & Hölscher, C. (2010). Glucagon-like peptide-1 analogues enhance synaptic plasticity in the brain: A link between diabetes and Alzheimer's disease. *European Journal of Pharmacology*, *630*(1–3), 158–162. https://doi.org/10.1016/j.ejphar.2009.12.023

Menger, N., Pow, D. V., & Wässle, H. (1998). Glycinergic amacrine cells of the rat retina. *Journal of Comparative Neurology*, *401*(1), 34–46. https://doi.org/10.1002/(SICI)1096-9861(19981109)401:1<34::AID-CNE3>3.0.CO;2-P

Menger, N., & Wässle, H. (2000). Morphological and physiological properties of the A17 amacrine cell of the rat retina. *Visual Neuroscience*, *17*(5), 769–780. https://doi.org/10.1017/S0952523800175108

Miura, K. (2020). Bleach correction ImageJ plugin for compensating the photobleaching of time-lapse sequences. *F1000Research*, *9*, 1–17. https://doi.org/10.12688/f1000research.27171.1

Mora, F., Expösito, I., Sanz, B., & E., B. (1992). Selective release of glutamine and glutamic acid produced by perfusion of GLP-1(7–36) amide in the basal ganglia of the conscious rat. *Brain Research Bulletin*, *29*(3–4), 359–361. https://doi.org/10.1016/0361-9230(92)90068-9

Müller, T. D., Finan, B., Clemmensen, C., Di Marchi, R. D., & Tschöp, M. H. (2017). The new biology and pharmacology of glucagon. In *Physiological Reviews* (Vol. 97, Issue 2). https://doi.org/10.1152/physrev.00025.2016

Nickla, D. L., & Totonelly, K. (2011). Dopamine antagonists and brief vision distinguish lens-induced- and form-deprivation-induced myopia. *Experimental Eye Research*, *93*(5), 782–785. https://doi.org/10.1016/j.exer.2011.08.001

Nickla, D. L., Totonelly, K., & Dhillon, B. (2010). Dopaminergic agonists that result in ocular growth inhibition also elicit transient increases in choroidal thickness in chicks. *Experimental Eye Research*, *91*(5), 715–720. https://doi.org/10.1016/j.exer.2010.08.021

Norton, T. T., Essinger, J. A., & Mcbrien, N. A. (1994). Lid-suture myopia in tree shrews with retinal ganglion cell blockade. *Visual Neuroscience*, *11*(1), 143–153. https://doi.org/10.1017/S0952523800011184

O'Brien, J. A., Sebe, J. Y., & Berger, A. J. (2004). GABAB modulation of GABAA and glycine receptor-mediated synaptic currents in hypoglossal motoneurons. *Respiratory Physiology & Neurobiology*, *141*(1), 35–45. https://doi.org/10.1016/j.resp.2004.03.009

Pardue, M. T., Stone, R. A., & Iuvone, P. M. (2013). Investigating mechanisms of myopia in mice. *Experimental Eye Research*, *114*, 96–105. https://doi.org/10.1016/j.exer.2012.12.014

Parmet, W. E., & Sinha, M. S. (2020). Covid-19 — The Law and Limits of Quarantine. *New England Journal of Medicine*, *382*(15), e28. https://doi.org/10.1056/NEJMp2004211

Patton, T. B., Uysal, A. K., Kellogg, S. L., & Shimizu, T. (2017). Brain Mapping Using the Immediate Early Gene Zenk. In *Lateralized brain functions* (Vol. 122, Issue 3, pp. 313–329). https://doi.org/10.1007/978-1-4939-6725-4_10

Popova, E. (2014). Ionotropic GABA Receptors and Distal Retinal ON and OFF Responses. *Scientifica*, *2014*, 1–23. https://doi.org/10.1155/2014/149187

Popova, E. (2015). ON-OFF Interactions in the Retina: Role of Glycine and GABA. *Current Neuropharmacology*, *12*(6), 509–526. https://doi.org/10.2174/1570159X13999150122165018

Qiao, S.-N., Zhang, Z., Ribelayga, C. P., Zhong, Y.-M., & Zhang, D.-Q. (2016). Multiple cone pathways are involved in photic regulation of retinal dopamine. *Scientific Reports*, *6*(1), 28916. https://doi.org/10.1038/srep28916

Rebosio, C., Balbi, M., Passalacqua, M., Ricciarelli, R., & Fedele, E. (2018). Presynaptic GLP-1 receptors enhance the depolarization-evoked release of glutamate and GABA in the mouse cortex and hippocampus. *BioFactors*, *44*(2), 148–157. https://doi.org/10.1002/biof.1406

Remington, L. A. (2012). Retina. In *Clinical Anatomy and Physiology of the Visual System* (pp. 61–92). Elsevier. https://doi.org/10.1016/B978-1-4377-1926-0.10004-9

Rohrer, B., Spira, A. W., & Stell, W. K. (1993). Apomorphine blocks form-deprivation myopia in chickens by a dopamine D 2 -receptor mechanism acting in retina or pigmented epithelium. *Visual Neuroscience*, *10*(3), 447–453. https://doi.org/10.1017/S0952523800004673

Roy, S., & Field, G. D. (2019). Dopaminergic modulation of retinal processing from starlight to sunlight. *Journal of Pharmacological Sciences*, *140*(1), 86–93. https://doi.org/10.1016/j.jphs.2019.03.006

Runge, S., Wulff, B. S., Madsen, K., Bräuner-Osborne, H., & Knudsen, L. B. (2003). Different domains of the glucagon and glucagon-like peptide-1 receptors provide the critical determinants of ligand selectivity. *British Journal of Pharmacology*, *138*(5), 787–794. https://doi.org/10.1038/sj.bjp.0705120

Rymer, J., & Wildsoet, C. F. (2005). The role of the retinal pigment epithelium in eye growth regulation and myopia: A review. *Visual Neuroscience*, *22*(3), 251–261. https://doi.org/10.1017/S0952523805223015

Saw, S. M., Gazzard, G., Shin-Yen, E. C., & Chua, W. H. (2005). Myopia and associated pathological complications. *Ophthalmic and Physiological Optics*, *25*(5), 381–391. https://doi.org/10.1111/j.1475-1313.2005.00298.x

Schaeffel, F., & Feldkaemper, M. (2015). Animal models in myopia research. *Clinical and Experimental Optometry*, *98*(6), 507–517. https://doi.org/10.1111/cxo.12312

Schippert, R., Burkhardt, E., Feldkaemper, M., & Schaeffel, F. (2007). Relative axial myopia in Egr-1 (ZENK) knockout mice. *Investigative Ophthalmology and Visual Science*, *48*(1), 11–

17. https://doi.org/10.1167/iovs.06-0851

Schmid, K. L., & Wildsoet, C. F. (2004). Inhibitory Effects of Apomorphine and Atropine and Their Combination on Myopia in Chicks. *Optometry and Vision Science*, *81*(2), 137–147. https://doi.org/10.1097/00006324-200402000-00012

Smith, B. J., Tremblay, F., & Côté, P. D. (2013). Voltage-gated sodium channels contribute to the b-wave of the rodent electroretinogram by mediating input to rod bipolar cell GABAc receptors. *Experimental Eye Research*, *116*, 279–290. https://doi.org/10.1016/j.exer.2013.09.006

Smith, E. L., Huang, J., Hung, L.-F., Blasdel, T. L., Humbird, T. L., & Bockhorst, K. H. (2009). Hemiretinal Form Deprivation: Evidence for Local Control of Eye Growth and Refractive Development in Infant Monkeys. *Investigative Opthalmology & Visual Science*, *50*(11), 5057. https://doi.org/10.1167/iovs.08-3232

Solmaz, V., Tekatas, A., Erdoğan, M. A., & Erbaş, O. (2020). Exenatide, a GLP-1 analog, has healing effects on LPS-induced autism model: Inflammation, oxidative stress, gliosis, cerebral GABA, and serotonin interactions. *International Journal of Developmental Neuroscience*, *80*(7), 601–612. https://doi.org/10.1002/jdn.10056

Stone, R. A. (2008). Myopia Pharmacology: Etiologic Clues, Therapeutic Potential. In *Ocular Therapeutics* (pp. 167–196). Elsevier. https://doi.org/10.1016/B978-012370585-3.50011-X

Stone, R. A., Lin, T., Laties, A. M., & Iuvone, P. M. (1989). Retinal dopamine and form-deprivation myopia. *Proceedings of the National Academy of Sciences*, *86*(2), 704–706. https://doi.org/10.1073/pnas.86.2.704

Tam, J. K. V., Lee, L. T. O., Jin, J., & Chow, B. K. C. (2014). Molecular evolution of GPCRs: Secretin/secretin receptors. *Journal of Molecular Endocrinology*, *52*(3). https://doi.org/10.1530/JME-13-0259

Tang, Z.-Q., Lu, Y.-G., Huang, Y.-N., & Chen, L. (2020). Cross-talk pattern between GABAA- and glycine-receptors in CNS neurons is shaped by their relative expression levels. *Brain Research*, *1748*(August), 147071. https://doi.org/10.1016/j.brainres.2020.147071

Tkatchenko, T. V., Shen, Y., & Tkatchenko, A. V. (2010). Analysis of Postnatal Eye Development in the Mouse with High-Resolution Small Animal Magnetic Resonance Imaging. *Investigative Opthalmology & Visual Science*, *51*(1), 21. https://doi.org/10.1167/iovs.08-2767

Travis, A. M., Heflin, S. J., Hirano, A. A., Brecha, N. C., & Arshavsky, V. Y. (2018). Dopamine-dependent sensitization of rod bipolar cells by GABA is conveyed through wide-field amacrine cells. *Journal of Neuroscience*, *38*(3), 723–732. https://doi.org/10.1523/JNEUROSCI.1994-17.2017

Troilo, D., Gottlieb, M. D., & Wallman, J. (1987). Visual deprivation causes myopia in chicks with optic nerve section. *Current Eye Research*, *6*(8), 993–999. https://doi.org/10.3109/02713688709034870

Trombley, P. Q., Hill, B. J., & Horning, M. S. (1999). Interactions Between GABA and Glycine at Inhibitory Amino Acid Receptors on Rat Olfactory Bulb Neurons. *Journal of Neurophysiology*, *82*(6), 3417–3422. https://doi.org/10.1152/jn.1999.82.6.3417

Tsukamoto, Y., & Omi, N. (2017). Classification of Mouse Retinal Bipolar Cells: Type-Specific Connectivity with Special Reference to Rod-Driven AII Amacrine Pathways. *Frontiers in Neuroanatomy*, *11*(October), 1–25. https://doi.org/10.3389/fnana.2017.00092

Veruki, M. L., & Wässle, H. (1996). Immunohistochemical localization of dopamine D1 receptors in rat retina. *The European Journal of Neuroscience*, *8*, 2286–2297. https://doi.org/10.1111/j.1460-9568.1996.tb01192.x

Vessey, K. A., Lencses, K. A., Rushforth, D. A., Hruby, V. J., & Stell, W. K. (2005). Glucagon Receptor Agonists and Antagonists Affect the Growth of the Chick Eye: A Role for Glucagonergic Regulation of Emmetropization? *Investigative Opthalmology & Visual Science*, *46*(11), 3922. https://doi.org/10.1167/iovs.04-1026

Vessey, K. A., Rushforth, D. A., & Stell, W. K. (2005). Glucagon- and secretin-related peptides differentially alter ocular growth and the development of form-deprivation myopia in chicks. *Investigative Ophthalmology and Visual Science*, *46*(11), 3932–3942. https://doi.org/10.1167/iovs.04-1027

Vielma, A. H., & Schmachtenberg, O. (2016). Electrophysiological fingerprints of OFF bipolar cells in rat retina. *Scientific Reports*, *6*(1), 30259. https://doi.org/10.1038/srep30259

Vielma, A. H., Tapia, F., Alcaino, A., Fuenzalida, M., Schmachtenberg, O., & Chávez, A. E. (2020). Cannabinoid Signaling Selectively Modulates GABAergic Inhibitory Input to OFF Bipolar Cells in Rat Retina. *Investigative Opthalmology & Visual Science*, *61*(3), 3. https://doi.org/10.1167/iovs.61.3.3

Wallman, J., & Turkel, J. (1978). Extreme myopia produced by modest changes in early visual experience. *Science*, *201*(SEPTEMBER), 1249–1251.

Wang, G. H., Zhang, Y. T., Zhao, J., Zhang, J., & Jiang, F. (2020). Mitigate the effects of home confinement on children during the COVID-19 outbreak. *Journal of Shanghai Jiaotong University (Medical Science)*, *40*(3), 279–281. https://doi.org/10.3969/j.issn.1674-8115.2020.03.001

Wang, J., Li, Y., Musch, D. C., Wei, N., Qi, X., Ding, G., Li, X., Li, J., Song, L., Zhang, Y., Ning, Y., Zeng, X., Hua, N., Li, S., & Qian, X. (2021). Progression of Myopia in School-Aged Children After COVID-19 Home Confinement. *JAMA Ophthalmology*, *139*(3), 293. https://doi.org/10.1001/jamaophthalmol.2020.6239

Wässle, H. (2009). Glycinergic transmission in the mammalian retina. *Frontiers in Molecular Neuroscience*, *2*. https://doi.org/10.3389/neuro.02.006.2009

Wersinger, E., Schwab, Y., Sahel, J. A., Rendon, A., Pow, D. V., Picaud, S., & Roux, M. J. (2006). The glutamate transporter EAAT5 works as a presynaptic receptor in mouse rod bipolar cells. *Journal of Physiology*, *577*(1), 221–234. https://doi.org/10.1113/jphysiol.2006.118281

Xiong, W. H., Pang, J. J., Pennesi, M. E., Duvoisin, R. M., Wu, S. M., & Morgans, C. W. (2015). The effect of PKCα on the light response of rod bipolar cells in the mouse retina. *Investigative Ophthalmology and Visual Science*, *56*(8), 4961–4974. https://doi.org/10.1167/iovs.15-16622

Yiu, W. C., Yap, M. K. H., Fung, W. Y., Ng, P. W., & Yip, S. P. (2013). Genetic Susceptibility to Refractive Error: Association of Vasoactive Intestinal Peptide Receptor 2 (VIPR2) with High Myopia in Chinese. *PLoS ONE*, *8*(4). https://doi.org/10.1371/journal.pone.0061805

Zhang, T., Ruan, H.-Z., Wang, Y.-C., Shao, Y.-Q., Zhou, W., Weng, S.-J., & Zhong, Y.-M. (2022). Signaling Mechanism for Modulation by GLP-1 and Exendin-4 of GABA Receptors on Rat Retinal Ganglion Cells. *Neuroscience Bulletin*, *38*(6), 622–636. https://doi.org/10.1007/s12264-022-00826-9

Zhang, Y., & Wildsoet, C. F. (2015). RPE and Choroid Mechanisms Underlying Ocular Growth

and Myopia. In *Cognitive Development* (Vol. 25, Issue 4, pp. 221–240). https://doi.org/10.1016/bs.pmbts.2015.06.014

Zhong, X., Ge, J., Smith, E. L., & Stell, W. K. (2004). Image defocus modulates activity of bipolar and amacrine cells in macaque retina. *Investigative Ophthalmology and Visual Science*, *45*(7), 2065–2074. https://doi.org/10.1167/iovs.03-1046

Zhou, X., Li, Q., An, J., Pan, M., Li, Y., Chen, J., & Qu, J. (2010). Development of Relative Hyperopia in Dopamine D2 Receptors Knockout Mice. *Investigative Ophthalmology & Visual Science*, *51*(13), 1197. http://dx.doi.org/

Zhou, X., Pardue, M. T., Iuvone, P. M., & Qu, J. (2017). Dopamine signaling and myopia development: What are the key challenges. *Progress in Retinal and Eye Research*, *61*, 60–71. https://doi.org/10.1016/j.preteyeres.2017.06.003